

NO_Z INTERFERENCE IN MEASURING NO₂ BY MOLYBDENUM
OXIDE CONVERSION AND CHEMILUMINESCENCE AT A
COASTAL SITE IN NOVA SCOTIA, CANADA

by

Alan Wilson

Submitted in partial fulfillment of the requirements
for the degree of Master of Applied Science

at

Dalhousie University
Halifax, Nova Scotia
August 2017

© Copyright by Alan Wilson, 2017

To the Meteorological Service of Canada

Table of Contents

List of Tables	vi
List of Figures	vii
Abstract	ix
List of Abbreviations and Symbols Used	x
Acknowledgements	xiv
Chapter 1 Introduction	1
1.1 Definitions of NO_x , NO_y and, NO_z	1
1.2 Science Questions	1
1.3 Hypothesis	2
1.4 NO_2 and the NO_x Cycle in the Troposphere	2
1.5 HO_x in the Troposphere	4
1.6 Other Reactive Oxides of Nitrogen - NO_y and NO_z	6
1.7 NO_2 and People - the AQHI	7
1.7.1 What is the AQHI?	7
1.7.2 The 2009 Expansion of the AQHI Program	8
1.7.3 Measurements, Modelling, and Forecasting	9
1.8 Methods of Real-time measurements of NO_2	14
1.8.1 Chemiluminescence	14
1.8.2 Direct Measurements by Spectroscopic Methods	16
1.8.3 Cavity Attenuated Phase Shift (CAPS)	18
1.8.4 Other Methods	20
1.8.5 Methods in Current Use	20
1.9 Catalytic Conversion of NO_2 Followed by Chemiluminescent Detection and NO_z Interference	20

1.10	NO _z Species	21
1.10.1	HNO ₃	21
1.10.2	PANs	22
1.10.3	HONO	24
1.10.4	pNO ₃	26
1.10.5	Other Minor NO _z species	26
1.10.6	Other Interfering Species	27
1.11	NO _z Interference - Other Works	27
Chapter 2	Materials and Methods	33
2.1	General Approach	33
2.2	Measurement Site	33
2.2.1	Location	33
2.2.2	Characteristics	34
2.3	Instrumentation	36
2.3.1	Teledyne - API (T-API) T200 NO _x Analyser	36
2.3.2	T-API T200 Modified for NO _y	36
2.3.3	T-API T500U NO ₂ Analyser	41
2.3.4	Sample Inlet and Sampling System	41
2.4	Calibration	41
2.4.1	T-API T700U Dynamic Dilution Calibrator	42
2.4.2	T-API 701H Zero Air Generator	42
2.4.3	Calibration Gas	43
2.4.4	T-API T300U CO Analyser and Thermo Scientific 49i Ozone Analyser	43
2.5	Data Collection	44
2.5.1	DR DAS Envidas Ultimate Software and PC	44

2.5.2	Meteorological Data	44
2.5.3	Data Preparation	47
2.6	Data Analysis	48
2.6.1	R and the OpenAir Package	48
2.6.2	Statistical and Other Methods	49
Chapter 3	Results and Discussion	50
3.1	Estimation of Experimental Error	50
3.2	Summary of Measured Species and Meteorological Data	52
3.2.1	Summary of Chemical Species	52
3.2.2	Summary of Meteorological Data	60
3.2.3	Temporal Variation of Selected Measurements	60
3.2.4	NO _z Interference Based on Wind Direction and Speed	61
3.3	NO _z Interference	68
3.3.1	Linear Regression of NO ₂ (T200) vs. NO ₂	68
3.3.2	Wilcoxon Signed-Rank Testing	72
3.3.3	Spearman Correlation Analysis for May and October	73
Chapter 4	Conclusion	78
	Bibliography	82
	Appendix A Calibration Valve Code	87
	Appendix B Certifications	91
B.1	Calibration Gas	91
B.2	T700U Calibrator Mass Flow Controllers (MFCs)	93
B.3	T700U Calibrator Ozone Generator Certification	99
	Appendix C Traffic Volume	103

List of Tables

Table 1.1	Estimated sources of present-day NO_x in the Troposphere (IPCC [Dentener et al., 2001])	3
Table 1.2	Health Risk Associated with AQHI Values.	7
Table 2.1	Instrument Specifications.	39
Table 2.2	Specifications for the T300U and 49i.	43
Table 2.3	Comparison of selected meteorological values between the MSC surface station AAW and the Davis station co-located at the measurement site.	45
Table 3.1	Summary of NO_y chemical species data; $n = 2692$	52
Table 3.2	Summary of median (interquartile range) NO_2 , NO and NO_z interference by month.	53
Table 3.3	1981-2000 Climate normals for Shearwater (CYAW) met station.	53
Table 3.4	Summary of meteorological data; $N = 2692$	60
Table 3.5	Data for extreme events, $\text{NO}_2(\text{T}200)/\text{NO}_2 > 1.15$	66
Table 3.6	Wilcoxon signed-rank test by month and for the complete dataset.	73

List of Figures

Figure 1.1	Lewis diagram for NO.	3
Figure 1.2	Summary of NO_x , NO_y and NO_z	6
Figure 1.3	NAPS sites across Canada in 2009. [Environment Canada, 2010b]	10
Figure 1.4	Example of the temporal variation of the NO_2 field at the measurement site.	13
Figure 1.5	Plot of light intensity incident on the detector as a function of phase angle.	19
Figure 1.6	Response of 5.6 ppb HNO_3 to various inlet materials.	22
Figure 1.7	Peroxyacetyl nitrate.	23
Figure 1.8	Monthly NO_2 and ΔNO_2 at two sites in the Swiss Alps.	28
Figure 1.9	Diurnal cycles of $(\text{NO}_2)_M/\text{NO}_2$ for both sites.	29
Figure 1.10	Diurnally averaged profiles for measured CL NO_x monitor interference, measured HNO_3 concentrations and modelled alkyl nitrate concentrations at La Merced, Mexico City site.	31
Figure 2.1	Location of the measurement site in Dartmouth, NS.	35
Figure 2.2	Instrument rack, measurement site in Dartmouth, Nova Scotia	37
Figure 2.3	Calibration valve control.	38
Figure 2.4	External shelter with the relocated MoO converter, sample / calibration gas selection valve, and post-converter particulate filter.	40
Figure 2.5	The Raspberry Pi model B used to collect data from the Davis Vantage Pro II weather station, with external TCXO real-time clock.	46
Figure 3.1	Box plots by month for NO and true NO_2	54
Figure 3.2	Box plots by month for NO_z , NO_x , and NO_y	55
Figure 3.3	Box plots by month for NO_z interference and NO_z interference for data with $\text{NO}_x > 1$ ppbv.	56
Figure 3.4	Box plots by month for NO_z and absolute humidity.	58

Figure 3.5	Polar plot of median NO and NO ₂ values.	59
Figure 3.6	Time variation plot for NO _z interference.	61
Figure 3.7	Time variation plot for NO ₂ (T200) / NO ₂	62
Figure 3.8	Time variation plot for NO ₂ as measured by the T200 and T500U.	62
Figure 3.9	Time variation plot for median wind speed.	63
Figure 3.10	Polar plot of median NO _z interference.	63
Figure 3.11	Polar plot of median NO _z values.	65
Figure 3.12	NO _z interference, NO ₂ (T200)/NO ₂ ratio > 1.15.	66
Figure 3.13	NO _z , NO ₂ (T200)/NO ₂ ratio > 1.15.	67
Figure 3.14	NO ₂ and NO ₂ (T200) pre and post Log transform	69
Figure 3.15	Histograms for NO ₂ and NO ₂ (T200), pre and post Log transform.	70
Figure 3.16	Autocorrelation function plot for Log NO ₂ and Log NO ₂ (T200).	71
Figure 3.17	Linear regression slopes by month, NO ₂ (T200, MoO/CL) vs. NO ₂ , with 95% CI bars.	72
Figure 3.18	Spearman correlation plot for May 2016.	75
Figure 3.19	Spearman correlation plot for October 2016.	76

Abstract

The common method of monitoring NO₂ (Nitrogen dioxide) in Canada may be subject to error by interference from other oxides of nitrogen. These other compounds are capable of causing instruments to over-report NO₂ concentrations. NO₂ is a toxic gas, a reasonable surrogate measure for mixed-pollutant air masses, and one of the pollutants used to calculate Canada's air quality risk communication tool, the AQHI (Air Quality Health Index). It is one of the pollutants commonly modelled in air chemistry models. The level of interference has been reported to be half or more of measured NO₂ in a variety of locations, from the Swiss Alps to Mexico City. Using measurements with some unknown amount of positive interference has the potential to introduce artifacts into air quality forecasts or induce model error. It is expected that there may be a significant, albeit poorly characterised, interference in NO₂ monitoring in Canada.

List of Abbreviations and Symbols Used

$\bar{\epsilon}_R(\lambda)$	Mie extinction at wavelegth λ averaged over pathlength l
$\bar{\epsilon}_R(\lambda)$	Rayleigh extinction at wavelength λ averaged over pathlength l
\bar{c}_i	Concentration of species i averaged over pathlength l
λ	Wavelength, especially of light or other electromagnetic radiation
ρ	Spearman rank correlation coefficient
$\sigma_i(\lambda)$	Absorbance cross-section of species i at wavelength λ
τ	Chemical lifetime
$I_0(\lambda)$	Intensity of light incident on a sample
$I_{tr}(\lambda)$	Intensity of light of wavelength λ transmitted through a sample
l	Within the context of the Beer-Lambert Law, l is the pathlength through an absorbing species
A	Constant, 6.116441
AH	Absolute Humidity
AN	Alkyl nitrate
AQ	Air Quality
AQHI	The Air Quality Health Index
C	Constant, 2.16679 gKJ ⁻¹
CAPS	Cavity Attenuated Phase Shift
cc³ min⁻¹	Cubic centimetres per minute
CL	Chemiluminescence
CRDS	Cavity Ring-down Spectroscopy

DI	Digital Input
DO	Digital Output
DOAS	Differential Optical Absorbance Spectroscopy
EC	Environment Canada. Name changed to Environment and Climate Change Canada (ECCC) in 2015
ECCC	Environment and Climate Change Canada
EM	Electromagnetic
FEP	Fluorinated ethylene propylene
FSDS	Federal Sustainable Development Strategy
FTIR	Fourier Transform Infrared Spectroscopy
GEM-MACH	Global Environmental Multiscale, Modelling Air Quality and Chemistry
GPT	Gas Phase Titration
HO_x	H + OH + HO ₂ ; radical species capable of oxidizing many trace species in the atmosphere
HONO	Nitrous acid
IR	Infrared
L min⁻¹	Litres per minute
LDL	Lower detection limit
Log₍₁₀₎	Base 10 Logarithm
m	Constant, 7.591386
MFC	Mass Flow Controller
MSC	Meteorological Service of Canada

NAPS	National Air Pollution Surveillance
NB	Province of New Brunswick, Canada
NO	Nitric oxide or Nitrogen monoxide
NO₂	Nitrogen dioxide
NO_x	$\text{NO}_x \equiv \text{NO} + \text{NO}_2$
NO_y	Total reactive nitrogen. Includes NO _x
NO_z	$\text{NO}_z \equiv \text{NO}_y - \text{NO}_x$
NS	Province of Nova Scotia, Canada
O₃	Ozone
OA	Objective Analysis
OI	Optimal Interpolation
P_{ws}	Saturated water vapour pressure, hPa
P_w	Water vapour pressure, hPa
PAN	Peroxyacetyl nitrate. IUPAC nomenclature nitroethaneperoxoate. Also refers to a group of compounds, including PPN.
PBL	Planetary Boundary Layer - that part of the atmosphere between the planet's surface and the free troposphere. Can be a few hundred to a few thousand metres in depth, depending on latitude, time of day, and other conditions. Also sometimes referred to as the mixed layer, as the PBL is turbulent, whereas the free troposphere above the PBL tends towards laminar flow
PMT	Photomultiplier tube
pNO₃	Particulate nitrates or particulate-bound nitrates
ppbv	Parts per billion by volume
PPN	Peroxypropionyl nitrate
pptv	Parts per trillion by volume
QA	Quality Assurance

RCS	Reference Climate Station
RDAQA	Regional Deterministic Air Quality Analysis. The ECCC operational OA product combining numerical prediction (model output) and surface AQ data using OI
rh	Relative humidity
RTC	Real-time Clock
SoC	System on Chip
T	Temperature, °C for equation 3.3, K for equation 3.2
T_d	Dewpoint temperature
T_n	Constant, 240.7263
TC	Transport Canada
TDLAS	Tunable Diode Laser Absorbance Spectroscopy
US EPA	United States Environmental Protection Agency

Acknowledgements

I would like to thank the following people: Dr. Steve Beauchamp and Bill Appleby, for making this possible. Dr. Mark Gibson, not only for acting as my supervisor, but also being a great collaborator and colleague. Dr. Susanne Craig and Dr. Jan Haelssig for taking the time to be on my committee. Dr. Cris Mihele for his insights and design suggestions for the NO_y modification. My wife, for putting up with the late nights and common absences. To my colleagues at the Meteorological Service of Canada, current and retired, who helped me get to where I am today. Vlado Keselj and all those before who helped develop and maintain the LaTeX dalthesis.cls template. And finally, to all of the MSC UA techs flying balloons in the remote corners of Canada - because no one else does.

Chapter 1

Introduction

1.1 Definitions of NO_x , NO_y and, NO_z

Below are the definitions for the various reactive oxides of nitrogen and chemical families referred to throughout this document:

- $\text{NO}_x = \text{NO} + \text{NO}_2$ (Nitric oxide and Nitrogen dioxide)
- $\text{NO}_y = \text{NO}_x + \text{peroxyacetyl nitrates (PANs)} + \text{alkyl nitrates (RONO)} + \text{Nitric acid (HNO}_3) + \text{Nitrous acid (HONO)} + \text{particulate-bound nitrates (pNO}_3) + \text{nitrate radical} + \text{other minor species}$
- $\text{NO}_z \equiv \text{NO}_y - \text{NO}_x$

1.2 Science Questions

The science questions for this work are:

1. What is the magnitude of NO_z interference at this urban coastal location (Dartmouth, NS, Canada)?
2. Is the magnitude significant to modelling, OA (Objective Analysis), or AHQI (Air Quality Health Index) forecasting?
3. What are the major temporal characteristics of the NO_z interference, especially diurnal, day of week and seasonal variation?
4. What relationships exist between meteorology and NO_z interference?
5. Is there a correction factor or factors evident from the data?

1.3 Hypothesis

Given current literature, I expect to find significant NO_z interference in the measurement of NO_2 with MoO/CL instruments. However, an easily identified correction factor is unlikely given the complexity of the NO_z , NO_x and HO_x chemistry and resultant concentration fields for individual NO_z species. GEM-MACH (Global Environmental Multiscale, Modelling Air quality and CHemistry, [Moran et al., 2012]) model output for NO_2 is for true NO_2 . Therefore, any non-trivial NO_z interference in the NO_2 monitoring network could have negative impact on model OA. As the OA output is used to seed the start of model runs, and to provide synthetic AQHI observations, NO_z interference in the monitoring network could impact model performance and AQHI products.

1.4 NO_2 and the NO_x Cycle in the Troposphere

Nitrogen dioxide (NO_2) is one of three criterion pollutants used to determine the Air Quality Health Index (AQHI). NO_2 was chosen as one of the constituent pollutants as it was shown to act as a reasonable indicator of adverse health outcomes [Stieb et al., 2008; Levy et al., 2014]. NO_2 is a toxic gas; Burnett et al. [2004] showed an increase in adverse health outcomes at concentrations as low as 22.4 ppbv [Burnett et al., 2004]. NO_2 , and other NO_y species, play an important role in tropospheric chemistry with regard to ozone and OH radical concentrations [Bottenheim et al., 1993].

In the context of ambient tropospheric conditions, NO and NO_2 exist within the NO_x cycle. Cycling between the two species within the troposphere is rapid, and they are usually considered within the context of the chemical family NO_x . Both NO and NO_2 are gasses in normal atmospheric conditions.

The majority of NO_x is emitted as NO. The major sources of NO in the troposphere are fossil fuel combustion and biomass burning. There are a variety of other minor sources as shown in Table 1.1.

NO is a free radical in the gas phase (Figure 1.4). As such, it reacts readily with a number of atmospheric constituents. NO is formed under high temperature and pressure conditions in the presence of molecular nitrogen and oxygen. The reaction

Source	Tg N yr ⁻¹ (2000)
Fossil fuel combustion	33.0
Biomass burning	7.1
Soils	5.6
Lightning	5.0
NH ₃ Oxidation	-
Aircraft	0.7
Transport from stratosphere	< 0.5

Table 1.1: Estimated sources of present-day NO_x in the Troposphere (IPCC [Dentener et al., 2001])

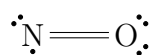
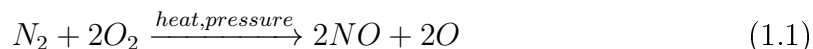
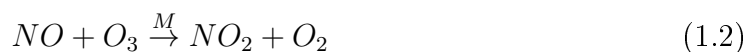


Figure 1.1: Lewis diagram for NO. Note the unpaired electron.

series can be summed up as:



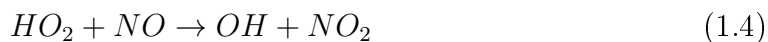
In the presence of O₃, NO undergoes the reaction:



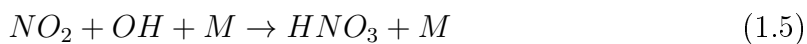
Within the NO_x cycle, NO₂ can undergo photolysis in the presence of O₂ to reform NO.



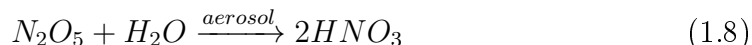
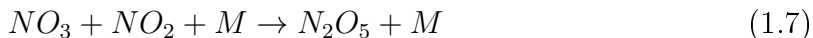
Reaction rates for 1.2 and 1.3 are fast in the troposphere. Taking the two together results in a null cycle. Cycling between the two NO_x species also occurs between reactions 1.3 and 1.4.



HNO₃ is the major NO_x sink. During the day, it is formed by:



Once the sun sets, photochemical production of the hydroxyl radical ceases (reactions 1.9 to 1.11). Production of HNO_3 at night occurs through a series of reactions, ending with heterogeneous reaction 1.8:



These mechanisms give a chemical lifetime (τ) for NO_x in the lower troposphere of about one day. HNO_3 can be photochemically converted back to NO_2 . However, the reaction rate for this conversion is slow compared to the wet deposition rate of HNO_3 in the troposphere, considered to be a few days in the lower troposphere and few weeks in the upper troposphere [Jacob, 1999].

1.5 HO_x in the Troposphere

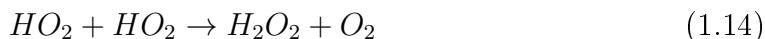
A major oxidizing species of the troposphere is OH, the hydroxyl radical. OH is usually considered within the chemical family HO_x . However, OH is the most abundant species of the HO_x family within the troposphere [Jacob, 1999]. Most general atmospheric chemistry texts and references include more detail on NO_x and HO_x chemistry in the troposphere. Jacob [1999] and Seinfeld and Pandis [2006] were used for this and Subsection 1.4.

OH is formed by the reaction of $\text{O}(^1\text{D})$ with water vapour. $\text{O}(^1\text{D})$ is produced by the photolysis of O_3 by UV radiation. Within the troposphere, sufficient UV radiation between 300 and 320 nm penetrates the atmosphere to allow the formation of $\text{O}(^1\text{D})$ in situ. $\text{O}(^1\text{D})$ can then either go to ground state monatomic oxygen, O, via collisional quenching (1.10), or react with water vapour to form OH (1.11).



OH oxidation plays an important role in removing a variety of pollutants. For example, CH₄ and CO oxidation within the troposphere occur primarily via OH. Within the context of NO_x and NO_y, OH plays an important role in the formation of some NO_z species, such as HNO₃ and PAN. HONO acts as a reservoir for both HO_x and NO_x [Calvert et al., 1994]. Refer to Subsection 1.10 for details on NO_z species.

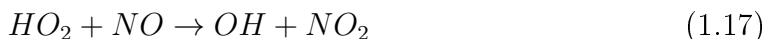
Much like NO_x, the HO_x family cycles between species in the troposphere. Oxidation of CO by OH forms carbon dioxide and the hydrogen radical. The hydrogen radical can then react with molecular oxygen in the presence of a third body to form HO₂. HO₂ can then combine with itself to form H₂O₂.



H₂O₂ is water soluble, with a lifetime against wet deposition ($\tau_{wetdeposition}$) of approximately one week. It can act as a HO_x sink in this manner. However, H₂O₂ can also photolyse or react with OH, regenerating HO_x.



In the presence of NO, HO₂ can also regenerate OH and NO₂:



The NO₂ can then photolyse (reaction 1.3), regenerating O₃ which can then itself photolyse (reaction 1.9) and produce 2 more OH. Reactions 1.12 + 1.13 + 1.17 + 1.3 result in a chemical chain mechanism whereby HO_x and NO_x catalyse O₃ production in the troposphere. Interestingly, HO_x and NO_x catalyse O₃ destruction in the stratosphere, due to differing reaction kinetics and increased atomic oxygen, O₃ and HO_x concentrations there.

NO_x and HO_x chemistry in the troposphere are linked, and thus NO_x has a direct effect on the oxidative capacity of the troposphere. As HO_x chemistry is important in

$\text{NO}_x = \text{NO} + \text{NO}_2$	NO_y :
	- NO_x
	- PANs
$\text{NO}_y = \text{NO}_x + \text{others}$	- R- NO_2
	- HNO_3
	- HONO
$\text{NO}_z \equiv \text{NO}_y - \text{NO}_x$	- p NO_3
	- NO_3 radical
	- Etc.

Figure 1.2: Summary of NO_x , NO_y and NO_z .

so many reaction pathways of trace species, accurate characterisation of both the NO_x and HO_x fields is necessary to gain accurate chemical modelling of our atmosphere. Modelling that has become important in terms of provision of a Canadian public health metric, known as the Air Quality Health Index (AQHI see Subsection 1.7). Accurate NO_2 measurements are required for model verification and model Objective Analysis (OA). OA is described in sub-Subsection 1.7.3 under "GEM-MACH and OA".

1.6 Other Reactive Oxides of Nitrogen - NO_y and NO_z

It is difficult to consider tropospheric NO_x in isolation. While the major source of tropospheric NO_x is NO, typical daytime 12 hour average ratios for NO/ NO_2 in the lower troposphere is about 0.1 [Seinfeld and Pandis, 2006]. NO_2 is a reactive species and can form many NO_z species by day and night. In the lower troposphere, reaction 1.5 tends to dominates NO_x lifetime, with $\tau_{\text{NO}_x} = 1$ to 2 days [Seinfeld and Pandis, 2006]. Besides removal as HNO_3 , NO_2 can also form a variety of NO_z species, where NO_z is defined as $\text{NO}_y - \text{NO}_x$. Figure 1.2 summaries the various nomenclatures. Subsection 1.10 gives more details on the major NO_z species.

The major NO_y species are generally considered to be NO_x , HNO_3 , HONO, the nitrate radical ($\text{NO}_3(g)$), PAN and associated homologs, N_2O_5 , HNO_4 , a variety of alkyl and peroxyalkyl nitrates, pNO_3 and $\text{NO}_3^-(aq)$ on aerosol and other surfaces [Seinfeld and Pandis, 2006].

As these species can form from NO_x , either directly or otherwise, so can they convert back to NO_x . In measuring NO_2 by catalytic conversion with MoO, where NO_2 is converted to NO for subsequent detection, other NO_z species are also converted to NO. This may cause measurements of NO_x and NO_2 values in excess of what is actually present in the air being sampled.

1.7 NO_2 and People - the AQHI

1.7.1 What is the AQHI?

The AQHI, as developed by Stieb et al. [2008], is a risk communication tool. It was developed to help communicate potential short-term health risks based on ambient air quality. The AQHI is based on three criterion pollutants, those being O_3 , particulate matter with an aerodynamic diameter of $2.5 \mu\text{m}$ or less ($\text{PM}_{2.5}$), and NO_2 . CO and SO_2 were also considered, but were not found to have good correlation with short-term acute health effects [Stieb et al., 2008]. It uses a unitless scale from 1 to 10+, with levels of acute risk to health associated with the values as shown in Table 1.2. Risk statements were developed for both the general population and for those at increased risk of adverse effects due to air pollution, such as those with asthma, children, and the elderly.

AQHI Value	Category
1-3	Low
4-6	Moderate
7-10	High Risk
10+	Very High Risk

Table 1.2: Health Risk Associated with AQHI Values.

The formula used by Environment Canada to report the AQHI is:

$$AQHI = \frac{10}{10.4} (100(e^{0.000871 * \text{NO}_2} - 1) + e^{0.000544 * \text{O}_3} - 1 + e^{0.000487 * \text{PM}_{2.5}} - 1)) \quad (1.18)$$

where the pollutant values are the 3-hour moving averages of hourly average values. NO_2 and O_3 are given in ppbv and $\text{PM}_{2.5}$ in $\mu\text{g m}^{-3}$. The value calculated is then rounded, with zero being set to 1, and values greater than 10 reported as 10+. The AQHI value is more sensitive to NO_2 than to the other constituents. A rough rule of thumb is that about 12 ppbv change in NO_2 will change the AQHI value by one, and 20 ppbv / $\mu\text{g m}^{-3}$ change in ozone or $\text{PM}_{2.5}$ will do the same.

1.7.2 The 2009 Expansion of the AQHI Program

Originally, the AQHI program was limited to areas near NAPS (National Air Pollution Surveillance) AQ (Air Quality) monitoring stations. These are largely located in urban areas as shown in Figure 1.3. AQHI measurements and forecasts were limited to locations with monitoring sites.

In 2009 the Government of Canada sought to expand the AQHI program. The desired results of the expansion are to "Continue development of the AQHI and continue implementation in all provinces and major communities in the North to achieve access for 80% of the Canadian population", as stated in the Federal Sustainable Development Strategy (FSDS) [Environment Canada, 2014]. Given the large size of the Canadian land mass, expansion of the surface monitoring network sufficient to gain coverage for 80% of the population would be entirely impractical, if not impossible. It was necessary to look at ways to provide regional versus point AQHI measurements and forecasts. Satellite retrievals are a candidate. However, the usual methods for using satellite retrievals are affected by meteorological and other conditions such as cloud cover, high surface albedo (snow cover), and darkness (arctic winter). The obvious means to do this is by modelling the necessary air chemistry and AQHI constituent species within the context of the meteorological modelling. It was at this point that the notions of synthetic AQHI observations and regional forecasting from the model came to be a larger part of EC's air quality research.

In 2011, MSC (Meteorological Service of Canada) Atlantic Region started a study on evaluating the GEM-MACH model against instrumentation. Campbellton, NB was chosen as the study site due to its location in the northerly reaches of the Maritime provinces of Canada, and because of its small urban size. The northerly location helped in having only occasional influxes of aged pollution plumes from the

eastern seaboard of North America, as synoptic weather patterns tended to keep such airmasses further to the south and east. Choosing a small, remote town ensured modelling was for a location with anthropogenic local sources (and thus a population for which to forecast), but otherwise of a rural nature. The surrounding rural land and air masses were important, as other work had already been done in urban areas, both for its own sake and to improve the model Objective Analysis (OA). Results were generally promising, but showed known issues with localised pollution sources, source inventories and PBL (Planetary Boundary Layer) modelling on a local scale [Wilson et al., 2014].

The issue of NO_z interference presented as a possible source of model/measured divergence in the NO_2 field during literature review for the Campbellton AQHI study. It was at this point that the planning for an NO_z interference study in the Atlantic Region of MSC began. OA for the GEM-MACH NO_2 field was a driving reason for conducting this work. Similar studies were started in the oil sands of Alberta and other locations in Canada.

1.7.3 Measurements, Modelling, and Forecasting

AQHI constituent pollutants are measured by the NAPS network in cooperation with provincial, territorial and other partners across Canada. Figure 1.3 shows the network as of 2009. The goal and scope of ECCC's (Environment and Climate Change Canada) NAPS program is to:

... provide accurate and long-term air quality data of a uniform standard across Canada. NAPS was established in 1969 to monitor and assess the quality of ambient (outdoor) air in the populated regions of Canada. NAPS is managed using a cooperative agreement among the provinces, territories and some municipal governments. In 1969, eight provinces – Nova Scotia, New Brunswick, Quebec, Ontario, Manitoba, Saskatchewan, Alberta and British Columbia – joined the program. In the first annual data report 36 monitoring sites reported to the Canada-wide database. Today there are 286 sites in 203 communities located in every province and territory. [Environment and Climate Change Canada, 2013]

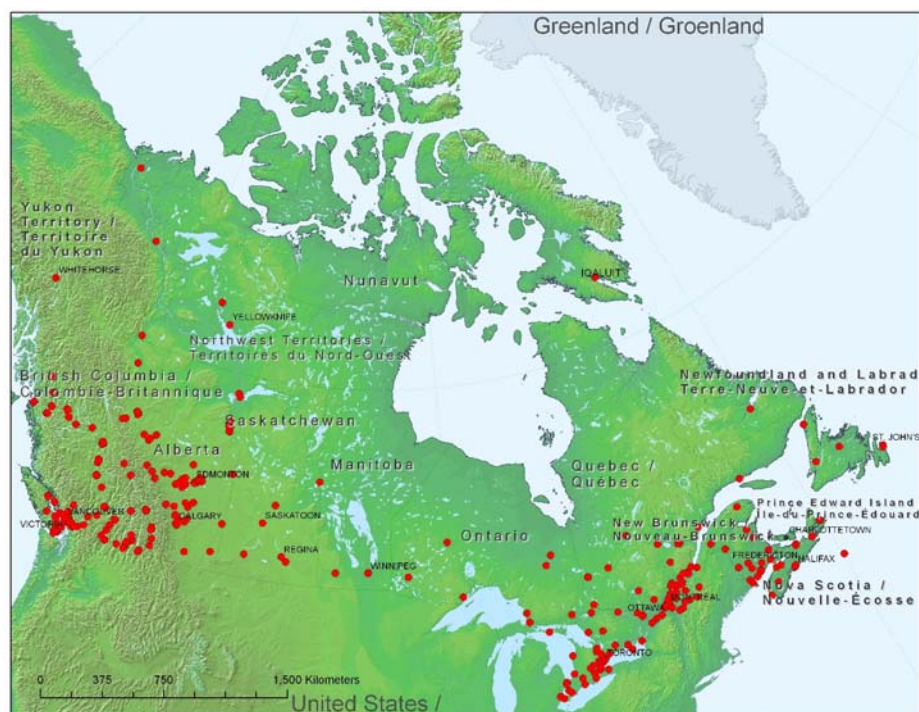


Figure 1.3: NAPS sites across Canada in 2009. [Environment Canada, 2010b]

The National Atmospheric Pollution Surveillance (NAPS) Network

NAPS provides support in terms of instrumentation, calibration gases, annual calibrator certification and other support. Using Nova Scotia as an example, the provincial Department of Environment operates and maintains the monitoring sites, provides data QA/QC and performs the necessary site audits and instrument calibrations in accordance with NAPS procedures. While there are variations on the details of the Federal - Provincial/Territorial cooperation agreement, the Nova Scotia example demonstrates the general nature of how the network monitoring is managed.

Within Canada, NO_2 is monitored as part of ECCC's NAPS AQHI monitoring network. The standard means of measuring ambient NO_2 within the NAPS network is with instruments that measure NO_2 concentration by conversion to NO via a heated molybdenum oxide (MoO) catalyst, followed by chemiluminescence (CL) detection [Environment Canada, 2010a]. Data used for the development of the the AQHI by Stieb et al. [2008] were from the NAPS network.

GEM-MACH and OA

AQHI monitoring stations are not inexpensive. A "back of the envelope" number for just instrumentation and supporting communications equipment would be CAD\$100 000 in 2016. Increasing the number of monitoring station sufficient to cover 80% of Canadians is not practical. One solution to 'fill in' between monitoring stations is modelling. The MSC uses GEM-MACH as its operational model for AQHI. The operational version of the model domain encompasses all of North America. It is based on a 10 km horizontal grid, and 80 σ - p vertical layers from the surface to 0.1 hPa. Equation 1.19 defines σ - p pressure coordinates, where $p(x,y)$ is pressure at the considered grid point, $p_s(x,y)$ the surface pressure, and p_t the pressure at the top of the domain). GEM-MACH is an inline model, which is to say that meteorology and chemistry are modelled together. Output is hourly. This is contrasted by other types that model meteorology first, then air chemistry. There are other experimental models, with smaller geographic domains and horizontal grid sizes (2.5 km). However, given the large computational expense, these are limited to specific studies and other research. They are not yet suitable for constant, full domain use at this time [Moran et al., 2012].

$$\sigma(x, y, p) = \frac{p(x, y) - p_t}{p_s(x, y) - p_t} \quad (1.19)$$

Work continues within MSC to use GEM-MACH and associated Objective Analysis (OA) to provide synthetic AQHI observations as well as AQHI forecasts for regions without an AQHI monitoring station near by. OA for O₃ and PM_{2.5} have been operational and available in real time since 2012. OA for the NO₂ field has become available recently. The original goals of the OA product were, and remain, to inform forecasters on current surface chemistry conditions and quality of the model output - large differences between the model output and OA product may indicate model issues - and to provide the initial fields necessary for an assimilation system. Such a system is required because unlike meteorological modelling, where meteorology is sensitive to initial conditions, air quality is largely controlled by chemical sources and sinks, boundary conditions and atmospheric conditions, and are highly variable in space and time. Therefore AQ fields, both the AQHI constituent pollutants and

other pollutants necessary for effective modelling of atmospheric chemistry, within the model require assimilation of hourly AQ data. The OA provides the initial AQ fields for the start of the model run [Robichaud and Ménard, 2012].

The method used by ECCC to provide AQ OA is an Optimal Interpolation (OI) method combining numerical prediction (output from the GEM-MACH model) and hourly monitoring data from the AIRNow near real-time output from monitoring stations in the USA and Canada. The model requires data from outside of Canada, as its domain is North America. The operational OA product for MSC is called the Regional Deterministic Air Quality Analysis (RDAQA) [Robichaud and Ménard, 2012].

The RDAQA OA method acquires the necessary air quality data in real time. These data are passed through a series of quality control tests. The background field is provided from the GEM-MACH model output. OI is then applied. OI uses an exponential decaying function based on distance, from the H.-L. method [Hollingsworth and Lönnberg, 1986], with a series of modifications that improve both bias and error variances in the analysis. Final bias corrections are then applied, such as those for seasonal biases in the $PM_{2.5}$ field, and the final product is complete [Robichaud and Ménard, 2012].

As the OA product is used both to seed the initial AQ conditions in GEM-MACH, and is used by forecasters to both improve AQ forecasts and make judgments on the quality of the model output, it is evident that the best possible quality of OA output is important. the RDAQA OA product is also a candidate source for synthetic AQ observations for most of Canada where there is no local monitoring station. The best possible OA product relies on accurate AQ data. Should NO_x interference prove to be large and common, this would have a negative impact on the OA product, model validation, forecasts, and synthetic observations needed to meet the FSDS goal of AQHI program expansion to 80% of Canadians. The problem becomes increasingly difficult with increasing temporal resolution and NO_x species mixture complexity.

Forecasting

Ideally, model output would be sufficient to provide AQHI forecasts for any given region. However, it is recognised that the model has difficulty with the PBL. While

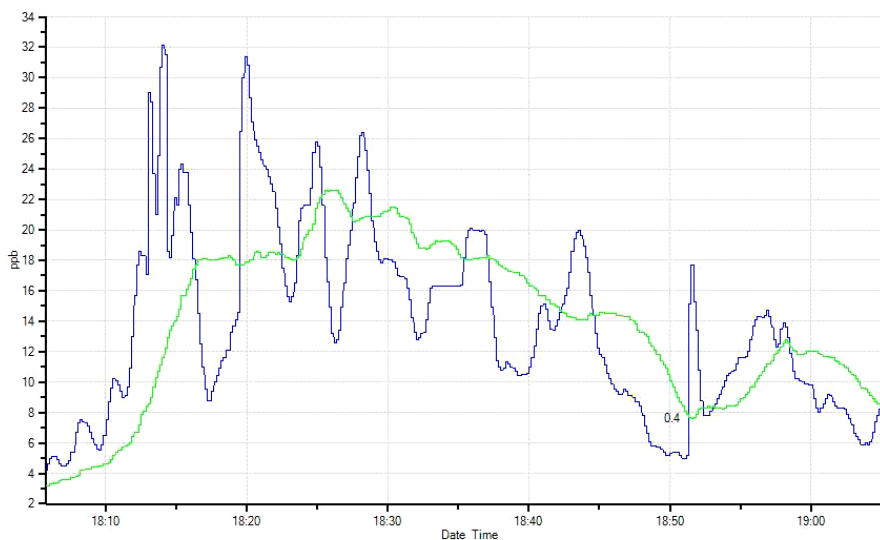


Figure 1.4: Example of the temporal variation of the NO_2 field at the measurement site. Note the finer temporal resolution of the T500U (blue) vs. the multi-channel T200 (green).

ozone is generally considered a regional pollutant, $\text{PM}_{2.5}$ and NO_2 both vary in concentration on a horizontal spatial scale much smaller than the 10 km grid of the GEM-MACH model. The NO_2 concentration field is also noisy, and can vary by 100's of percent over a period of minutes in low NO_x regimes. Therefore, forecaster intervention is helpful in improving AQHI forecasts based on model output. Initial results of a test of forecaster intervention versus only model output in northern New Brunswick in 2012-2013 showed improvement of the AQHI forecast. Instances such as winter night-time inversions trapping pollutants in a small valley such as in the area of Campbellton, NB can be recognised and accounted for by a forecaster, while such local meteorological phenomena are not necessarily resolved in the 10 km grid of the model [Wilson et al., 2014]. However, the large size of the Canadian land mass does not allow for individual forecaster intervention for all AQHI forecast regions. The task is simply too large to "do by hand".

Since forecaster intervention is not possible for all of the populated areas in Canadian land mass, modelling and OA products may be able to provide forecasts for most Canadians. While the AQHI was developed using NO_2 data with some unknown amount of NO_2 interference, and therefore essentially may have a partial or

near-complete correction factor built in, this is not the case for GEM-MACH. It models true NO_2 . A correction factor for NO_z interference, if necessary, would both improve model verification and the OA products, thus improving AQHI forecasting based on model output. Given current literature, NO_z interference is expected to be measurable and significant, at least in terms of modelling.

1.8 Methods of Real-time measurements of NO_2

1.8.1 Chemiluminescence

MoO Catalysts

The accepted method of NO_2 measurement within the NAPS network are analysers that have received US EPA (United States Environmental Protection Agency) "Automated Reference Method" for NO_2 [Environment Canada, 2010a]. The US EPA periodically updates that list, as found on their website (www.epa.gov at time of writing). Most appear to be of the standard thermal/metal converter CL type.

For this type of instrument, the sample stream is switched between two paths in the instrument. One path is for the detection of NO via reaction with excess O_3 in the reaction chamber and subsequent detection by chemiluminescence.



followed by either:



or



The excited electron can return to ground state by either third-body quenching or photon emission. Photons via reaction 1.22 tend to be in the 600 - 3000 nm range, with a 1200 nm peak. It is this photon emission (CL) that is used as a means of detection, as there is a linear relationship between photon signal and concentration of NO_2 [Fontijn et al., 1974]. The photon signal is detected and amplified by a PMT (Photo Multiplier Tube), and the PMT signal converted to a reported concentration. The PMT requires only moderate cooling (typically held around 4°C). Excessive third-body quenching is avoided by using a reduced reaction chamber pressure.

The second path switches the sample flow to move through a converter, converting NO_2 to NO , after which the sample is directed through the reaction chamber and detected as above. The most common converter in the current network is a Molybdenum oxide converter, where the sample flows through a heated Section with MoO chips or screens at about 320°C . In the presence of oxygen, this catalytically reduces NO_2 to NO while temporarily oxidizing MoO to MoO_2 and MoO_3 [McClenny et al., 2002; Gerboles et al., 2003]. MoO is then regenerated. After the conversion of the NO_2 to NO , the sample stream is directed through the CL detection pathway as noted above for NO . NO_2 is now present as NO . This converted NO , plus the NO already in the sample is detected via CL and reported as the total NO_x concentration [Heard, 2006]. The MoO/CL methodology is subject to some interference, including positive interference from NO_z species. Some NO_z species are also converted. Conversion efficiencies vary from the order of 10-20% to quantitative conversion, pending on NO_y species and physical conditions such a sample and converter .

CO and Gold

There are other converter types used in the detection of NO_2 followed by CL detection. Instead of a MoO substrate, a heated gold substrate at similar temperatures to the MoO type, with CO as a reducing agent, is used to convert NO_2 to NO , with chemiluminescence as a detection method. This has proven to be susceptible to interferences in manner similar to the molybdenum converters. It requires a source of CO gas, which is not always convenient in remote monitoring locations. This and the MoO methods can collectively be considered as thermal-type converters. There are other, less common metal/thermal type converters in use for research purposes [Heard, 2006; McClenny et al., 2002].

Photolysis

Another converter type relies on NO_2 being photolysed in the UV/visible blue range. This can be used to selectively photolyse NO_2 to NO for subsequent CL detection [Bollinger et al., 1984]. Photolytic converters have some issues that need to be considered. Photolysis is not quantitative, and is not linearly related to NO_2 concentration. There have been reports of radical formation in the photolytic converter by certain

volatile organic compounds (VOCs), such as glyoxyls (including oxidation products of isoprene), resulting in under-reporting of NO_2 . Atmospheric VOC photolysis products introduce negative interference as well [Villena et al., 2012]. HONO has also been reported as a source of interference in photolytic converters. The reported conversion efficiency of HONO by photolytic converters is in the 20-30% range [Ryerson et al., 2000].

Luminol

NO_2 (and O_3) react with some organic compounds resulting in chemiluminescence. By using PMTs, this reaction can provide a usable electrical signal for measuring NO_2 concentrations. The method was found to be fast and showed initial promise in very low detection limits, on the order of tens of pptv. However, in measuring NO_2 with just luminol a number of interferences were found, both positive and negative. O_3 , PAN, HNO_3 , CO_2 , and other species were found to give interfering signals. Modifications such as additives to change pH or otherwise remove interfering species, inlet filters and other methods were all tried, and most were successful. However, PAN interference was never completely solved, and the method fell out of favour. In instances where interfering species are not a factor, luminol-based instruments are small, use little power, and can provide low detection limits with fast reaction times. However, for ambient monitoring where interfering species are a concern, luminol is not the best method [Heard, 2006].

1.8.2 Direct Measurements by Spectroscopic Methods

Direct detection of NO_2 can be made by various techniques. Tunable Diode Laser Absorbance spectroscopy (TDLAS) and Fourier Transform Infrared (FTIR) spectroscopy use the IR part of the EM spectrum and the absorbance spectra of NO_2 (and other species of interest) via a variety of detection and data processing techniques to derive NO_2 concentrations. The IR source can be active, such as heated filaments or tunable lasers, or passive, such as the sun. Measurements are usually taken through a long pathlength. Open path methods sample through the atmosphere, either with the source at one end of the path and detector at some distance away, or with reflectors.

In the case of reflectors, the detector and IR source can be co-located, with the path-length twice that of the distance between source and reflector. UV-visible Differential Optical Absorbance Spectroscopy (DOAS) methods can also use open long path measurement, making use of a different region of the EM spectrum. These methods can be quite selective, and are capable of low detection limits, the exact nature of which depends on the absorbance spectra of the species in question, atmospheric conditions, and other factors. Open path methods have limitations for use in ambient monitoring such as interference from water vapour, no way to introduce calibration gases into the sample, limited time of day for the passive IR methods (when the sun is below the horizon, it cannot be used as the IR source), screening of the sun as the IR source by clouds, and overlapping spectra for some species of interest. Also, these methods rely on varying degrees of post-processing of the data to get meaningful results. As such, they have limited utility in continuous ambient monitoring of NO₂ [Heard, 2006].

There are a number of closed path spectroscopic methods as well. Most closed path measurements use the visible or UV part of the EM spectrum. By using highly reflective mirrors at the ends of a measurement chamber and multiple reflection within that chamber, pathlengths of thousands of metres can be achieved within a relatively small instrument case. Cavity ring-down spectroscopy (CRDS) and a variety of other methods based on DOAS can be used within a closed path instrument. DOAS is based on the Beer-Lambert Law, describing the exponential decrease of light intensity at a given wavelength on passing through a sample with an absorbing species. In considering measuring an absorbing species such as NO₂ in a sample of ambient air, the Beer-Lambert equation is modified to treat Rayleigh (molecular scattering) and Mie (aerosol scattering) extinction as analogous to molecular absorption. This is then averaged over the pathlength, yielding equation 1.23, where $I_{tr}(\lambda)$ is the intensity of light of wavelength λ transmitted through the sample containing species i with a concentration c_i , $I_0(\lambda)$ is the intensity of light incident on the sample, l is the pathlength, $\sigma_i(\lambda)$ is the absorbance cross-section at wavelength λ , pressure (P) and temperature (T) (P and T are omitted in equation 1.23), and the barred terms are the concentration of species i , Rayleigh and Mie extinction terms averaged over

pathlength l for wavelength λ .

$$I_{tr}(\lambda) = I_0(\lambda) \exp\left(-l \left(\sum_{i=1}^n \sigma_i(\lambda) \bar{c}_i + \bar{\epsilon}_R(\lambda) + \bar{\epsilon}_M(\lambda) \right)\right) \quad (1.23)$$

In the atmosphere most species of interest are always present. Also, Rayleigh and Mie scattering always occur. As such, I_0 cannot be determined free of any extinction. Therefore, direct application of 1.23 cannot occur. However, if the absorption spectrum of a species of interest has a fine scale variation, it can be used as a "fingerprint" for that species. The absolute cross-section is considered as a sum of a rapidly varying component and another, slowly varying component. Subtracting the slow component leaves a differential cross-section. While useful, newer methods using absorbance spectroscopy have been developed recently. These simplify measurements and instrument design [Jacob, 1999; Keabian et al., 2008].

1.8.3 Cavity Attenuated Phase Shift (CAPS)

Cavity Attenuated Phase Shift (CAPS) detection of NO_2 is similar to, and derived from, cavity ring-down spectroscopy (CRDS), but does not require phase locking or a coherent light source. It makes use of NO_2 's absorption spectra and long pathlengths via highly reflective mirrors resulting in a measurable phase shift in a beam of light within the absorption spectrum passed through the sample chamber. CAPS takes advantage of NO_2 's strong absorbance band in the blue visible region of light. A series of light pulses, or shots, are emitted into the sample chamber, and the pathlength (or time) of the intensity peak is measured. Calibration of the instrument with zero air allows for the calculation of the pathlength or time between the shot and peak intensity at the detector as the light "leaks" through the mirrors at the ends of the chamber. The introduction of an absorbing species decreases the absolute value of the intensity at the peak. The introduction of an absorbing species also decreases the pathlength, or time, at which the intensity peak occurs. This change, or phase shift, is directly proportional to the concentration of the absorbing species. Figure 1.5 demonstrates the phase shift between air with and without an absorbing species present in the sample.

This method has its own interferences. Most, but not all of these can be addressed in instrument design. For example, absorption bands for 1,2-dicarbonyl compounds

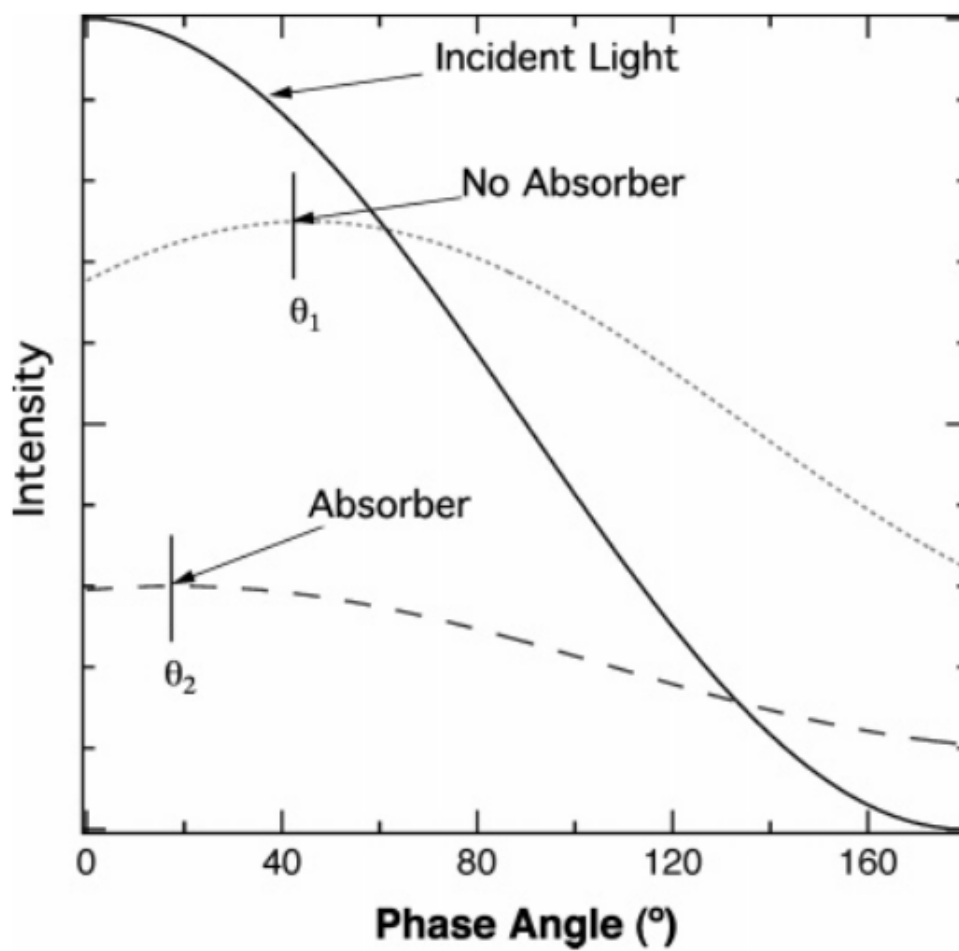


Figure 1.5: Plot of light intensity incident on the detector as a function of phase angle. Phases with and without an absorbing gas are shown. [Kebabian et al., 2005]

(products of photolysis of certain VOCs) overlap that of NO₂ [Kebabian et al., 2008, 2005]. Glyoxal is an example, and is one of the products of the photolysis reaction pathways of isoprene. Glyoxal is also one of the major contributors to the negative interference in photolytic converters [Villena et al., 2012]. This can largely be mitigated by shifting the light source wavelength away from the overlapping portions of the band associated with the interfering species, and introducing narrow band-pass optical filters in front of the detector. In some cases, this is not possible. The absorption bands for some halogen compounds show significant overlap with that of NO₂. It is usual to consider that these compounds are not found in sufficient quantities to cause issues during normal monitoring. 3σ detection limits for NO₂ measurements by CAPS are in the range of around 60 pptv for 10 second resolution. The measurements are linear ($R^2=0.9999 \pm 1$ ppbv for and range of 0-320 ppbv), and instrument drift is very low (less than ± 0.5 ppb over a month) [Kebabian et al., 2008].

1.8.4 Other Methods

There are several more methods for determining ambient NO₂ concentrations. Heard [2006] and McClenny et al. [2002] provide a good overview.

1.8.5 Methods in Current Use

The most common method of ambient NO₂ monitoring in the NAPS network is MoO conversion / CL detection. There were a few photolytic converter types being run for inter-comparisons with MoO/CL types, and other methods are likely in the field outside of the NAPS network. However, the author is not aware of the nature or quantity of other types in operational use.

1.9 Catalytic Conversion of NO₂ Followed by Chemiluminescent Detection and NO_z Interference

A known issue with the use of MoO and other thermal-type converters of NO₂ is that the conversion is not selective for NO₂ [Grosjean and Harrison, 1985; Winer et al., 1974]. Some NO_z species ($\text{NO}_z \equiv \text{NO}_y - \text{NO}_x$), such as peroxyacetyl nitrate (PAN), convert as effectively as NO₂ [Heard, 2006]. If there are non-trivial concentrations of

these interfering species, NO_2 is over-reported. While the AQHI was developed using data with such interference, that interference has not been well characterised. Also, models such as those used by ECCC (e.g. GEM-MACH) model true NO_2 . Therefore, using the network data with some unknown amount of positive interference from NO_z species has the potential to introduce artifacts into products such as the OA and AQHI forecast. Several studies have suggested that photochemistry plays a role in the production and lifetime of the interfering NO_z species, with sunny afternoons showing some of the highest interference [Gerboles et al., 2003; Dunlea et al., 2007].

1.10 NO_z Species

1.10.1 HNO_3

HNO_3 is a significant NO_z species. It is created both during the day and night, acts as a significant NO_x sink in the lower troposphere, and in the presence of NH_3 can contribute to aerosol formation (NH_4NO_3 - see pNO_3 below) [Seinfeld and Pandis, 2006; Jacob, 1999]. In terms of measuring NO_x and NO_y , HNO_3 poses certain problems, "sticking" to inlet materials. HNO_3 can also "unstick" from inlet materials as atmospheric conditions change, such as temperature and humidity. It can thus providing a NO_y signal that is not present in the current sample, but rather was present some unknown time in the past. This is often referred to as a memory effect [Neuman et al., 1999]. Figure 1.6 shows the response to 5.6 ppb HNO_3 moving through various inlet materials. Section 1.4 covered the major reactions for the formation of HNO_3 in the NO_x cycle.

Original attempts to determine the conversion efficiency of HNO_3 by thermal methods such as MoO failed. There was found to be significant conversion, but it could not be quantified [Gerboles et al., 2003; Winer et al., 1974]. Subsequent work found that HNO_3 could be efficiently converted by a thermal type MoO converter. Reports of 85-100% efficiency for a MoO were reported, with a converter temperature of 340°C [Williams et al., 1998]. HNO_3 can make up to tens of percent of total NO_y [Harrison et al., 1999], and therefore may contribute significantly to NO_z interference in MoO/CL methods. However, quantification of that contribution remains difficult to achieve.

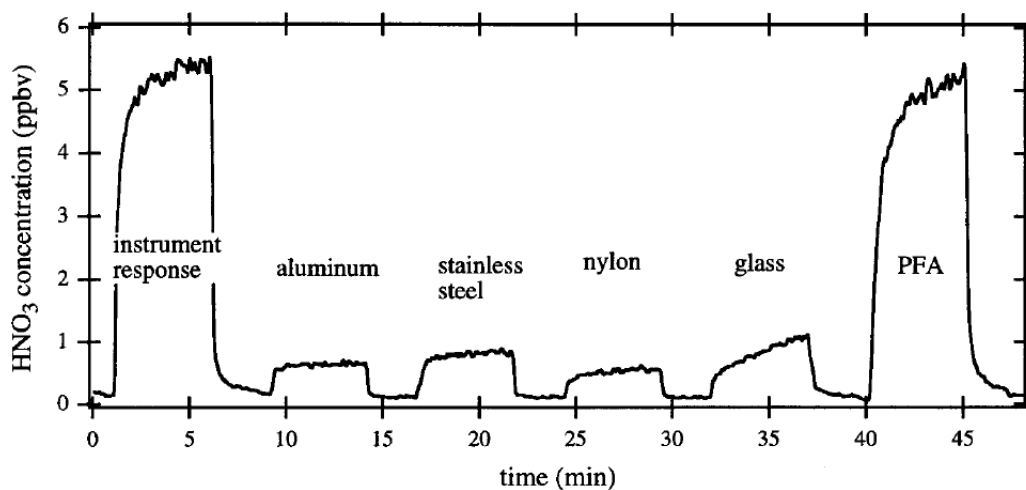
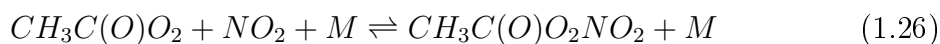
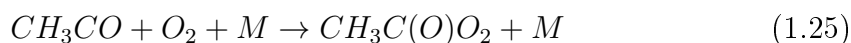
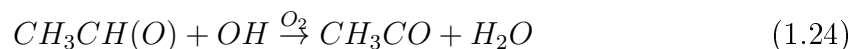


Figure 1.6: Response of 5.6 ppb HNO_3 to various inlet materials. Note the passivation of glass as time progresses [Neuman et al., 1999]

1.10.2 PANs

A class of NO_2 reservoir species collectively known as *peroxyacetyl nitrates* or PANs are compounds of the general form $\text{RC}(\text{O})\text{OONO}_2$. Peroxyacetyl nitrate (PAN) and peroxypropionyl nitrate (PPN) are the most commonly considered species of PANs, as others dissociated too rapidly to be of significance as an NO_x interfering species. PANs are produced by the oxidation of carbonyl compounds in the presence of NO_x . The carbonyls are the product of photochemical oxidation of hydrocarbons from both biogenic sources (such as isoprene) and anthropogenic sources. While there are many more PAN species that are possible, few have sufficiently long chemical lifetimes in tropospheric conditions to be of any significant influence on total NO_y or NO_x . In the simplest case of acetalehyde, the formation of PAN can be summarised as:



The thermal decomposition of PAN (right to left reaction of equilibrium 1.26) is highly temperature dependent. The lifetime of PAN against thermal decomposition is about an hour at 298 K, but several months at 250 K [Jacob, 1999]. Should PAN

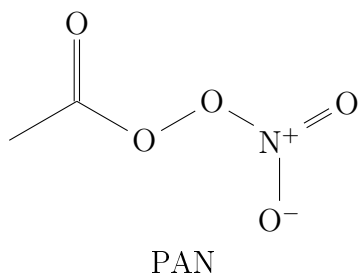


Figure 1.7: Peroxyacetyl nitrate.

be lofted into the upper troposphere, it can be carried over synoptic scale distances (1000s of km), where it can then descend with its associated airmass and undergo thermal decomposition, adding NO_2 to the lower troposphere. PAN is also quantitatively converted to NO (and products) in MoO and other thermal-type converters. Depending on conditions, PAN can account for tens of percent of total NO_y [Harrison et al., 1999]. Given this large dependence on temperature with regard to chemical lifetimes of PAN, it is easy to see that PAN could contribute to significant NO_z interference during the winter months at mid and high latitudes.

Alkyl Nitrates

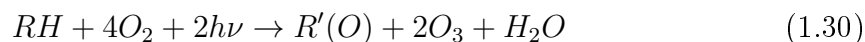
There is general agreement that there is an incomplete understanding of alkyl nitrates (ANs) chemistry in the troposphere. They are of the general form RONO_2 , where R represents an alkyl group. They are of interest for several reasons. ANs can be converted in MoO converter to NO and products, resulting in NO_z interference with varying degrees of efficiency. For example, the fairly simple ethyl nitrate has been found to convert quantitatively [Winer et al., 1974]. There is some evidence that ANs can account for most or all of the "missing" NO_y others have reported in measuring total NO_y against the sum of individually measured NO_y species. ANs have their origin in a terminating branch of the catalytic formation of tropospheric O_3 by NO_x and HO_x [Day et al., 2003]. The production of ANs begins with oxidation of a hydrocarbon by OH. The source of the hydrocarbon can be biogenic or anthropogenic. This is also the start of the catalytic production of O_3 by NO_x and HO_x .



At which point the reaction can branch:



Reaction 1.29b terminates the catalytic chain, but is slower than reaction 1.29a for many hydrocarbons under normal lower tropospheric conditions. From reaction 1.29a, the chain continues, with the net reaction shown as reaction 1.30 [Day et al., 2003].

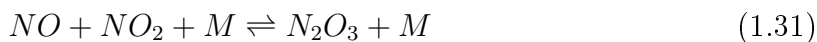


The resultant carbonyl compound can itself undergo further reactions, including the formation of additional NO_z species. In the case of acetaldehyde, it can form PAN. The formation of ANs is linked to NO_x and HO_x cycling, formation of tropospheric O_3 , and provides for a potential source of NO_z interference in routine NO_x monitoring. Some have found that total ANs account for 10-20% of total NO_y over a year in a rural site [Day et al., 2003]. With an incomplete understanding of $RONO_2$ chemistry and amounts found in the troposphere, it is possible that ANs could prove to be a significant source of NO_z interference under the right conditions.

1.10.3 HONO

HONO is often ignored in NO_y studies. It is often felt that the concentrations are too low to make any significant contribution [Harrison et al., 1999]. However, there is evidence that this is not always the case. HONO formation is thought to primarily be a night-time heterogeneous reaction on wet surfaces (ground, structures, aerosols, etc). A number of studies in the 1980's found > 1 ppb night-time concentrations in a variety of air mass types at night in the lower troposphere. The exact nature of

HONO formation remains questionable. However, reactions 1.31 and 1.32 represent the accepted general reactions. The specific mechanisms within this heterogeneous system remain unclear [Calvert et al., 1994].



While the equilibrium shown in reaction 1.31 heavily favours the left side in ambient conditions, it is forced to the right in high NO_x conditions, such as those at vehicle exhausts. During the day, photodissociation and fast daytime reactions keep HONO concentrations low. HONO absorbs strongly in daylight below 390 nm. The quantum yield of reaction 1.33 is near unity within its absorbance band.



Besides keeping HONO concentrations low during daylight hours, reaction 1.33 is thought to provide a pulse of OH (and NO) soon after sunrise, before reactions 1.9 to 1.11 have a chance to get started. Therefore, HONO can be considered a night-time reservoir of both OH and NO [Calvert et al., 1994]. MoO/CL conversion of HONO has been reported as efficient and near quantitative [Gerboles et al., 2003; Heard, 2006; Williams et al., 1998]. However, there is limited data on the quantification of HONO conversion in thermal MoO converters. HONO concentrations are usually low with regard to total NO_y and NO_z . However, one study in the southeast of England found the night HONO concentrations were on the same level as HNO_3 the following day, albeit in the sub-ppb range [Kitto and Harrison, 1992]. Therefore, in circumstances where conditions favour HONO formation (high NO_x air masses), HONO could be expected to be a direct contributor to NO_z interference. It could also have secondary effects in its action as a night-time OH/NO reservoir, the associated OH "push" at sunrise, and NO_z species arising from OH oxidation of NO_x , alkyl nitrates and other NO_z precursors. There is little literature that specifically addresses HONO conversion in MoO converter, allowing for a degree of uncertainty with regard to this NO_z species acting as an interfering signal in MoO/CL monitoring of NO_2 and NO_x .

1.10.4 pNO₃

There are a variety of mechanisms for the formation of particulate-bound nitrates (pNO₃). HNO₃ in the presence of NH₃ can form NH₄NO₃ fine aerosols. HNO₃ can also react on the surfaces of coarse aerosols (sea salts and crustal material) to form nitrates. NO₃ can also be found in larger sea salt aerosols without HNO₃ involvement. Little work has been done to quantify the degree of pNO₃ conversion to NO in thermal converters. One study found that sub-micron particulate nitrates were efficiently converted. Coarse mode particulate nitrates (such as NaNO₃ from sea salts) showed lowered efficiency [Harrison et al., 1999]. A summary of total NO_y versus NO_y by species from a variety of studies as shown in Harrison et al. [1999] suggests that 5-15% of total NO_y may be particulate-bound nitrate. However, as little information is available as to the efficiency of conversion by the studies cited is available, and the data provided were total study means, it is difficult to quantify NO_z in MoO converters based on this information. Absolute 8-hour means for all studies cited showed pNO₃ values in the sub-ppb equivalent range. Therefore, this NO_z species is of more interest in secondary effects, such as the sequestration of HNO₃ [Harrison et al., 1999]. It is possible that occasional, short-period spikes in concentration may occur, with an associated NO_z interference episode.

1.10.5 Other Minor NO_z species

Other minor NO_z species include a variety of nitrated organic compounds, the NO₃ radical, N₂O₅, and others. Most of these are either formed in very low concentrations (organics), or rapidly return to their precursors through thermal decomposition or photolysis. For example, the night-time formation mechanism for HNO₃ shown in reactions 1.6 to 1.8 are only possible at night, as the nitrate radical and N₂O₅ are rapidly photolysed back to their originating species. NO₂⁻ and NO₃⁻ anions can be found in the aqueous phase on wet aerosol and other surfaces. Work on the nature of conversion efficiency for these other NO_z species is sparse. These other species are generally short-lived and in low concentrations [Harrison et al., 1999; Jacob, 1999; Seinfeld and Pandis, 2006].

1.10.6 Other Interfering Species

Some non- NO_y species can also be reduced or otherwise form NO in MoO converters. HCN and NH_3 are example species that have shown positive interference. Most work looking at these species show less than quantitative conversion, usually in the 2-20% range. However, some work with different types of thermal converter have shown near-quantitative levels. HCN levels are not usually of concern for ambient monitoring. NH_3 can be an issue near certain industrial and agricultural activities, and must be considered in equipment use and design, such as placing an NH_3 filter in line with the sample stream [Heard, 2006; Williams et al., 1998; Fahey et al., 1985].

1.11 NO_z Interference - Other Works

NO_z is defined as $\text{NO}_y - \text{NO}_x$, where $\text{NO}_x \equiv \text{NO} + \text{NO}_2$, and NO_y is generally considered to be all reactive oxides of nitrogen, such as $\text{NO}_x + \text{HNO}_3$, PAN, ANs, N_2O_5 , particulate bound nitrates, HONO, and additional minor species [McClenny et al., 2002].

Some NO_y species are converted as efficiently as NO_2 (PAN, some alkyl nitrates), or partially (HNO_3 , some ANs). There are also some non- NO_y species (for example HCN) that can be converted to NO by the method in question. Accounting for HNO_3 poses additional issues, as it has been demonstrated that HNO_3 exhibits memory effects at the sample inlet, line losses and temperature and humidity related losses [Volz-Thomas et al., 2005; Steinbacher et al., 2007]. Measuring total NO_y requires taking these effects into account when designing instrumentation, inlets, and other experimental apparatus and installation techniques (Neuman et al. [1999], for example).

At low NO_x concentration, interference can result in over-reporting of NO_2 by a significant amount [Gerboles et al., 2003]. Gerboles et al. reported NO_z interference accounting for up to one third of the NO_2 value reported. Steinbacher et al. reported that during a spring/summer measurement campaign in Switzerland, only 70-83% of reported monthly NO_2 by MoO/CL was actually NO_2 , the remainder being NO_z interference. This was for a site at Teanikon, a plateau site in the Alps. At a higher altitude site of Rigi, 630 m above the plateau, 43-76% of reported monthly NO_2 as

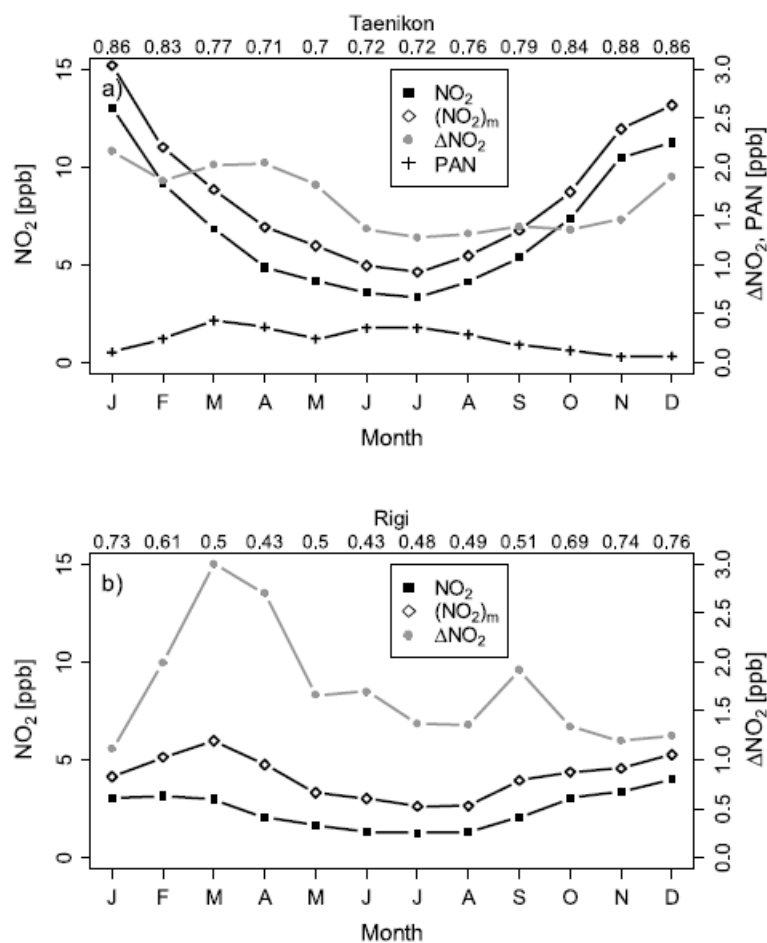


Figure 1.8: Monthly NO_2 and ΔNO_2 at two sites in the Swiss Alps. Note that Rigi is 630m above the plateau and is less impacted by human activity. The numbers over the top of each graph are monthly $\text{NO}_2/(\text{NO}_2)_M$ [Steinbacher et al., 2007]

measured by MoO/CL was actual NO_2 , with the remainder being NO_z interference [Steinbacher et al., 2007]. NO_2 concentrations for Steinbacher et al. were in the 0-10 to 0-15 ppbv range. They used a photolytic converter as an inter-comparison instrument, with the assumption that the photolytic instrument provided an accurate measure of true NO_2 concentrations.

Figure 1.8 shows monthly NO_2 , $(\text{NO}_2)_M$ (NO_2 as measured with a MoO converter), and ΔNO_2 values for two sites in Switzerland. Some key points to note are that the delta is actually larger (in ppbv) at the higher (and less impacted by pollution) site, and the different seasonal trends between the two sites. Steinbacher et al.

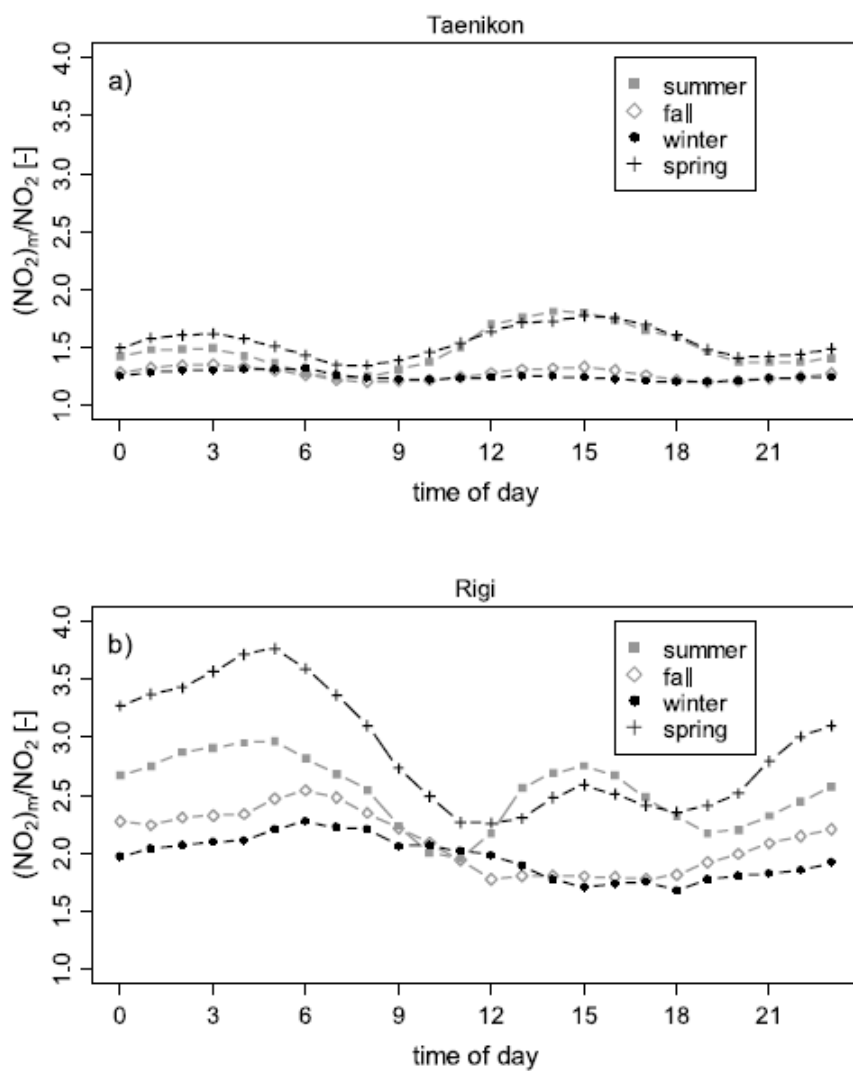


Figure 1.9: Diurnal cycles of $(NO_2)_M/NO_2$ for both sites. Each season is presented separately. [Steinbacher et al., 2007]

suggested that at least part of the difference in winter could be attributed to particulate nitrates and equipment design. They suggested that at Taenikon, the lower and warmer site in winter, could show a positive bias as compared to colder Rigi due to increased evaporation from nitrates trapped on particle filters inserted into the sample stream to keep particulate matter out of the instrumentation. Both sites showed some agreement between the daily averages of ΔNO_2 and daily total nitrates. Springtime interference maximas for both sites coincided with the usual spring ozone maxima in the northern hemisphere. Seasonal and diurnal data along with case studies suggest that local meteorological, photochemistry and transport conditions play a role in the amount of NO_z interference found in MoO/CL instruments.

From their work, Steinbacher et al. [2007] developed a correction factor based on a multiple linear regression approach. This was done by fitting modelled ΔNO_2 to that of the measured ΔNO_2 for each site. The model equation developed is shown in equation 1.34.

$$\Delta\text{NO}_2 = a \cdot (\text{NO}_2)_m + b \cdot \text{O}_3 + c \cdot \text{factor}(\text{month}) + d \cdot \text{factor}(\text{day/night}) + e + \varepsilon \quad (1.34)$$

In equation 1.34, a through d represent the developed coefficients, e is the intercept, ε is a residual, $(\text{NO}_2)_m$ is the measured NO_2 value via CL instruments, and O_3 is used as an indicator of photochemistry potential. Initial application to sites of similar geographic NO_x regimes showed some promise. See Steinbacher et al. [2007] for details and the various coefficients developed.

For higher NO_x regimes, NO_z interference can account for half or more of the NO_2 concentration measured. Work in Mexico City examined MoO thermal conversion / CL detection in comparison with spectroscopic techniques (TDLAS, DOAS) to determine the difference between MoO/CL reported concentrations and true NO_2 concentration measured via spectroscopy. It was found that up to half of averaged afternoon NO_2 concentrations as measured by a thermal MoO instrument were not NO_2 . The major contributor to the interference signal were believed to be HNO_3 , alkyl nitrates, and multi-functional alkyl nitrates [Dunlea et al., 2007].

Figure 1.10, from Dunlea et al. [2007], shows averaged daily values for interference

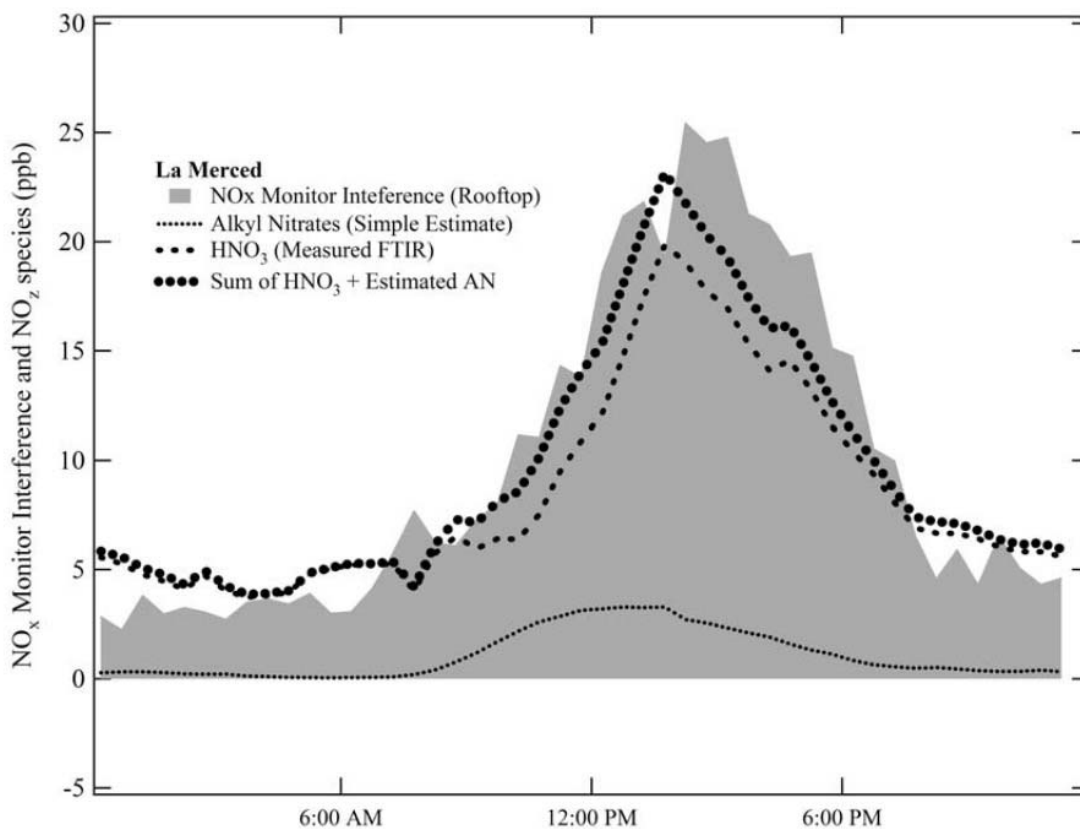


Figure 1.10: Diurnally averaged profiles for measured CL NO_x monitor interference, measured HNO₃ concentrations and modelled alkyl nitrate concentrations at La Merced, Mexico City site. Profiles averaged over entire campaign. Also included is sum of HNO₃ and modelled alkyl nitrate concentration. Time of day is local. [Dunlea et al., 2007]

in the NO_2 values, HNO_3 , and modelled alkyl nitrate levels. There is a strong diurnal signal evident.

Villena et al. [2012] reported NO_2 concentrations over-reported by up to a factor of four during the afternoon for a measurement campaign in Santiago, Chile. The peak interference corresponded well with that of the afternoon ozone peak. This corresponding ozone peak was also reported by Dunlea et al. [2007]. It is thought that the ozone peak is co-varying with NO_2 interference, rather than directly related. Some interfering species are resultant from NO_y photochemistry, and thus their concentrations might be expected to peak with those of photochemically produced ozone. In the case of Villena et al. [2012], NO_2 concentrations presented were in the 10-50 ppbv range. For comparison, the range for NO_2 in the case of Dunlea et al. [2007] were about 20-120 ppbv [Villena et al., 2012; Dunlea et al., 2007].

The strong afternoon peaks shown by Dunlea et al. [2007] and Villena et al. [2012] suggest that photochemistry likely plays a dominant role for NO_z interference in MoO/CL NO_2 measurements in higher NO_x concentrations. The spring and summer diurnal plots shown in Figure 1.9 also show afternoon peaks in the interference signal for both sites. This may be suggestive of a photochemical interference signal at lower NO_x locations as well.

Chapter 2

Materials and Methods

2.1 General Approach

The general approach to data collection was that of a continuous monitoring network. In doing so, methods used were to approximate a continuous monitoring station. This approach was selected to determine the nature and extent of NO_z interference within a monitoring context. However, in order to minimise the amount of data correction, a compromise audit/calibration cycle was selected. While NAPS monitoring stations require auditing every three months, once a month was chosen to minimise instrument drift [Environment Canada, 2010a]. Also, recalibration was done for instances of span drift equal to or greater than 5%, and when zero drift exceeded the LDL (lower detection limit). Approaches that would result in high precision data, such as nightly recalibration, were rejected as the purpose of this work was to characterise NO_z interference within an ambient continuous monitoring context. In choosing a monthly audit cycle with calibration thresholds lower than the NAPS monitoring network, data collected required little correction while still acting as a reasonable representation of both ambient monitoring techniques and actual NO_2 concentrations. It is believed that this approach provided for an acceptable compromise between high precision data and simulating a monitoring network with an operating error of an unknown amount up to $\pm 15\%$, as the NAPS recalibration threshold allows for up to that amount.

2.2 Measurement Site

2.2.1 Location

The measurement site was located at the ECCC office in Dartmouth, Nova Scotia, Canada, $44^{\circ}42' \text{ N } 063^{\circ}36' \text{ W}$, at an elevation of approximately 20 m. The building complex consists of an 18 story office tower, with a three story extension to the

south and associated multi-level parking garage to the east and southeast. Rooftop access is available for both portions of the building. There is a multi-lane roadway to the west with several transit routes and a multistory building across the street forming a road canyon. Secondary/tertiary streets are on the other three sides of the building complex. Traffic volumes (mixed data from 2013-2016) for Alderney Drive, as provided by the municipality, are approximately 12 000 to 16 000 vehicles per day during the work week (Monday to Friday), and lower on the weekends. Rush hour peak volumes of 1200 to 2000 vehicles per hour were measured. Refer to Appendix C for the traffic volume data received from the municipality. Halifax Harbour is within 100 m of the site to the west. The site has exposure to the outer harbour and open North Atlantic to the south. Figure 2.1 shows overhead views of the site.

2.2.2 Characteristics

Located mid latitudes along the Atlantic Coast of Nova Scotia, Canada, the measurement site experiences climatological moderation, with some cooling influences in the spring and summer, and warming influences due to the proximity of the Gulf Stream offshore during the winter. Being adjacent to Halifax Harbour and the North Atlantic Ocean, the site is considered "Coastal Marine" in meteorological terms. At 20 m, the site is within the PBL. It is also likely often within the marine boundary layer, which is generally lower than the terrestrial boundary layer, and often sufficiently 'strong' to prevent mixing down of airmasses and associated long-range transport of pollutants.

The location of the site next to several roadways and their associated road traffic provide a level of primary NO_x emissions for most of the day, with increased levels during morning and evening rush hours. The presence of several multistory buildings in the immediate area make measurements of wind speed and direction from the measurement site largely meaningless in terms of regional and synoptic flow, hence the use of wind data from the MSC station AAW.

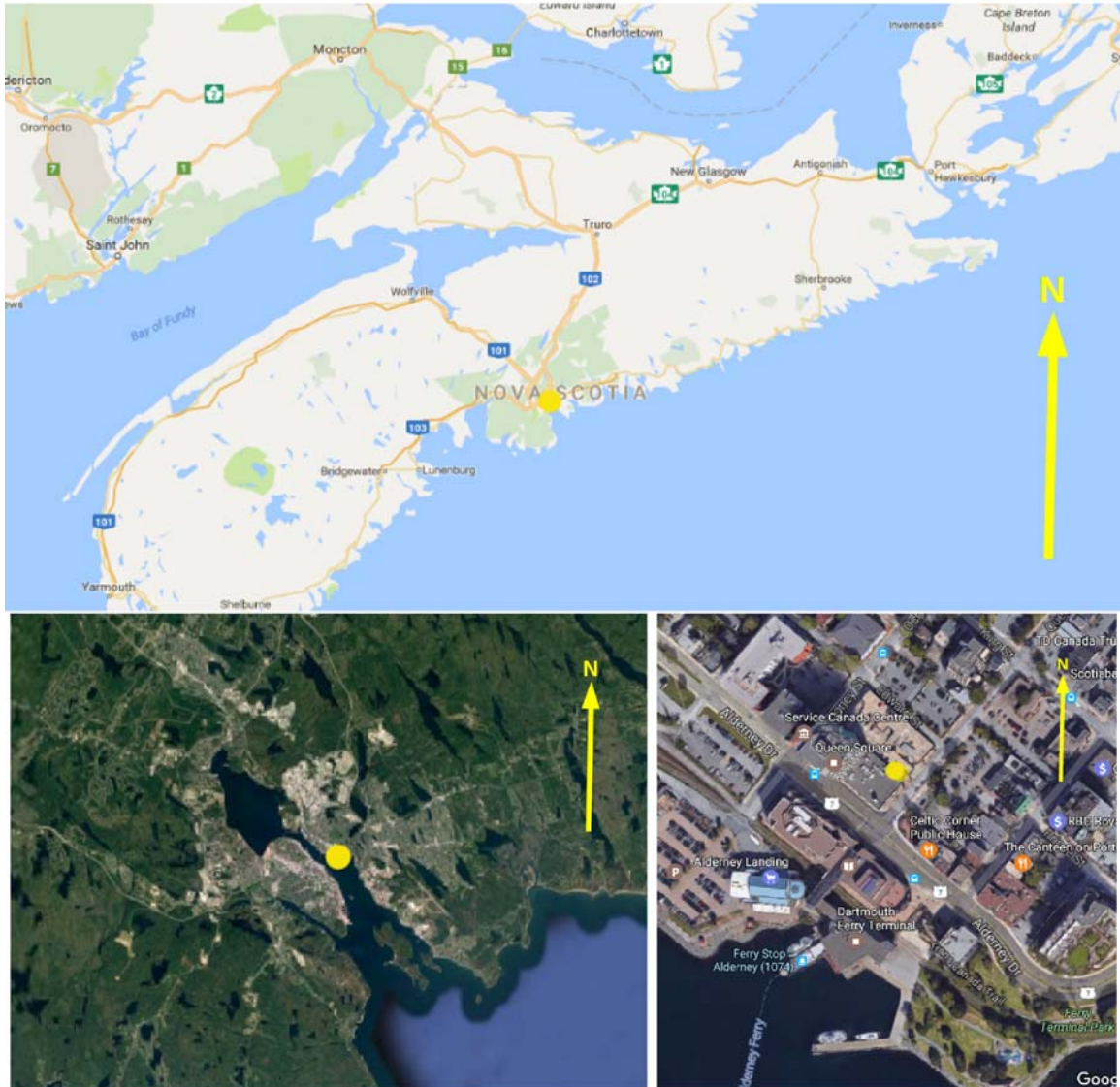


Figure 2.1: Location of the measurement site in Dartmouth, NS. The yellow dots mark the approximate location (Images from Google Earth).

2.3 Instrumentation

2.3.1 Teledyne - API (T-API) T200 NO_x Analyser

The Teledyne - Advanced Pollution Instruments (T-API) T200 NO_x analyser uses a heated MoO converter and CL detection, as described in Section 1.9. The manufacturer's key specifications are in Table 2.1. Two T200s were used during the measurement campaign. T200 s/n 208 replaced s/n 2165 late May 2016 in order that s/n 2165 could undergo annual maintenance. Once the annual maintenance was completed on 2165 and it was allowed to run on ambient air for a few weeks, it was put back into service, and s/n 208 was withdrawn for its own annual maintenance period. T200 s/n 2165 came with the ambient Z/S (zero/span) option, allowing calibration gas to be supplied to the instrument without modifying the sample inlet stream. Calibration gas could be introduced to the instrument by selecting the ambient zero or ambient span option with instrument controls. These controls switched internal valves from taking gas from the sample inlet path to the zero or span gas paths. T200 s/n 208 required substituting the sample inlet line with the calibration gas line, as it did not have the ambient Z/S option. All T200s were operated with the measurement range of 0-200 ppbv. Figure 2.2 shows the instruments as used at the measurement site.

2.3.2 T-API T200 Modified for NO_y

T-API T200 s/n 680 was modified in order to use it as an NO_y analyser by the remote location of the MoO converter outdoors to the area of the sample inlet. The converter was installed in a weatherproof enclosure, along with a Cole-Parmer part number 01540-17 15 psi 12 VDC three-way solenoid valve used to switch from ambient sampling to a calibration gas stream. Figure 2.4 shows the external box with the sample/calibration valve and remotely located MoO converter. Switching from ambient air to calibration gas was accomplished by a relay on a PiFace Digital board attached to the GPIO header of a Raspberry Pi model B SoC single board computer. The PiFace Digital board was connected to the T700U calibrator digital out #1, and is shown in Figure 2.3. The calibrator was programmed with a number of calibration sequences, including zero air and 160 ppbv NO, which set the onboard digital output



Figure 2.2: Instrument rack, measurement site in Dartmouth, Nova Scotia

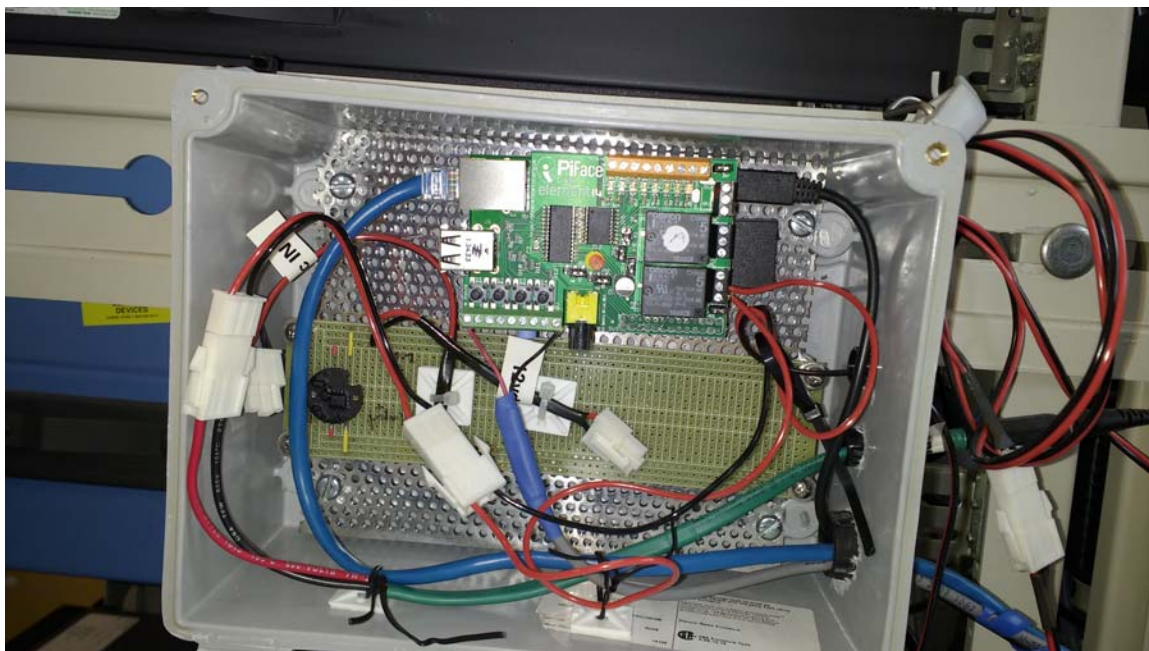


Figure 2.3: Calibration valve control; the PiFace Digital board mounted on a Raspberry Pi model B

(DO) #1 to high. A simple program written in Python 3 listened to the PiFace board for the digital input (DI) connected to DO #1 on the T700U. When the DI went high, a relay inline with the power source of the solenoid valve was closed, opening the NC path of the solenoid valve and allowing calibration gas from the T700U to flow in place of the ambient sample stream of the NO_y modified T200. The Python program also logged the changing state of the calibration valve. The program can be found at Appendix A. This modification allows for a short pathlength for the sample before reaching the MoO converter, ensuring little adsorption of HNO_3 in the sample line. The Raspberry Pi was connected to the lab LAN via wired Ethernet connections.

The inlet for the modified T200 consisted of a inline 47 mm PTFE filter holder without a filter in place, a short length of 1/4" FEP tubing, the three way calibration valve, another short piece of tubing, the MoO converter, another PTFE 47 mm filter holder with a 47 mm 1 micron PTFE filter (Savilex) to protect the instrument from any remaining particulates, and additional tubing of approximately 10 m to carry the converted NO_y sample to the analyser. The filter holder at the inlet was used as a weather shield and a screen for insects and coarse debris, as the 47 mm filter

included a sub-millimetre PTFE grid. The total pathology from inlet to converter was longer than the 10 cm as suggested in Section 1.10.1, and the increase in the converter temperature was somewhat conservative. While these factors may suggest that not all HNO_3 may have been available for conversion, and the conservative increase in the MoO converter may not have allowed quantitative conversion for some other NO_y species, it is believed the error introduced was minimal, and the benefits of the design compromises (easy access in the inlet shelter, and not overheating the converter) were justified.

The temperature of the MoO converter was increased to 330°C over the usual 315°C . This was done in order to achieve a more complete conversion of various species to NO. An Ozone Solutions model ODS-1 inline ozone scrubber was placed in the exhaust stream, as the usual scrubber was removed from the pneumatic stream in these modifications. The usual external pump was also replaced by a KNF model PU425-N026.3-8.90 pump with PTFE internals. This was done to ensure pump longevity in case ozone generated in the instrument was not completely removed by the inline ozone scrubber. These modifications were based on the suggestions and diagrams from Dr. Cris Mihele, Science and Technology Branch, ECCC, Downsview, Ontario. They are largely to ensure the best possible capture and conversion of HNO_3 . They were provided by Dr. Mihele based on modifications he has used in the past for a similar instrument from another manufacturer. The NO_y modified T200 s/n 680 was also placed in NO_x only measurement mode, which is to say that it did not alternate between NO and NO_x (modified for NO_y) channels, but measured only the NO_y channel, on a continuous basis.

	T200	T500U
Range used	200 ppb	200 ppb
Sample Flow Rate	0.5 LPM $\pm 10\%$	0.9 LPM $\pm 10\%$
Lag Time	20 s	not given
Rise/Fall Time	< 60 sec to 95%	< 30 sec to 95%
LDL	0.4 ppb	< 40 ppt
Zero Noise	< 0.2 ppb (RMS)	< 20 ppt (RMS)
Span Noise	< 0.5% of reading above 50 ppb	< 0.2% of reading plus 20 ppt
Precision	0.5% above 50 ppb	0.5% of reading above 5 ppb
Linearity	1% of full scale	< 1% of full scale

Table 2.1: Instrument Specifications. Note that Lag Time of the NO_y modified T200 was reduced as it was set to measure only one channel.

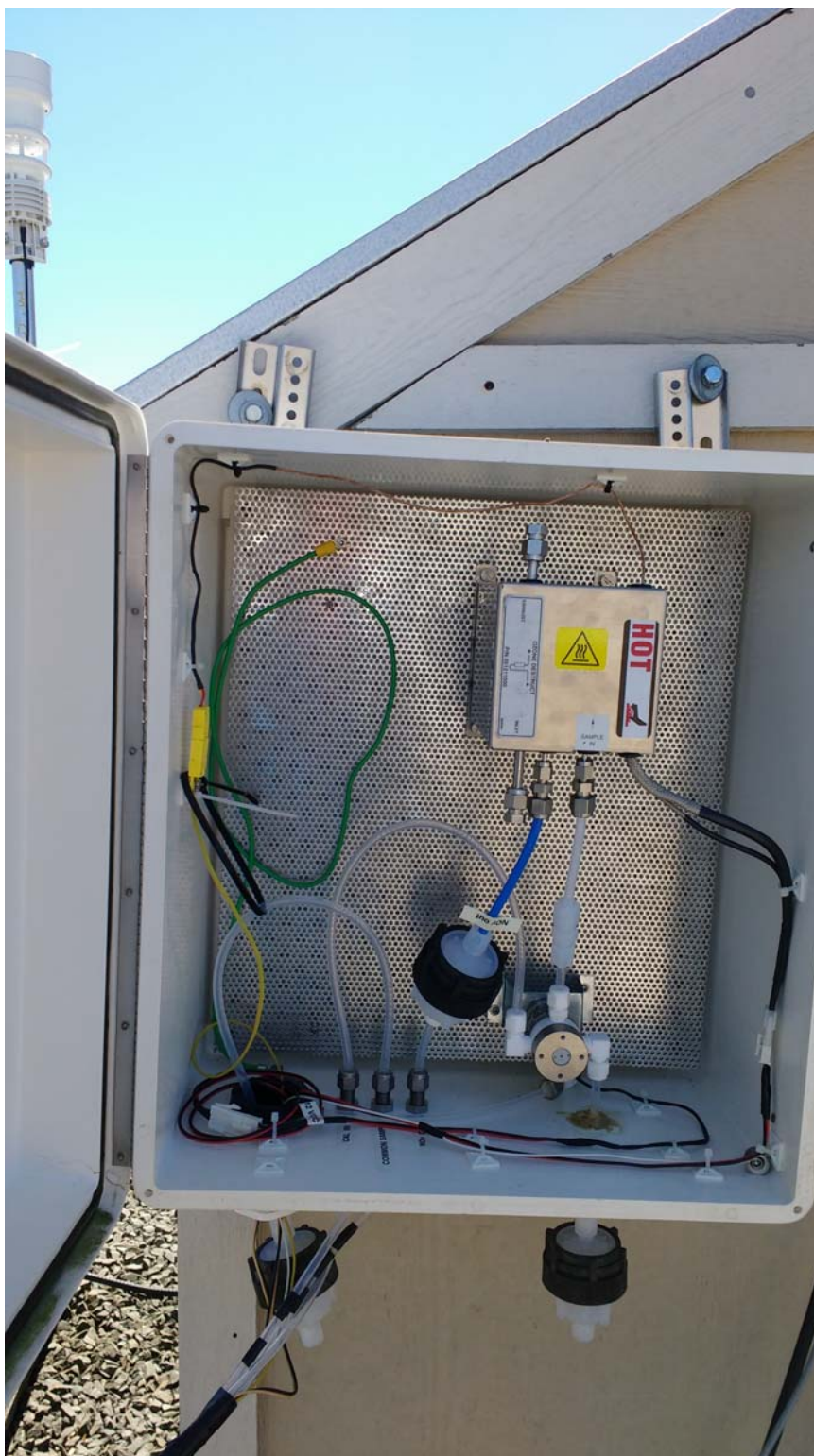


Figure 2.4: External shelter with the relocated MoO converter, sample / calibration gas selection valve, and post-converter particulate filter.

2.3.3 T-API T500U NO₂ Analyser

The T-API T500U is an NO₂ analyser using the CAPS method as detailed in Chapter 1. Key instrument specifications are found in Table 2.1. The T500U came with the ambient Z/S option, as described for the T200 above.

2.3.4 Sample Inlet and Sampling System

The original sample and inlet system consisted of two separate inlets. Sampling for the T500U and T200 occurred through a single line in a "candy-cane" configuration, leading to a glass manifold in the lab via thin walled 3/8" FEP tubing. The second inlet was for the NO_y modified T200, and is described in Subsection 2.3.1. The candy-cane inlet was located about 3 m above the roof surface, while the NO_z inlet was at the bottom of the exterior shelter, approximately 1.5 m above the roof. At the end of August 2016, the equipment on the roof was required to be removed for roof maintenance. At this point the NO_y inlet shelter box was moved down off the roof and onto a fence on the upper level of the building parking structure, with the inlet about 2 m from the surface. The inlet for the regular T200 and T500U were also relocated to the shelter box at this time, using 1/4" FEP tubing to the glass manifold.

2.4 Calibration

Calibrations were conducted by a T-API T700U dynamic dilution calibrator, T-API 701H zero air generator, and calibration (span) gas provided by NAPS. NO₂ for calibrating the T500U was generated via gas phase titration (GPT) of excess NO from the NAPS calibration gas and ozone as generated by the T700U O₃ generator in the desired NO₂ concentration.

All instruments were calibrated at the beginning of the measurement campaign. They were then checked for both zero and span accuracy at approximately one month intervals. Instruments were first checked for zero and calibrated if the zero was outside of \pm the LDL. Each was then checked for span at 80% of full range. If the span drift was near or above 5%, the span was calibrated. It has been found by the author during other work that changing the span slope on a T200 usually

necessitates a re-zeroing of the instrument. The manufacturer's manual does not show this as necessary. However, previous experience shows this to be so. As such, if a change was necessary to the span slope, the T200 in question was zeroed again. This did not prove to be necessary for the T500U. Instruments were also checked for linearity at regular intervals (every two or three months) via a multipoint span check. All instruments remained linear throughout the measurement campaign. The MoO converters were checked for efficiency after the measurement campaign was concluded. They remained within manufacturer's specification.

2.4.1 T-API T700U Dynamic Dilution Calibrator

The calibrator used for the duration of the measurement campaign was a T-API T700U dynamic dilution calibrator. The calibrator was itself calibrated by NAPS at the River Road facility in Ottawa, Ontario, Canada. The calibration certificates are shown in Appendix B. The T700U had an additional span gas MFC rated for $1\text{-}10\text{ cc}^3\text{ min}^{-1}$. However, as that MFC was not calibrated by NAPS, and was found to not be in agreement with the main span MFC, low concentration calibrations with the $0\text{-}10\text{ cc}^3\text{ min}^{-1}$ MFC were not done. The calibrator precision was $\pm 1\%$ per MFC (one each for span gas and zero air/dilutant). It was capable of providing up to 10 L min^{-1} total gas. However, calibration and zero gas was provided at 9 L min^{-1} for all audits and calibrations. The T700U provides gas from a manifold which is vented to the outside in order that gas is supplied at ambient pressures. Gas was supplied to the manifold in excess of the total draw of all instruments being calibrated in order to ensure the gas drawn for calibrations was at ambient pressure and only gas as supplied by the calibrator was sampled by the instruments, without drawing in outside air through the manifold vent.

2.4.2 T-API 701H Zero Air Generator

The T-API 701H zero air generator output pressure was set to 30 psi. It was capable of supplying up to 20 L min^{-1} of dry zero air. The generator included O_3 and NO_x scrubbers, as well as a catalytic CO and hydrocarbon scrubber. It was operated as per the manufacturer's directions, including routine maintenance. It was found that after replacing the O_3 and NO_x scrubbing chemicals, the generator needed to be run

for up to 5 days before the generator could provide air at the minimum dew point of -16°C . This was in excess of the manufacturer's documentation.

2.4.3 Calibration Gas

The calibration gas was supplied by NAPS. The calibration gas Certificate of Analysis is found in Appendix B. The NO and CO in the mixture were calibrated against a NIST primary standard. NO₂ for calibration of the T500U and conversion efficiency checks of the MoO converters was provided by gas-phase titration (GPT) of NO with O₃ as provided by the T700U calibrator. The O₃ generator certification is also found in Appendix B. NO was provided in excess (at least 10%), with the concentration of O₃ determining the concentration of NO₂ provided by the calibrator.

2.4.4 T-API T300U CO Analyser and Thermo Scientific 49i Ozone Analyser

A T-API T300U was used to measure CO. A Thermo 49i was used to measure O₃. Both instruments were removed from service at the end of August. This was necessitated by roof maintenance requiring the removal of the sample inlet (candy-cane) used by these instruments. It was decided not to relocate the candy-cane during this roof maintenance period. Specifications for the instruments are found in Table 2.2.

	T300U	49i
Range used	2000 ppb	200 ppb
Sample Flow Rate	1800 cc/min $\pm 20\%$	1.5 LPM $\pm 10\%$
Lag Time	10 s	10 s
Rise/Fall Time	< 60 sec to 95%	20 s
LDL	< 20 ppb	1.0 ppb
Zero Noise	< 10 ppb (RMS)	0.25 ppb (RMS) for 60 s average time
Span Noise	< 0.5% of reading above 2.5 ppmb	not given
Precision	0.5% of reading	not given
Linearity	1% of full scale	$\pm 1\%$ of full scale

Table 2.2: Specifications for the T300U and 49i.

2.5 Data Collection

2.5.1 DR DAS Envidas Ultimate Software and PC

Instrument data collection was done with the Envidas Ultimate software package running on an Advantec 510 industrial PC chassis running the Windows 7 Professional operating system. The system was supplied by the Dr. DAS company, located in the USA. The system was originally running the Windows XP operation system. It was upgraded to Windows 7 prior to the measurement campaign. The computer chassis included a Moxa brand PCI serial port expansion board that provided an additional 8 9-pin RS-232 serial ports. Data was collected by the software via RS-232 approximately every 300 ms. The software package then stored data for 1-minute averages, and from the 1-minute data calculated and stored 15, 60 and 180 minute averages on demand. All gas instruments were also connected to the lab LAN via Ethernet. The Ethernet connections were used with the relevant manufacturers' software for instrument control where direct access to the instrument control panels was less practical than at the computer.

2.5.2 Meteorological Data

The meteorological data used was largely from a nearby MSC automatic surface weather station, with solar radiation from a Davis Vantage Pro II system located at the measurement site. The Davis was removed from service at the end of August, as there was work to be done on the roof where the measurement site was located. As such, comparison of temperature, relative humidity, and station pressure were made between the Davis and the MSC station (AAW) for the period in which data were available for both. The R package "lmodel2" was used with the following script:

```
## merge met date
MET <- merge(aaw_utc, hr_qs_met, by="date")

## comparisons - type met_comp_VAR or
## plot.met_com_VAR to see

met_comp_t <- lmodel2(outTemp ~ T, data = MET,
```

```

'interval', 'interval', 99)
met_comp_p <- lmodel2(pressure ~ stn_p, data = MET,
'relative', 'relative', 99)
met_comp_rh <- lmodel2(outHumidity ~ rh, data = MET,
'relative', 'relative', 99)

```

Standard Major Axis results are reported in Table 2.3. For temperature, range.y and range.x were set to "interval". For the pressure and relative humidity, range.y and range.x were set to "relative". Permutations were set to 99 for all tests. Type 2 regression was chosen to account for errors in both sets of meteorological sensors.

Given that the slopes for all three compared values were near 1, and the R^2 values were high, it was decided to take the AAW values for the entire measurement period. This allowed for these values to be available for the duration of the measurement period without possibly introducing a step function by switching data sources part way through the measurement campaign.

Data was collected from the Davis datalogger by a Raspberry Pi model B using WeeWX software [Keffer, 2016]. The WeeWX software package stored data collected in an SQLite database. The Raspberry Pi used for collecting the meteorological data from the Davis was also fitted with a temperature compensated crystal oscillator (TCXO) real-time clock (RTC) with battery backup. This was necessary as Raspberry Pis do not come with a real-time clock, unlike most PCs. Rather, Raspberry Pis use emulation of a system clock and time data from the internet. The addition of a RTC ensured that data collected was stored with an accurate time stamp, independent of internet connectivity, as shown in Figure 2.5.

	Value	f(x)	R^2
Temperature ($^{\circ}\text{C}$)		$1.03(T) + 0.2$	0.98
Relative Humidity (%)		$0.97(\text{rh}) + 5.0$	0.96
Station Pressure (hPa)		$1.00(p) - 1.8$	1.00

Table 2.3: Comparison of selected meteorological values between the MSC surface station AAW and the Davis station co-located at the measurement site. AAW was taken as the independent variable for the comparison.

The surface weather station is the automatic station located near the main gate of CFB Shearwater, approximately 6 km south of the measurement site. It is known by

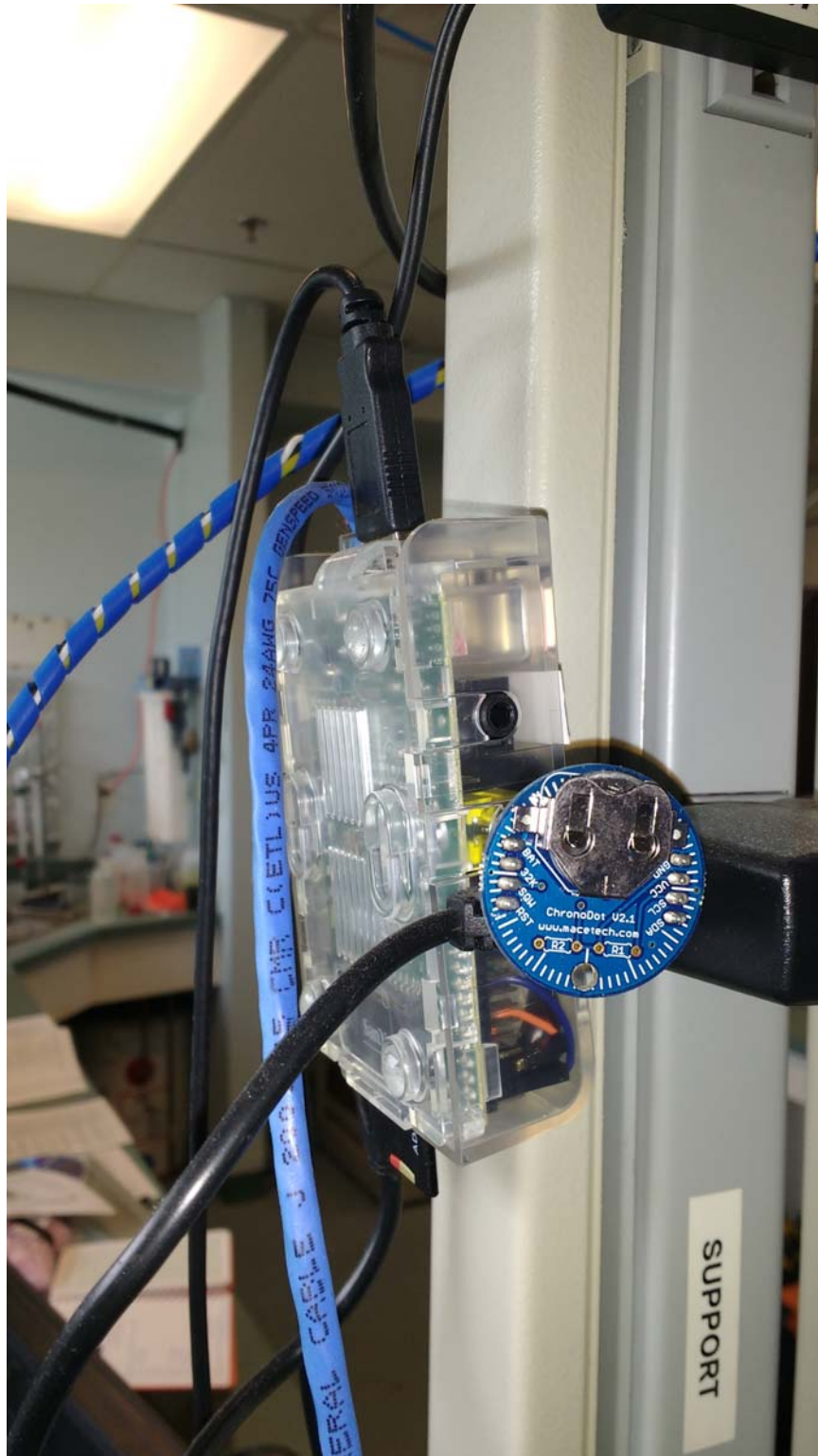


Figure 2.5: The Raspberry Pi model B used to collect data from the Davis Vantage Pro II weather station, with external TCXO real-time clock.

the Transport Canada (TC) identifier AAW. There is also a human observer program at Shearwater (TC identification YAW), but it is only active during Canadian Forces flying operations from Shearwater. Hence, the autostation was chosen as it provided continuous data. The immediate vicinity of office towers and other multistory buildings around the measurement site made local wind measurements from the Davis largely meaningless. Therefore, the wind direction and speed were taken from AAW as well as the temperature, relative humidity and station pressure as noted above. As such, the only meteorological factor taken from the Davis was solar radiation.

2.5.3 Data Preparation

The QA processes allowed for fairly simple data preparation and processing. The calibrations and maintenance processes are documented elsewhere in this Chapter. Calibration certificates are shown in Appendix B. Once the data was collected, diagnostic values and digital statuses were examined for each of the instruments. Data that were associated with instrument errors were removed. Data for the twelve hours following significant maintenance or extended downtime were also removed. The instrument manufacturer's recommendation were shorter than twelve hours. However, in the author's experience during previous work an extended period to allow for thermal equilibrium within the instruments, and additional time for autoreference and autozero measurements ensured high-quality data. Data were then corrected between audits / calibrations where zero and/or span drift exceeded the limits set for this work (\pm LDL for zero drift, \pm 5% for span drift). Drift was assumed to be linear, and corrected as such. However, limited data was subjected to this correction, as most audits showed drift to be within the limits set. The meteorological data was then added to the dataset. Data from known weekly generator tests for backup generators located near the sample inlets were then removed. These tests were just after 14:00 UTC on Wednesdays and 13:00 UTC on Thursdays. Data pairs missing either NO₂ value, or both, were then stripped from the dataset. The data were then subsetted by removing the first and 99th percentile of the T500U NO₂ values. All datapoints with NO or NO_x below the lower detection limit of the T200, that being 0.4 ppbv, were then removed. This left 2692 hourly data points of a possible 4416 hours in May to October 2016, or 61% of the total possible values. Eight of the 39% of values excluded

were for reasons other than being below detection limits for the T200.

2.6 Data Analysis

2.6.1 R and the OpenAir Package

Data analyses were conducted using R version 3.3.0 [R Core Team, 2017] within RStudio version 0.1.2. Normalisation, autocorrelation function analysis, linear regressions, Wilcoxon Sign-Ranked Tests and Spearman correlations were conducted either through the base R package or one of the statistical packages available. AQ analyses, such as pollutant roses, time variation plots, etc., were completed with the OpenAir package from King's College, London [Carslaw and Ropkins, 2012]. Other R packages used included Hmisc, ggplot2, reshape, and stats. The package xtables was used for some automation of Table generation from R into LaTeX (used to prepare this document). The OpenAir polarPlot function was used to produce a series of polar plots of various measurements and calculated values. The polar coordinates are wind speed and direction. The plots were prepared by the following script in R, using the OpenAir [Carslaw and Ropkins, 2012] package function polarPlot. An example R script for the polar plots:

```
polarPlot(noz_data, pollutant = c("no", "no2"),
  statistic = "median",
  force.positive = FALSE,
  min.bin = 2,
  units = "m/s",
  strip = FALSE,
  key.footer = expression('NO, NO'[2]),
  key.header = 'median, ppbv',
  main = expression('Polar Plot for NO, NO'[2]))
```

Min.bins was set to two versus the default one in order to require at least two data points for each wind speed / direction bin. The exception was for the subset dataset for large NO₂(T200)/NO₂ ratios developed during data analysis. There were insufficient data points to develop a polar plot unless min.bin = 1. The specific headers and plotted pollutants were changed as necessary.

2.6.2 Statistical and Other Methods

The initial approach was to apply linear regressions to NO_2 (independent variable) and $\text{NO}_2(\text{T200})$ (dependant) by month, after applying Log_{10} transforms, assessing normality of the transformed data, autocorrelation analysis and averaging at the decorrelation point. As AQ data is not normally considered parametric, non-parametric methods were then explored. The Wilcoxon Signed-Rank test was applied to the NO_2 and $\text{NO}_2(\text{T200})$ pairs for the data by month and for the complete dataset. Spearman correlations were then applied to months that were determined to have non-zero NO_z interference. These determinations were made on the basis of the summary statistics (monthly medians) and the results of the Wilcoxon Signed-Rank testing by month. Polar and Time Variation plots of NO , NO_2 , NO_x , NO_z interference, and other selected measurements were also prepared.

Chapter 3

Results and Discussion

3.1 Estimation of Experimental Error

The assessed sources of error are as follows:

1. Calibrator Mass Flow Controllers - 1% for each MFC used = 2%
2. Span Gas certification - 2%
3. T200 Instrument Span Noise - 1%
4. Instrument Calibration Tolerance - 5%

Instrument span noise and instrument calibration tolerance were considered to be dependant, and were summed. The same approach was chosen for the two MFCs of the calibrator (remembering that the third trace level MFC was not previously calibrated, and was therefore not used).

The Calibrator MFCs are as per the manufacturer's documentation. Errors for the MFCs are not independent, as both the dilutant/zero air and span gas MFCs are in use for anything other than zero checks and calibrations. The errors for each MFC are therefore considered as additive. Span noise and the recalibration threshold are considered in the same manner. The span gas error is from the calibration certificate from NAPS, the supplier of the span gas. The error for the T200 is believed to be dominant over that of the T500U, given that the T500U's LDL and zero noise are an order of magnitude below that of the T200, and the span noise is one fifth that of the T200. Therefore, the error introduced by the T500U was discounted. Had it been necessary, drift corrections would have been applied to the T500U data as they were for the T200s. However, drift of zero (LDL) and span ($\pm 5\%$) values for the T500U remained below the chosen correction thresholds for both zero and span drift between every calibration audit.

The instrument calibration tolerance value is an arbitrary value chosen at the start of the measurement campaign, as discussed in Section 2.1. When instrument audits found significantly less than 5% span drift, the span calibration was left as found. This was felt to be a good compromise between data that did not require correction and conducting data collection in a similar manner to a standard monitoring site in which recalibration is not mandatory until 15% drift [Environment Canada, 2010a]. The same was true of zero drift, in that instruments showing well below \pm LDL in zero drift were left as found.

Adding these grouped errors in quadrature (see equation 3.1), as the groups were assessed to be independent, results in an estimated error of $\pm 8\%$.

$$\Delta NO_2 = \sqrt{\sum_{i=1}^n (\delta x_i)^2} = 8\% \quad (3.1)$$

Zero noise was also considered. The published zero noise for the T-API T200 is 0.2 ppbv RMS (root mean square). For low concentrations of NO_x ($NO_x < 1$), the span noise and zero drift become dominant over other error sources. The data must be considered with this in mind. As such, the estimated error for these data is $\pm 8\%$ of the measured value and ± 0.4 ppbv. For values below 1 ppbv, the ± 0.4 ppbv will dominate over the 8% portion of estimated error. The exception are data from the T500U. The T500U zero noise is an order of magnitude below that of the T200 series. It is expected that for the T500U data only, the $\pm 8\%$ estimated experimental error will dominate.

Subsetting the data such that T200 NO_x values were greater than 1 ppbv was tried. This was done to try and eliminate low concentration values and their associated large uncertainties. However, it was found that the dataset was then 45% of the original available data. This large of an exclusion was rejected. The following data summaries and analysis use the non-zero data set as described in Chapter 2, unless specifically stated.

3.2 Summary of Measured Species and Meteorological Data

Data summaries for chemical and meteorological data are presented in Tables 3.1 and 3.4.

3.2.1 Summary of Chemical Species

Table 3.1 summarises the chemical species measured and calculated. The number of missing values for CO and O₃ are largely due to those instruments being taken off-line as a result of being required to move equipment from the original roof location. See Chapter 2 for details. These are summarised from the developed dataset as laid out in Subsection 2.5.3. Four values are calculated, as shown. In this Section, NO₂ refers to NO₂ concentrations measured by the T500U, and accepted as true NO₂ values, and NO₂(T200) are those values measured by the MoO/CL T200 instrument, and are therefore subject to NO_z interference. Table 3.2 summarises the median and interquartile range of key species by month. It corresponds to figures 3.1 and 3.3 (left hand plot).

$$NO_z \text{ Interference} = NO_2(T200) - NO_2$$

$$NO_z = NO_y - (NO + NO_2)$$

$$NO_x = NO + NO_2$$

$$NO/NO_x = NO/(NO + NO_2)$$

	CO	NO ₂	NO	NO ₂ (T200)	NO _x	NO _y	O ₃	NO _z	NO _z Int	NO/NO _x	NO ₂ (T200)/NO ₂
Min	37	0.5	0.4	BDL	0.7	-0.5	0.5	-56.1	-5.7	0.026	0.25
1st Quartile	116	3.2	0.9	3.2	4.5	4.2	16.8	-1.0	-0.2	0.19	0.96
Median	139	5.5	1.9	5.6	7.9	7.5	23.0	-0.1	0.1	0.29	1.01
3rd Quartile	166	9.0	3.7	9.2	13.0	12.3	29.5	0.4	0.4	0.38	1.07
Max	454	20.2	92.4	52.7	129	174	51.3	96.3	42.2	0.87	5.02
NA's	908					36	889	36			

Table 3.1: Summary of NO_y chemical species data; n =2692. All units are ppbv, less NO/NO_x ratio and NO₂(T200)/NO₂.

Table 3.3 shows the summary climatological statistics for the weather station at Shearwater. This station is approximately 6 km south of the measurement site. Note

	NO ₂	NO	NO ₂ (T200)	NO _z Int	NO/NO _x
May	4.8 (2.9, 8.2)	1.8 (1.0, 3.4)	5.1 (3.0, 8.9)	0.3 (0.1, 0.8)	0.30 (0.22, 0.38)
June	5.8 (3.3, 8.5)	2.2 (1.1, 4.4)	5.7 (3.4, 8.3)	0.0 (-0.1, 0.2)	0.31 (0.21, 0.39)
July	6.4 (3.7, 10.3)	2.1 (1.0, 4.0)	6.5 (3.6, 10.3)	0.0 (-0.3, 0.2)	0.29 (0.19, 0.38)
August	3.9 (2.5, 6.3)	1.7 (0.8, 3.4)	3.9 (2.3, 6.8)	-0.1 (-0.2, 0.2)	0.33 (0.22, 0.42)
September	6.8 (4.2, 10.5)	2.1 (1.0, 4.2)	6.4 (4.0, 10.7)	0.0 (-0.3, 0.3)	0.25 (0.18, 0.36)
October	6.2 (3.7, 9.5)	1.5 (0.8, 3.1)	6.4 (3.7, 10.1)	0.2 (0.0, 0.6)	0.23 (0.15, 0.33)

Table 3.2: Summary of median (interquartile range) NO₂, NO and NO_z interference by month. All units are ppbv.

	Jan	Feb	Mar	Apr	May	Jun	Jul	Aug	Sep	Oct	Nov	Dec	Year
Temperature (°C)													
Daily Average	-4.6	-4.2	-0.7	4.3	9.2	14.3	18.1	18.5	15.1	9.6	4.5	-1.0	6.9
Daily Maximum	-0.3	0.2	3.3	8.3	13.6	18.8	22.4	22.6	19.4	13.6	8.1	2.9	11.1
Daily Minimum	-9.0	-8.6	-4.7	0.2	4.8	9.8	13.7	14.3	10.8	5.5	0.9	-5	2.7
Precipitation													
Rainfall (mm)	84.6	69.1	96.9	105.3	118.9	117.9	103.4	91.8	103	130.3	130.2	110	1261.2
Snowfall (cm)	50.5	40.7	31.1	11.9	1.7	0	0	0	0	0.2	10.4	35.2	181.6
Wind													
Speed (km/h)	17.9	18	17.5	16.8	14	12.6	11	10.9	12.6	14.9	16.7	17.7	15.1
Most Frequent Direction	W	NW	N	N	S	S	S	S	SW	W	W	W	W
Bright Sunshine													
Total Hours	109.5	127.2	142.8	156.6	193.3	220.7	235.2	226.6	180.5	157.8	107.4	105.2	1962.5
Days with measurable	22.1	21.2	23	22.4	24.2	26.2	27.5	27.5	25.5	25.3	22.5	22.7	289.9
% of possible daylight hours	38.2	43.3	38.7	38.8	42.1	47.5	49.9	52.1	47.9	46.2	37.2	38.2	43.3
Extreme Daily	9.8	10.8	12.6	13.7	15.3	15.1	15.2	14.4	13.0	11.2	10.1	9.0	

Table 3.3: 1981-2000 Climate normals for Shearwater (CYAW) met station.

that the climate normals are for the Shearwater airfield, located several hundred metres to the east and about 20 metres higher than that of the RSC station (AAW) used for the meteorological data in this study, also located at the Shearwater airfield [Environment and Climate Change Canada, 2016].

Figure 3.1 summarise NO and NO₂ values. Figure 3.3 summarises NO_z interference for both the data set and for values of NO_x > 1 ppbv. The box plots are interesting in that there is a 'U' shape to the median NO_z interference values. This may show a seasonal trend in NO_z interference for this location.

Figure 3.2 shows NO_z, NO_x, and NO_y. Interestingly, the first three months show negative median values for the calculated NO_z field. The reason for this could not be fully determined. Before the end of August, the inlets for the T200 and T500U were separated from the inlet for the NO_y modified T200 by several meters, as noted in Chapter 2. The NO_y modified T200 was set to measure the NO_y channel only, not switching between NO and NO_y. As such, increased temporal variation was noted in measured NO_y as compared to NO_x measured by the T200 MoO/CL instrument. This difference in fine scale temporal variation was also noted between the T200 and

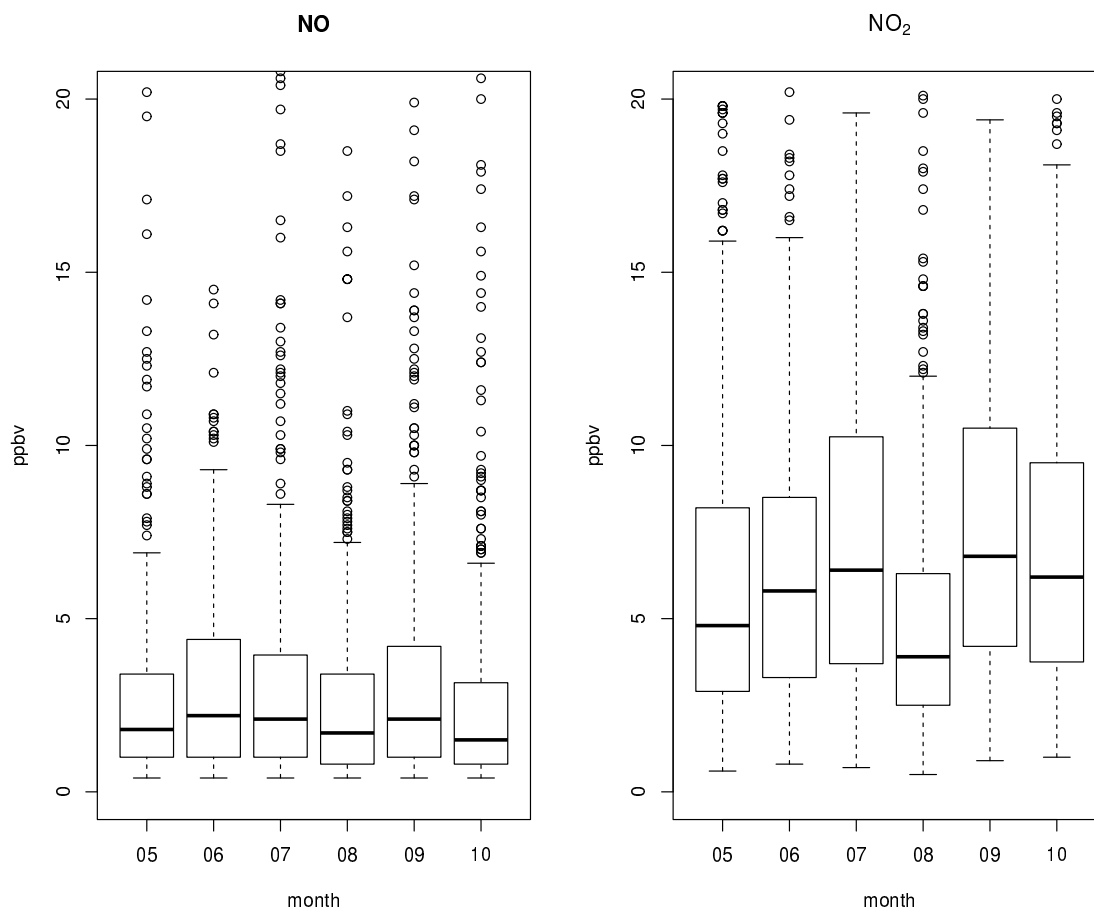


Figure 3.1: Box plots by month for NO and true NO₂; y axis limited to 21 ppbv. The bold lines are medians, boxes for interquartile range, whiskers extend $1.5 \times$ interquartile range, and circles for outliers.

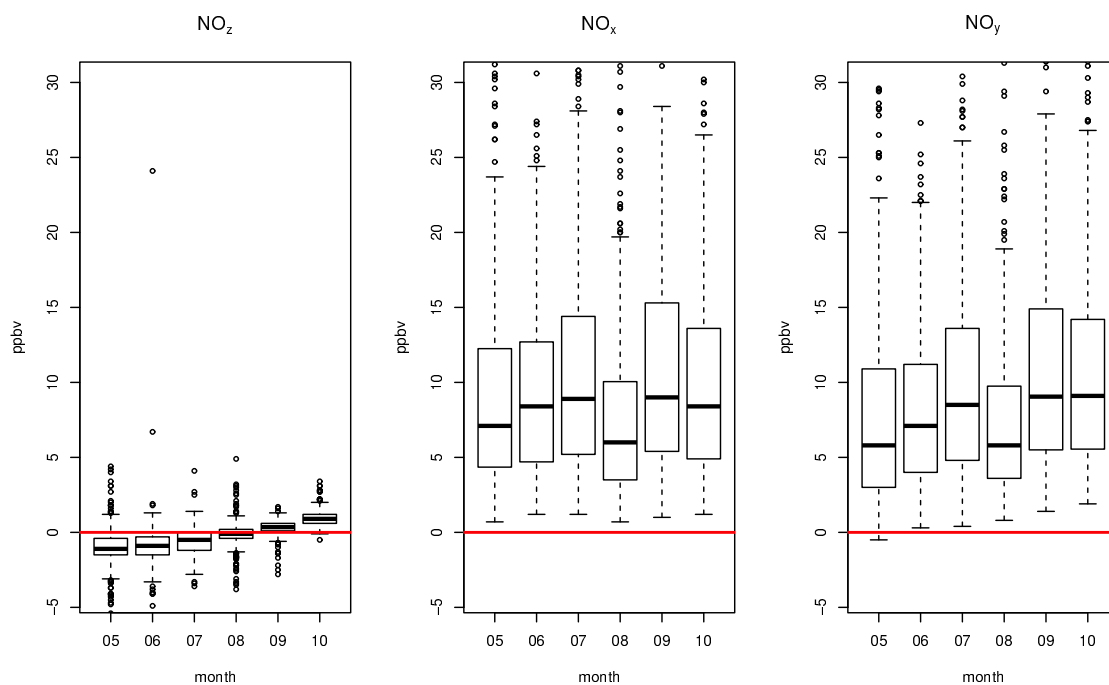


Figure 3.2: Box plots by month for NO_z , NO_x , and NO_y . y axis limited to 30 ppbv. The bold lines are medians, boxes for interquartile range, whiskers extend $1.5 \times$ interquartile range, and circles for outliers.

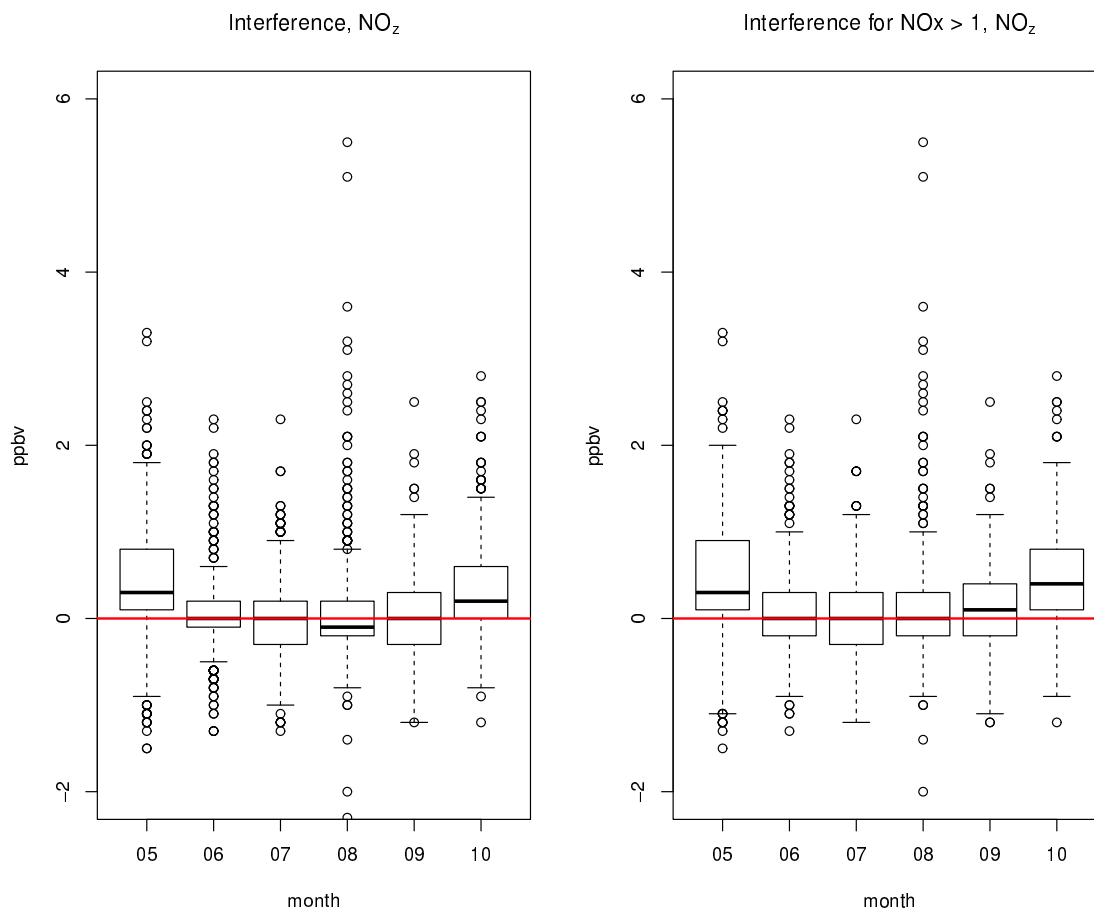


Figure 3.3: Box plots by month for NO_z interference and NO_z interference for data with NO_x > 1 ppbv; y axis limited between -2 to +6 ppbv. The bold lines are medians, boxes for interquartile range, whiskers extend 1.5 × interquartile range, and circles for outliers.

T500U. It is suspected that the smoothing algorithms of the T200 when switching between NO and NO_x channels, coupled with the separation and fine scale spatial variations of local primary source (road motor traffic) NO_x may account for the negative values of NO_z calculated for the first half of the measurement campaign, before the sample inlets were moved. NO_z was calculated using NO_x values as calculated from NO from the T200 and NO₂ from the T500U, followed by the simple subtraction of NO_z = NO_y - NO_x. Trying the NO_x values as measured directly from the T200 (that is to say, using the NO₂ values from the T200 as well as the NO) resulted in insignificant change in the summary statistics for NO_z by month, and was not pursued further.

The size of sample inlet was reduced from 3/8" to 1/4" FEP tubing during the move in late August. This reduced the internal surface area per unit length of sample line, and thus the total area on which HNO₃ could be adsorbed.

As shown in Figure 1.6, HNO₃ is known to adsorb onto glass until the surface is passivated and further adsorption is hindered. However, HNO₃ can also be released from these surface given the right physical conditions. It is possible that the T200 measured HNO₃ released from the glass manifold that had accumulated in the past, and that the NO_y modified T200 would not be able to measure as it sampled directly to the MoO converter, rather than through a longer inlet and glass manifold. As the manifold may have accumulated significant HNO₃ through adsorption, and then release what could be considered and 'integrated sample' in a short period of time, this may account for values of NO_x from the unmodified T200 being significantly higher than those measured by the NO_y modified T200. The same can be said for FEP tubing below 10°C. Also, adsorption appears to increase with humidity. The amount of adsorption that is reversible for FEP and glass have not been quantified, but it has been shown that once warmed (above 20°C), some adsorbed HNO₃ is released, at least in the case of PFA, and presumably other PTFE analogues such as FEP [Neuman et al., 1999]. Examination of the correlation between various meteorological parameters, including absolute humidity, and NO_z shows some negative correlation between temperature, absolute humidity and NO_z. There does not appear to be any correlation between relative humidity and NO_z.

Other unknown factors are likely at play. Despite the negative values of NO_z

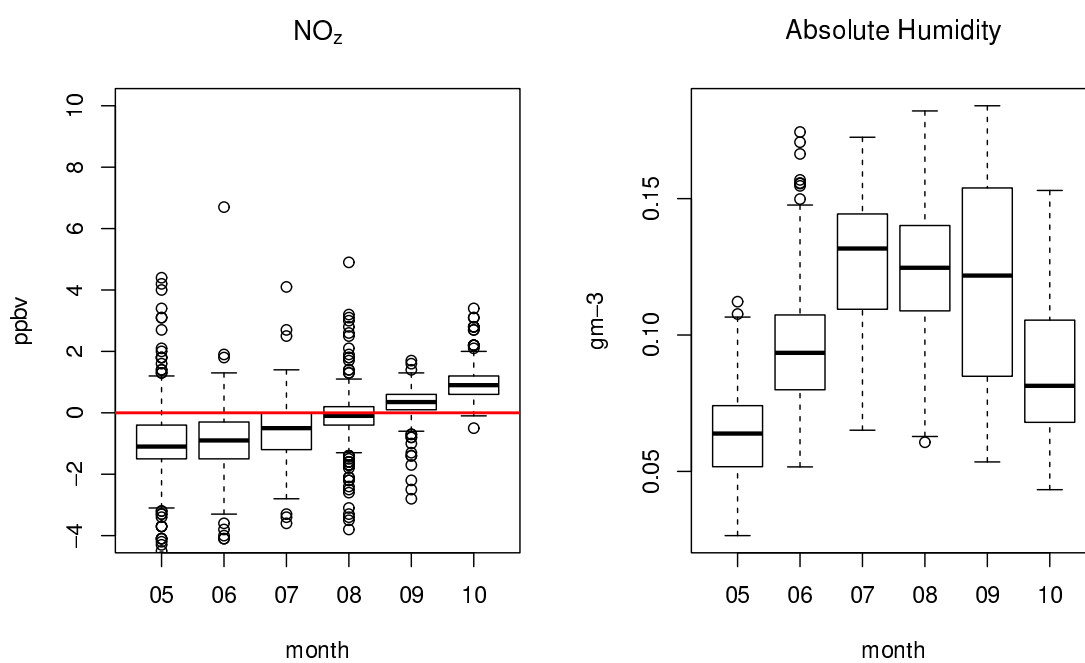


Figure 3.4: Box plots by month for NO_z and absolute humidity. y axis limited to 10 ppbv for NO_z. The bold lines are medians, boxes for interquartile range, whiskers extend $1.5 \times$ interquartile range, and circles for outliers.

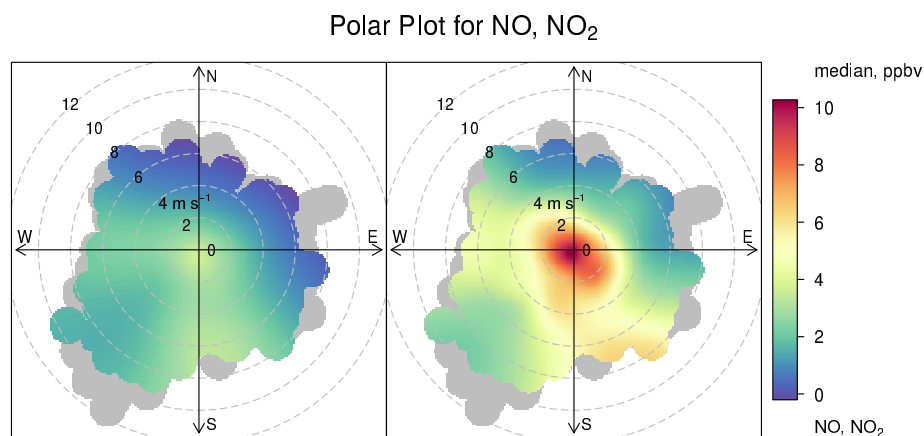


Figure 3.5: Polar plot of median NO and NO₂ values. The polar coordinates are wind speed and direction.

calculated for May, NO_z interference held the the highest median value for NO_z interference by month.

Figure 3.5 is a polar plot of NO and NO₂ median values. The polar coordinates are wind speed and direction. The plot was prepared by the following script in R, using the OpenAir [Carslaw and Ropkins, 2012] package function polarPlot:

```
polarPlot(noz_data, pollutant = c("no", "no2"),
  statistic = "median",
  force.positive = FALSE,
  min.bin = 2,
  units = "m/s",
  strip = FALSE,
  key.footer = expression('NO, NO' [2]),
  key.header = 'median, ppbv',
  main = expression('Polar Plot for NO, NO' [2]))
```

Higher NO₂ concentrations tend to occur when winds are from the west and south. This appears to be true across a variety of wind speeds.

3.2.2 Summary of Meteorological Data

The number of NA's for the Humidex (Hmdx) and Wind Chill (WC) values are unsurprising given the time of year, especially for WC. The number of NAs for Radiation is the result of moving the Davis Vantage Pro 2 station off of the roof along with the CO and O₃ inlet, and the resultant loss of those measurements for the remainder of the measurement campaign. The Shearwater RCS (AAW) does not measure solar radiation. The 18 NAs for the meteorological measurements were for missing station pressure values. As the status of the station for those times could not be determined, all meteorological values for those 18 hours with missing station pressure were excluded from the combined chemistry/meteorology dataset used for subsequent analysis.

	T (°C)	Td (°C)	rh (%)	wd (°True)	ws (ms ⁻¹)	Stn P (hPa)	Hmdx	WC	Radiation (Wm ⁻²)
Min	-0.2	-7.6	23	000	0.0	985.2	25	-1	0.0
1st Quartile	11.4	6.60	65	150	1.7	1007.4	26	-1	0.0
Median	16.4	11.3	80	210	2.8	1012.6	27	-1	105.9
3rd Quartile	19.5	15.6	91	260	4.2	1017.1	29	-1	457.5
Max	28.3	21.2	97	360	11.4	1031.0	34	-1	1128.2
NA's	18	18	18	18	18	18	2235	2691	859

Table 3.4: Summary of meteorological data; N = 2692.

3.2.3 Temporal Variation of Selected Measurements

Figures 3.6, 3.7 and 3.8 summarise the temporal variation of NO_z interference, both NO₂ measurements, and the ratio of NO₂ measured by MoO/CL to true NO₂. The 'U' shaped curve of the monthly values is evident for NO_z interference and the NO₂(T200)/NO₂ ratio. Note the significant decrease in median NO₂ concentrations for the month of August. This may be due to August being a popular vacation month, resulting in lower traffic volumes in the area, and the concomitant reduction in primary NO_x emissions. Looking at the hour of day variation of both the NO₂(T200)/NO₂ ratio and NO_z interference amounts, the highest values are noted in the 03:00 to 06:00 UTC timeframe (00:00 to 03:00 local time). The peak photochemistry period of 15:00 to 18:00 UTC shows some of the lowest interference and NO₂

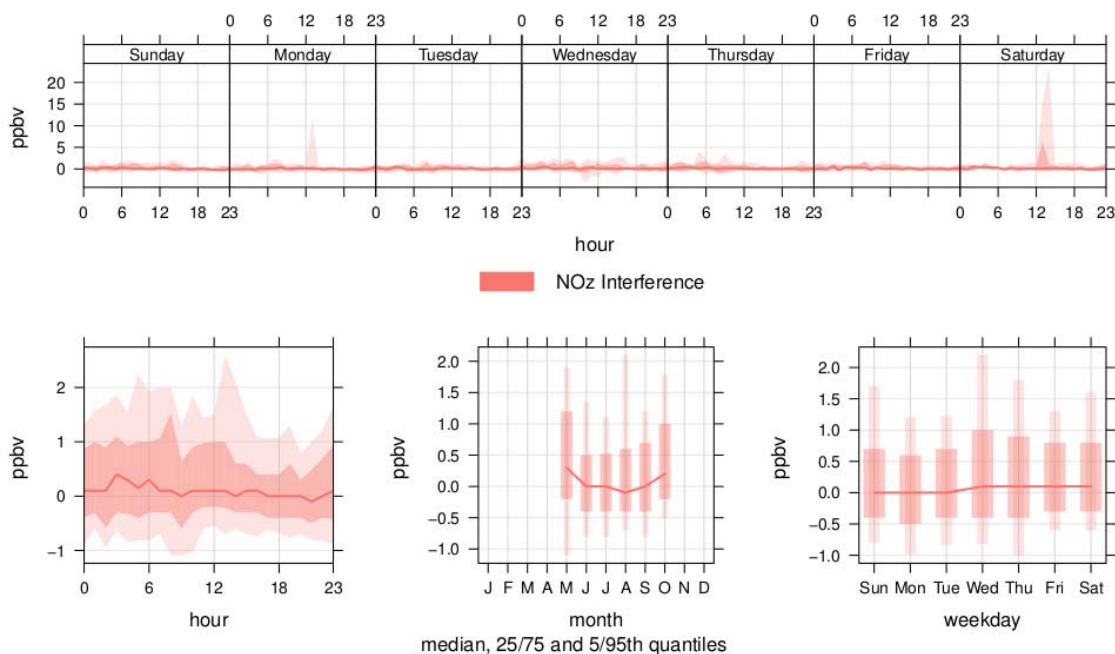


Figure 3.6: Time variation plot for NO_z interference. Note the non-zero median value between 03:00 and 06:00 UTC in the hour plot, lower left (midnight to 3 AM local time).

ratio values. The peaks noted around 13:00 on Saturdays are likely a result of a local backup generator testing. However, unlike the Wednesday and Thursday tests, the Saturday tests are monthly, but not necessarily the same week each month. As there was no way to confirm whether or not a generator test had occurred, these data were not excluded. The Saturday generator tests may also show some NO_z production. Anecdotal observation of real-time data at the measurement site on generator startup showed short duration NO_z spikes. It is not known if this was due to actual NO_z production on an cold diesel engine start, or was caused by some unknown issue in methodology. These spikes were not investigated further.

3.2.4 NO_z Interference Based on Wind Direction and Speed

All data

Figure 3.10 shows a polar plot of median NO_z interference. The polar coordinates are wind speed and direction. The plot was made using the polarPlot function from

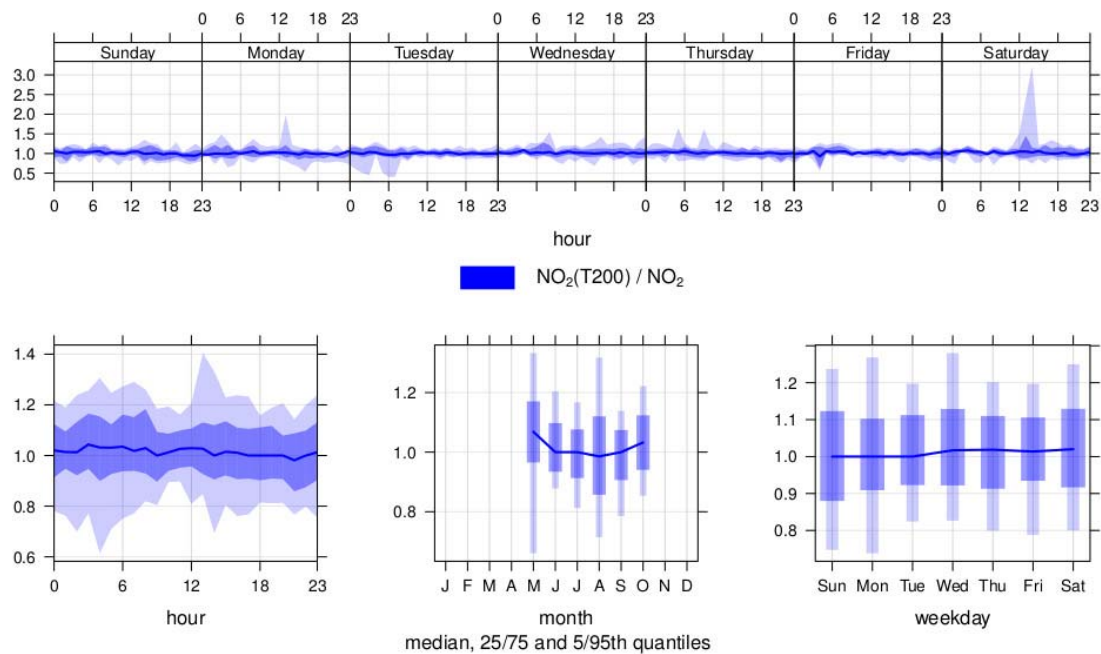


Figure 3.7: Time variation plot for $\text{NO}_2(\text{T200}) / \text{NO}_2$.

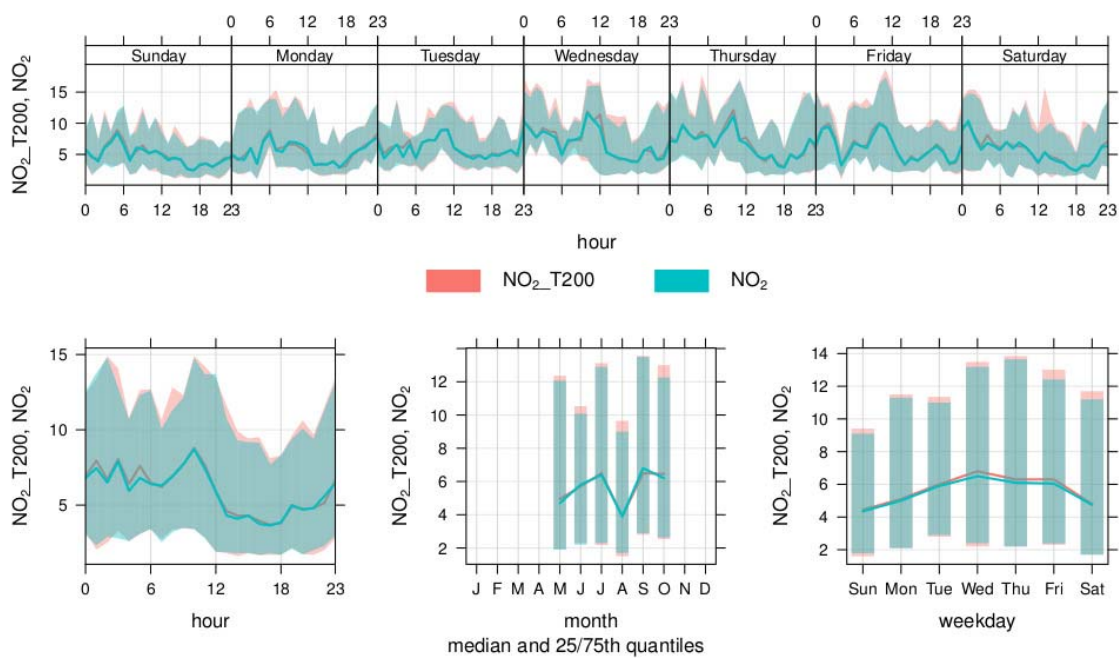


Figure 3.8: Time variation plot for NO_2 as measured by the T200 and T500U.

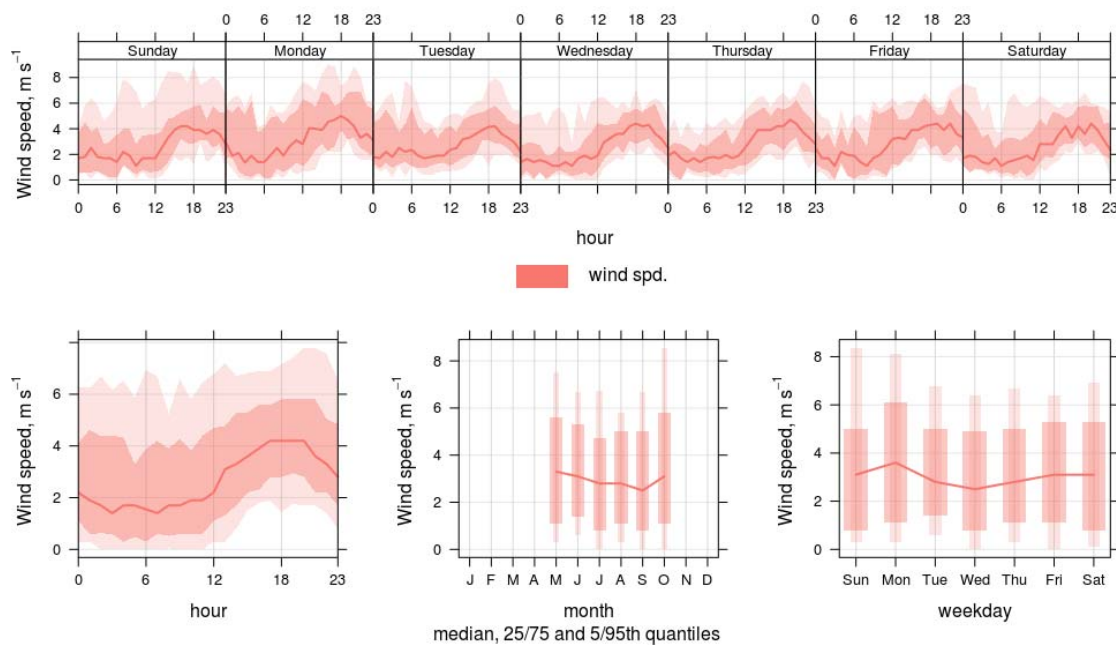


Figure 3.9: Time variation plot for median wind speed. Note the diurnal variation.

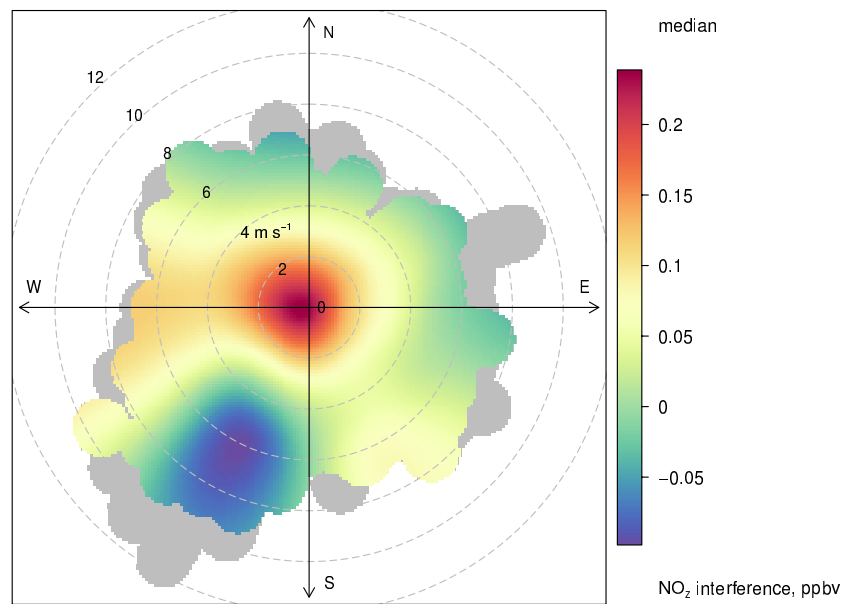


Figure 3.10: Polar plot of median NO_z interference. Polar coordinates are wind speed and direction

the OpenAir package in R, using the following script:

```
polarPlot(noz_data, pollutant = "noz_int",
  statistic = "median",
  force.positive = FALSE,
  min.bin = 2,
  units = "m/s",
  key.footer = expression("NO" [z] * "_interference", _ppbv))
```

Note that min.bin (minimum bins) was set to two rather than the default one. The greyed out parts of Figure 3.10 represent the areas with only one data point per bin, and were thus excluded from the plot interpolation and smoothing. A similar script was used to produce the same polar plot for calculated NO_z values, as shown in Figure 3.11. The highest median level of NO_z interference tends to be associated with low wind conditions and, to a lesser extent, westerly winds. The westerly component shows interference across wind all wind speeds, suggesting multiple sources. The peak for calm winds would suggest a non-buoyant and/or local source, such as vehicle traffic, backup generators, and the like.

However, the polar plot of median NO_z values exhibits different characteristics in terms of wind speed and direction. The maximum NO_z values are associated with higher wind speeds from the southeast. The higher windspeed suggests more buoyant NO_z plumes and/or greater mixing from a more turbulent (windy) PBL or marine BL. The direction is from off of the North Atlantic. Some possible sources include nitrates, nitrites, and ammonia aerosolised by wind and wave action due to oceanic biological activity (e.g. plankton), chemically aged plumes from the eastern seaboard advected ashore, emissions from industrial sites (former petroleum refinery, petroleum trans-shipment facility, marine fabricators as examples), or some combination thereof. The higher NO_z values in terms of the polar plot are from directions that include industrial and transport activity, including the downtown cores of Dartmouth and Halifax, shipyards, rail lines, and petroleum trans-shipment installations. Without speciation, it is difficult to move past speculation as to specific sources.

There appears to be either a negative interference for the T200 or positive interference for the T500U to the northeast. A positive interference for the T500U would

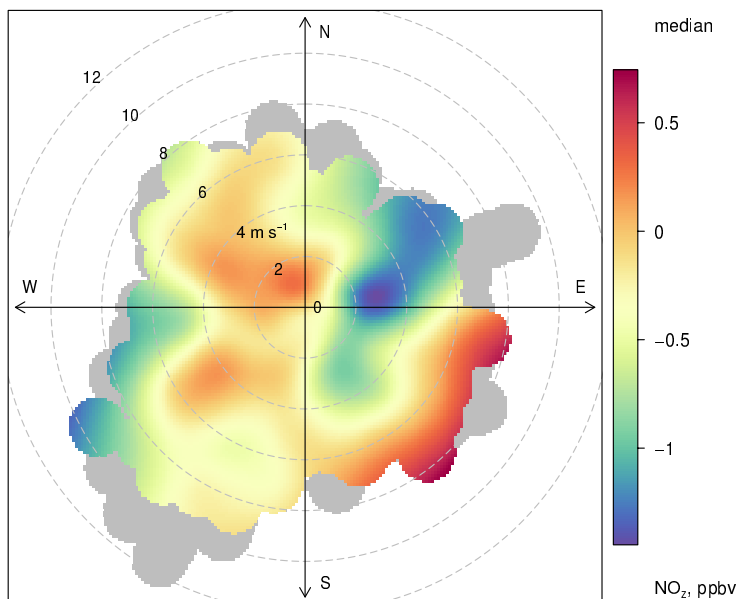


Figure 3.11: Polar plot of median NO_z values. The polar coordinates are wind speed and direction

be the more likely of the two possibilities. Locally, there is an industrial site (Dominion Diving, and former Dartmouth Shipyard grounds) several hundred meters to the east, and a laboratory (Ocean Nutrition Canada) approximately 1.8km to the east as well. The interference in question appears to be associated with lower wind speeds, suggesting a local source. As noted in Section 1.8.3, CAPS instruments are subject to positive interference from halogens, as they absorb in the same region as NO_2 . No investigation was made to identify the source of this interference.

High NO_z Interference

Looking at data where the $\text{NO}_2(\text{T}200)/\text{NO}_2(\text{T}500\text{U})$ ratio was 1.15 or greater (Figure 3.12, $N = 203$), there appeared to be a point source for NO_z interference to the west. A similar polar plot for NO_z values (Figure 3.13) shows a significant point source for NO_z from a similar wind direction and speed. There is also a point source of "negative NO_z " just to the north of the high NO_z source. All were associated with winds of about 3 m s^{-1} . As min.bin was set to 1 for these plots, there may be a single, or very few events that give rise to the point source shown in these two plots. Table 3.5 shows

data for extreme NO_z events thought to be associated with the point sources shown in the plots at figures 3.12 and 3.13. Large changes in the concentration of NO_x on very short time scales (seconds), coupled with differences in temporal resolution of the instruments may have given rise to the negative values of NO_z , remembering that NO_z was calculated as $\text{NO}_y - (\text{NO} + \text{NO}_2)$, where NO_z interference was calculated as $\text{NO}_2(\text{T200}) - \text{NO}_2$. As such, NO_z interference and NO_z were calculated using data from the T200 and T200(NO_y modified) instruments, respectively, with the T500U in common for true NO_2 . Additional discussion of possible causes for negative NO_z values are discussed in sub-Subsection 3.2.1.

Date	CO	NO ₂	NO	NO ₂ (T200)	NO _x	NO _y	O ₃	NO _z	NO _z	T	Td	rh	wd	ws	stn_p	radiation	NO _{-NO_x}	NO ₂ (T200)/NO ₂
2016-05-13 23:00	104.0	6.8	5.5	7.9	13.4	6.9	28.2	-5.4	1.1	6.4	4.5	87	140	1.1	1010.9	0.0	0.4	1.2
2016-05-21 10:00	162.0	19.8	52.6	36.1	87.1	62.4	27.1	-10.0	16.3	21.3	6.6	39	300	3.1	1014.1	793.2	0.7	1.8
2016-06-11 08:00	122.0	9.4	30.5	11.7	41.4	64.0	15.0	24.1	2.3	13.5	9.0	74	300	3.6	1010.8	469.8	0.8	1.2
2016-06-11 11:00	103.0	10.5	66.7	52.7	121.7	173.5	15.6	96.3	42.2	19.1	10.1	56	280	3.1	1009.7	572.2	0.9	5.0
2016-08-08 10:00	197.0	13.8	92.4	36.2	128.6	50.1	16.4	-56.1	22.4	21.6	12.6	57	300	3.6	1007.6	761.5	0.9	2.6

Table 3.5: Data for extreme events, $\text{NO}_2(\text{T200})/\text{NO}_2 > 1.15$

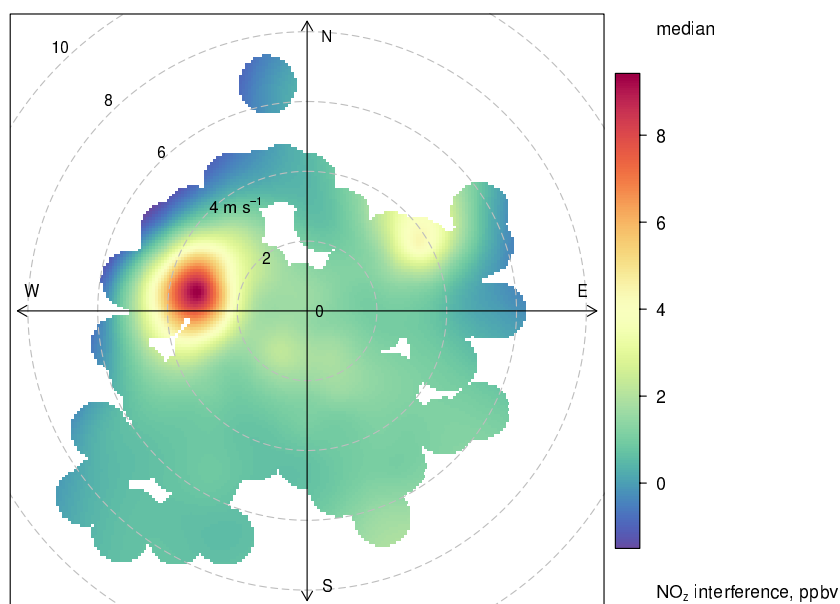


Figure 3.12: NO_z interference, $\text{NO}_2(\text{T200})/\text{NO}_2$ ratio > 1.15 .

It is important to note that there was insufficient data to run the polarPlot function with $\text{min.bin} = 2$. Therefore, individual hourly events had a greater effect in the production of the polar plots for the $\text{NO}_2(\text{T200})/\text{NO}_2 > 1.15$ data subset. A further

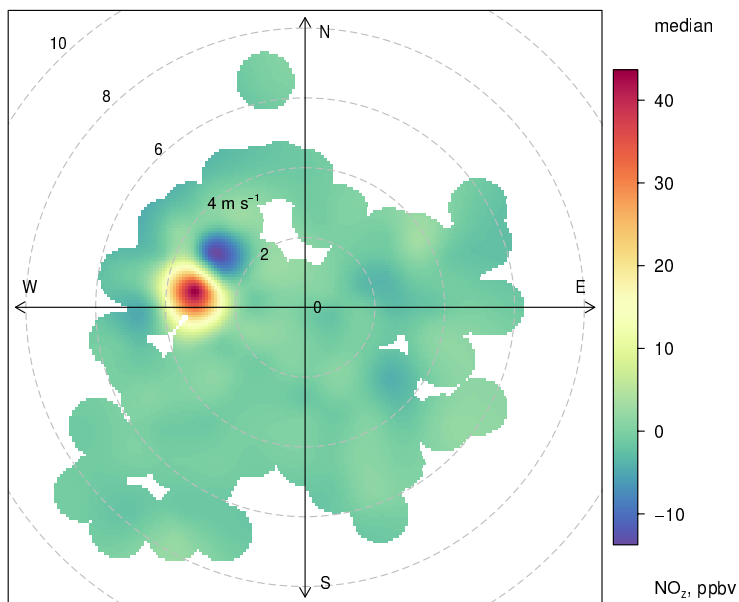


Figure 3.13: NO_z , $\text{NO}_2(\text{T200})/\text{NO}_2$ ratio > 1.15 . Note that the colour gradient scale is different from that of 3.12

subsetting of the modified data set was done with $\text{NO}_z > 4.9$ or < -4.9 . This was done to examine the point source to the west shown in Figure 3.13. Only five data points were produced by this further subsetting of the large NO_2/NO_2 ratio dataset. There were insufficient data to require multiple data points for each wind direction / wind speed bin. Therefore, each of these extreme events had significant impact on the plot. Table 3.5 shows the five data points.

Four of the five data point are mornings (08:00 to 11:00 UTC or 05:00 to 08:00 local), with winds out of the west near 3 ms^{-1} . These four data also exhibit high NO concentrations suggesting a local primary source. May 21st and June 11th are both Saturdays. May 13th was a Monday and August 8th a Friday. The May 13th data point differs from the other as it was at night, cooler and with lighter winds from the southeast. Excluding the May 13th datapoint, the remainder also had high NO/ NO_x ratios (0.7 to 0.9), suggesting a point source very near by. With such few data it is difficult to attribute these extreme events to a particular source. However, given their similarities, excepting the May 13th datapoint, I would speculate idling buses in the street canyon/bus terminal next to the measurement site, or idling locomotives

in the switching yard approximately 100 metres further to the northwest. Given the limited frequency of these events and the suspected cause, careful site selection should mitigate against such events for monitoring stations.

3.3 NO_z Interference

3.3.1 Linear Regression of NO₂(T200) vs. NO₂

Linear regression was looked at as a possible means of determining NO_z interference by looking at the slope of NO₂(T200)/NO₂. As air quality data is not parametric, Log₍₁₀₎ (base 10 Logarithm, hereafter referred to as Log) transforms were used on the NO₂ and NO₂(T200) values. Pre and post transform boxplots and histograms were then prepared in an attempt to judge whether the Log transformation normalised the data. Figure 3.14 shows the box plots for NO₂ and NO₂(T200), by month, before and after applying the Log transforms. Symmetry about the median appears to improve overall. However, June symmetry about the median for June decreases.

Figure 3.15 shows a comparison of the histograms for both NO₂ values pre and post Log transform. The post-Log transform values do take on a more "bell"-like shape. While they appear closer to a normal distribution, it would be difficult to claim that they are indeed normally distributed. However, the results did not preclude further investigation.

Next, autocorrelation was looked at with a view to finding the decorrelation point. Figure 3.16 shows the log transformed data as analysed by the R function "acf". The plot shows the autocorrelation function decaying prior to hour 20, with a bit of bump around 20. It was thought that by 24 hours the dataset was sufficiently decorrelated. The log transformed data were then averaged by day, and a linear regression of NO₂(T200) vs. NO₂, by month, was performed. As the T500U instrumental error is about an order of magnitude below that of the T200, it was discounted and a type 1 regression model was used. Figure 3.17 shows the results. With the exception of May, all months show slopes less than 1.08, inside of experimental error. The higher slope of May, couple with the large 95% CI bars, are likely due to a high NO_x day and several missing values toward the end of the month.

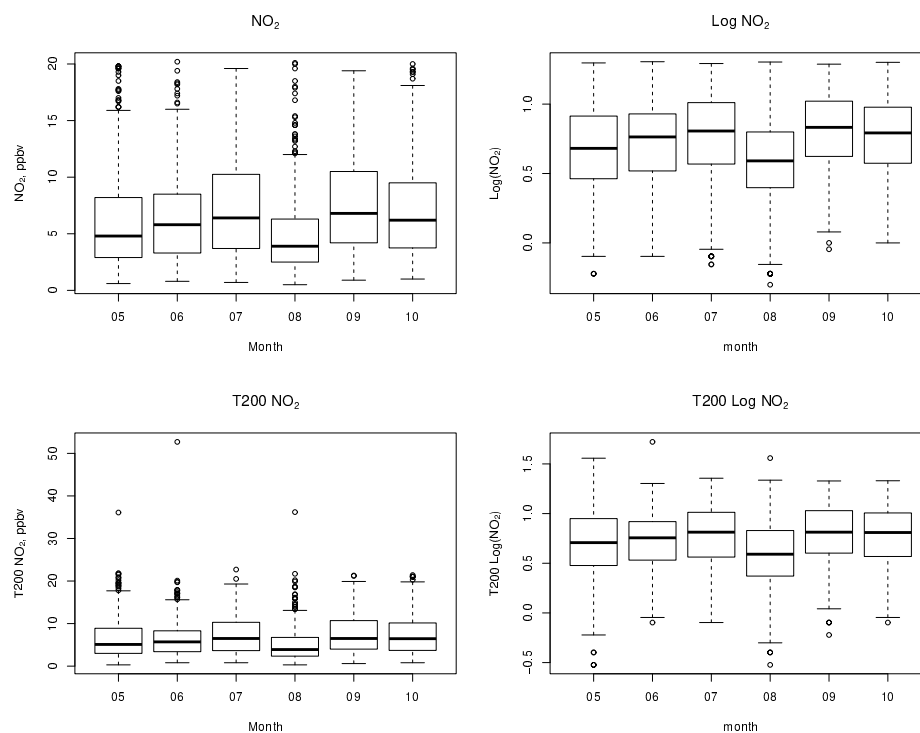


Figure 3.14: NO₂ and NO₂(T200) pre and post Log transform. The heavy line is the median, boxes are the interquartile range, whiskers extend $1.5 \times$ interquartile range, and circles for outliers.

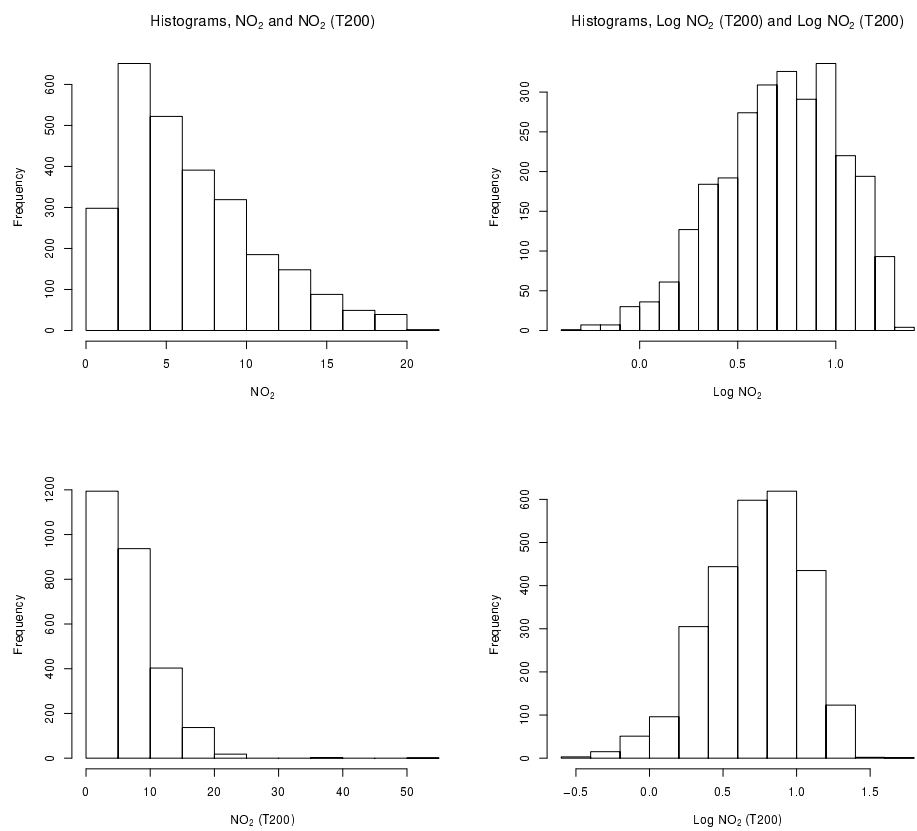


Figure 3.15: Histograms for NO_2 and NO_2 (T200), pre and post Log transform.

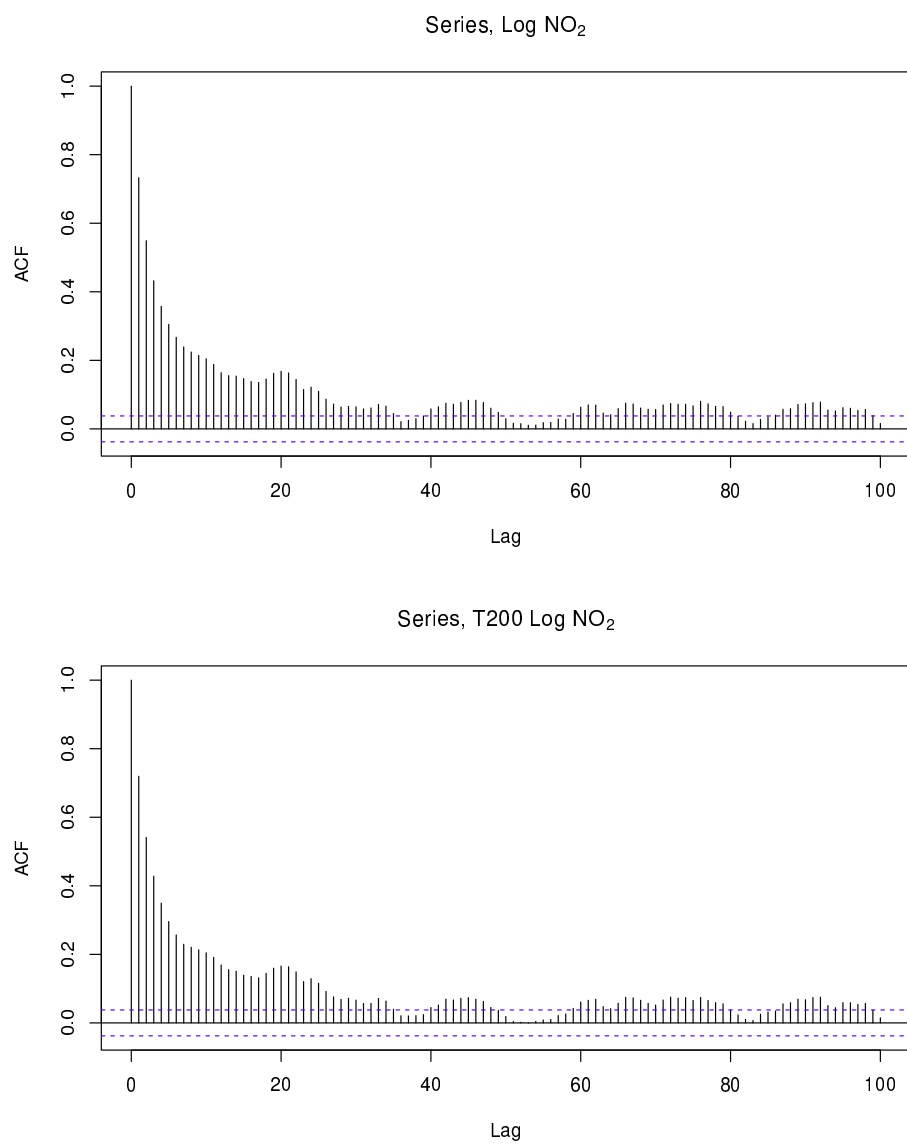


Figure 3.16: Autocorrelation function plot for Log NO₂ and Log NO₂ (T200).

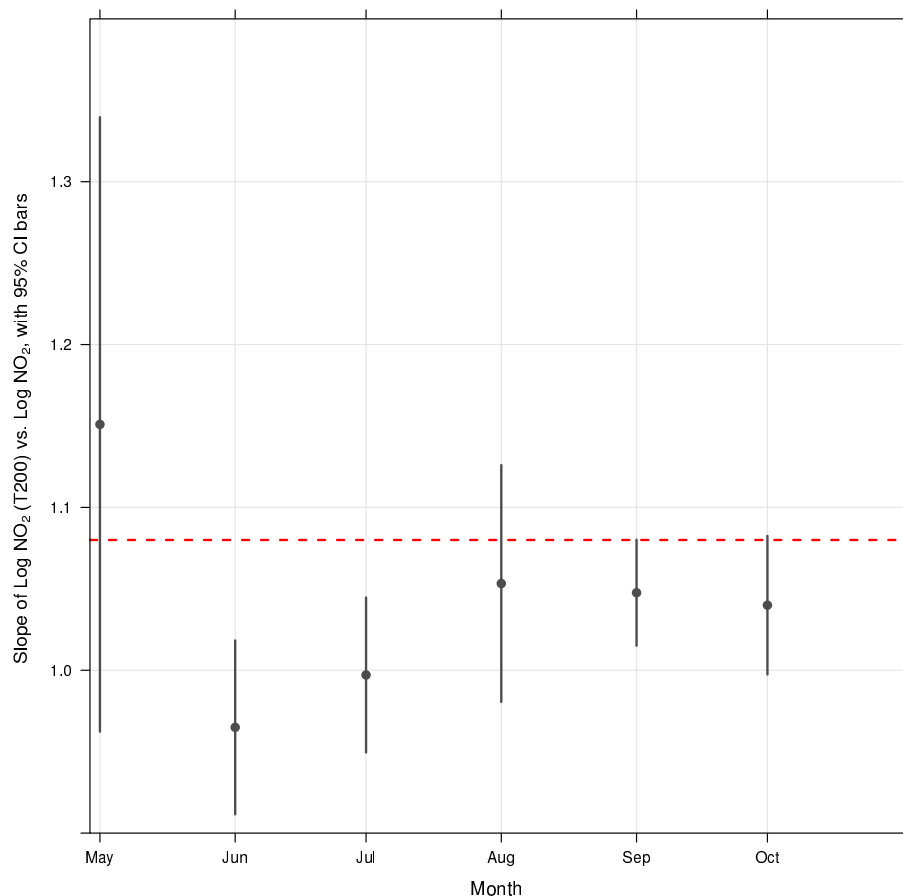


Figure 3.17: Linear regression slopes by month, $\text{NO}_2(\text{T200})$ vs. NO_2 , with 95% CI bars. NO_2 (T500U CAPS instrument) is taken as the true NO_2 value. The red dashed line is 1.08.

Given the results largely below experimental error, and the less-than-perfect normality of the Log transformed data, further parametric analyses were not pursued.

3.3.2 Wilcoxon Signed-Rank Testing

Parametric methods, even with attempts to normalise the data, proved ineffective. Subsequently, non-parametric analyses were performed. The Wilcoxon Signed-Rank test [Wilcoxon, 1945] (WSR) is a dependant variable, pairwise non-parametric hypothesis test of whether the two related samples are from the same population. It also provides for a pseudo median value, which is useful in comparing to the median measured values. The test was applied to the complete dataset as well as by month

in order to examine whether there was a difference between the NO₂ values measure by the T500U and T200.

	May	June	July	August	September	October	Complete Data
V	84001	35490	51638	42435	28926	56846	1804400
p	0.00	0.27	0.87	0.18	0.46	0.00	0.00
Lower Limit	0.3	0.0	-0.1	-0.1	-0.1	0.3	0.1
Upper Limit	0.5	0.1	0.0	0.0	0.1	0.4	0.2
Pseudo median	0.4	0.1	0.0	-0.1	0.0	0.3	0.2

Table 3.6: Wilcoxon signed-rank test by month and for the complete dataset. Note that p values of 0.00 indicate lower limits of the computer and associated software, and were reported by R as $p < 2.2e-16$.

The test indicated a difference between the two NO₂ measurements for the complete dataset, as well as for May and October. Each had near-zero p values. P values for June to September were quite high, suggesting the null hypothesis of the Wilcoxon Signed-rank test - there is no difference between datasets. The high p values coupled with near-zero pseudo medians is suggestive that there is no significant NO_z interference during these months.

There is similarity between the median monthly measured NO_z interference and the pseudo medians from the WSR test. The WSR results, in tandem with the median monthly values measured indicate that there is likely some amount of NO_z interference in May and October. This may be indicative of NO_z interference being related to the heating season, and largely separate from local road motor transport primary NO_x sources. However, this would need to be confirmed with additional measurements for the other six months of the year, and perhaps speciation of NO_y. Overall, the similarity between the calculated monthly medians and the pseudo-medians adds a degree of confidence in the monthly NO_z interference values.

3.3.3 Spearman Correlation Analysis for May and October

Given that the monthly medians and pseudo medians of NO_z interference for June to September are essentially zero, further analysis was limited to the shoulder months of the measurement period, being May and October.

Figures 3.18 and 3.19 show the Spearman correlation plots for May and October.

For May, the various NO_x and NO_y measurements show an expected level of correlation. Correlations between the NO_x - NO_y - NO_z values and meteorological conditions are not generally apparent. There is a weak correlation between station pressure and a variety of the $\text{NO}_x/\text{NO}_y/\text{NO}_z$ values. This matches well with the results of the polar plot showing the strongest NO_z interference associated with calm and weak winds. High pressure systems tend towards lower wind speeds. However, high pressure systems during the warm months are also associated with convection, higher PBL heights, and therefore not necessarily less turbulent conditions within the PBL, especially in the afternoon during the period of greatest insolation and surface heating. As would be expected from data presented in Subsection 3.2.1, wind speed shows a moderate negative correlation to the NO_x and NO_y species. It is expected that the higher wind speeds promote ventilation and dilution from surrounding rural and oceanic areas lacking in NO_x sources. The results are similar for October. However, an additional weak negative correlation shows up for October between all of the various NO_y species (NO , NO_2 , NO_x , NO_y , NO_z) and ambient temperature. It may be a simple increase in local fossil fuel combustion for structure heating, more people favouring motor vehicles over non-combustion transport, or other unknown factors. Also, there is a weak positive correlation in October for relative humidity and the NO_y species, except for NO . There is a weak correlation between NO and rh, but it is negative. It may be that higher rh helps in processing NO_x to NO_z species (e.g. night-time HNO_3 and HONO production). However, there is no supporting evidence to make any further comment on these weak correlations between meteorological factors and the various NO_x and NO_y species measured.

Given the weak correlation with rh and NO_z interference, absolute humidity (AH) was calculated, and spearman correlations run for May and October. AH was calculated by equation 3.2, where $C = 2.16679 \text{ gK/J}$ (constant), $P_w = \text{Vapour pressure of water in Pa}$, and $T = \text{Temperature in Kelvin}$. P_w was calculated using equation 3.3, where $P_w = \text{water vapour saturation pressure (} P_{ws} \text{) multiplied by relative humidity as a decimal}$. It was not corrected for the presence of other gases. These equations and constants were taken from [Vaisala Oyi, 2013].

$$AH = C \cdot P_w / T \quad (3.2)$$

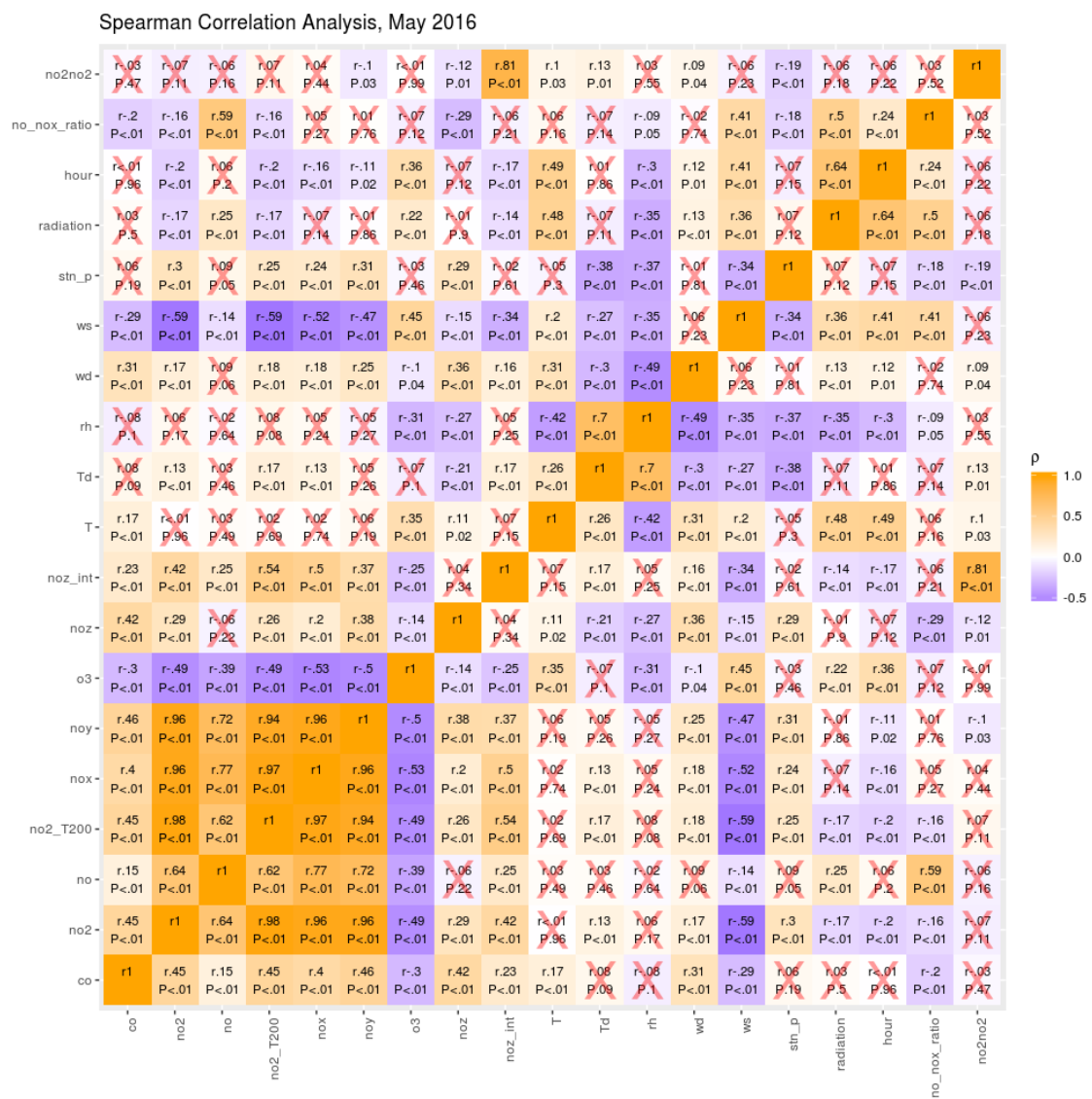


Figure 3.18: Spearman correlation plot for May 2016. Red 'X' indicates $p > 0.05$.

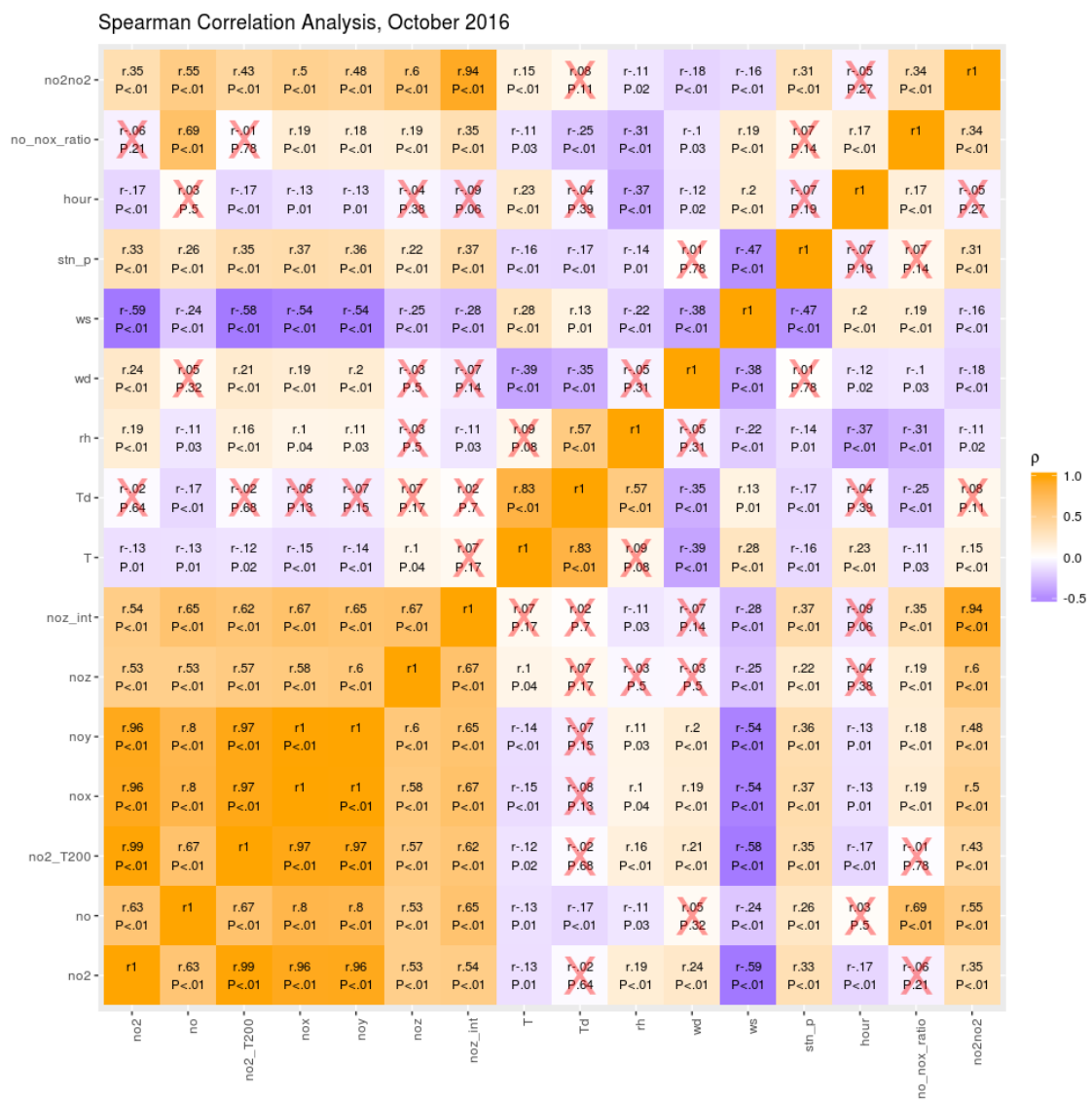


Figure 3.19: Spearman correlation plot for October 2016. Red 'X' indicates $p > 0.05$.

where

$$P_{ws} = A \cdot 10^{mT/(T+T_n)} \quad (3.3)$$

and

$$P_w = P_{ws} \cdot rh \quad (3.4)$$

where rh is expressed as a decimal value.

A weak correlation was found in May ($\rho = 0.13$, $p = 0.01$), but not for October. The correlation between AH and NO_z interference in May matched the values for temperature and NO_z interference closely ($\rho = 0.12$, $p = 0.01$). It is possible that the correlation between AH and NO_z interference may be another expression of the correlation with temperature, as warmer air can hold more water than colder air. The opposite may be true as well, with AH as an expression of warmer air rather than warmer air as an expression of AH. Given that there was no correlation in October, AH was not pursued further.

Chapter 4

Conclusion

The conclusions for each of the science questions posed in Chapter 1 are:

What is the magnitude of NO_z interference at this location?

The median NO_z interference between May and October 2016 is 0.1, with an interquartile range of -0.2 to 0.4. This value is within instrument error for standard MoO/CL instruments, and within the estimated experimental error. On a monthly basis, there was no statistically significant interference from June to September. While there was likely statistically significant positive interference for May and October, it was less than 1 ppbv for each.

Is the magnitude significant to modelling, OA, or AHQI forecasting?

For the months of May and October, the amount may have been significant to modelling in terms of model sensitivity to initial conditions (See Lorenz [1963] for an example) from a theoretical view. However, the measured NO_z interference was small enough in magnitude to be lost within the uncertainties of the monitoring network. It is also possible that current modelling methods are more robust in terms of sensitivity to small errors in initial conditions, thus limiting the effects of the low levels of NO_z interference found at this site. For the months of June to September, no significant NO_z interference was detected.

What are the major temporal characteristics of the NO_z interference, especially diurnal, day of week and seasonal variation?

No pattern was identified for day of week or most other short timeframe measures. However, there was a maximum for NO_z interference noted for time of day between 03:00 and 06:00 UTC (00:00 to 03:00 local). This time of day coincided with daily windspeed minima. Overall, the highest NO_z interference also coincided with low wind speeds, which may

be suggestive. NO_z interference for the period of measurement, that being May to October, was highest in May, decreased to zero for the summer, and increased again in October. It is thought that this pattern may be related to average ambient temperature and structure heating, but more work and measurements for the other six month would be required to investigate this hypothesis. In terms of correlation values between individual meteorological measurements and NO_z interference, there were seasonal differences between the months of May and October. However, it must be noted that even in May and October, the median level of interference was low (sub ppbv).

What relationships exist between meteorology and NO_z interference?

In May, weak Spearman correlations between NO_z interference and T_d and wind direction ($\rho = 0.17$ and 0.16 respectively), as well as negative correlations with wind speed, radiation and hour of day ($\rho = -0.34$, -0.014 , and -0.17). For October, there was a positive correlations with station pressure ($\rho = 0.34$), and negative correlations with relative humidity and wind speed ($\rho = -0.11$ and -0.26). The correlation between NO_z interference and station pressure in October may be related to the relation between station pressure and windspeed, where high pressure systems tend to bring low or calm winds. One might then expect a similar correlation for May. However, this was not so. The time of year and the location of the site may offer an explanation, in that biogenic production of volatile and semi-volatile organic compounds may tend to peak in the spring. These compound react readily with OH and other oxidizing species. A large flux of these compounds may reduce the local oxidative potential, and thus limit NO_z production from local primary source or transported NO_x .

Is there a correction factor or factors evident from the data?

No correction factor was evident for the months of June to September inclusive, as NO_z interference was below detection limits. For May and October, while NO_z interference was on the upper edge of experimental error, the general magnitude was of a sufficiently small size as to not affect AQHI calculation and forecasting. Given the inherent and unknown error

present in the NAPS AQHI monitoring network, any correction factor developed from this work would be lost in the "noise". This may not hold true for other months at this location, as the data suggest that there may be greater levels of NO_z interference in the colder months of the year. Data collection continued past October 2016. Future measurements and analysis should further characterise the nature of NO_z interference at this location.

In terms of my hypothesis, within a monitoring context, there was little NO_z interference between May and October in the small urban coastal site. NO_z interference in NO_2 monitoring by MoO/CL instruments was not a significant factor in NO_2 monitoring and AQHI calculation and forecasting. Within the context of model OA, NO_z interference was not likely a factor in the use of OA as a synthetic AQHI observation for areas without monitoring stations nearby. In use of OA to seed model runs, minor NO_z interference in the NO_2 field may be an issue. However, within the context of a monitoring network, and the precision available from such a network, a correction factor for areas similar in nature to this measurement site are unlikely to be had. There is too much uncertainty present in the current and past monitoring data to allow for a correction in such sites.

The lack of NO_z interference may be a result of the monitoring site being both a clean site, having relatively low primary NO_x production located nearby, coupled with being surrounded by clean space. That is to say that the monitoring site was surrounded by either rural land or open ocean, both having almost no anthropogenic primary NO_x sources. In the case of Steinbacher et al. [2007], while the measurement sites were in areas of low primary NO_x emissions (especially the higher elevation site), the major urban areas of Europe likely contributed aged NO_x plumes, and the associated NO_z species. This site showed significant ventilation in most circumstances, allowing for the dilution of all NO_y species, low overall NO_x , NO_y and NO_z concentrations, and levels of NO_z interference below detection limits for the methods used. It was during times of calm winds that demonstrated the highest levels of NO_z interference, although the highest levels of NO_z concentrations did appear to come from chemically aged sources to the southeast and west.

It is unknown whether the lack of literature showing little or no NO_z interference

in MoO/CL NO₂ measurements is a result of this measurement site being unique in nature, or that null results tend to be published with less frequency, or some other factor or combination of factors. The body of work on NO_z interference demonstrates that it can be an issue of concern for the measurement of NO₂ by thermal MoO/CL instruments. However, this work shows that within a monitoring context, NO_z interference may not be an issue within some geographic and/or meteorological contexts.

Bibliography

- Bollinger, M. J., Hahn, C. J., Parrish, D. D., Murphy, P. C., Albritton, D. L., and Fehsenfeld, F. C. (1984). NO_x measurements in clean continental air and analysis of the contributing meteorology. *Journal of Geophysical Research: Atmospheres*, 89(D6):9623–9631.
- Bottenheim, J., Barrie, L. A., and Atlas, E. (1993). The partitioning of nitrogen oxides in the lower Arctic troposphere during spring 1988. *Journal of Atmospheric Chemistry*, 17(1):15–27.
- Burnett, R. T., Stieb, D., Brook, J. R., Cakmak, S., Dales, R., Raizenne, M., Vincent, R., and Dann, T. (2004). Associations between short-term changes in nitrogen dioxide and mortality in Canadian cities. *Archives of Environmental Health: An International Journal*, 59(5):228–236. PMID: 16201668.
- Calvert, J. G., Yarwood, G., and Dunker, A. M. (1994). An evaluation of the mechanism of nitrous acid formation in the urban atmosphere. *Research on Chemical Intermediates*, 20(3):463–502.
- Carslaw, D. C. and Ropkins, K. (2012). openair — an r package for air quality data analysis. *Environmental Modelling & Software*, 27-28(0):52–61.
- Day, D. A., Dillon, M. B., Wooldridge, P. J., Thornton, J. A., Rosen, R. S., Wood, E. C., and Cohen, R. C. (2003). On alkyl nitrates, O_3 , and the "missing NO_y ". *Journal of Geophysical Research: Atmospheres*, 108(D16):2156–2202. 4501.
- Dentener, F., Derwent, R., Dlugokencky, E., Holland, E., Isaksen, I., Katima, J., Kirchhoff, V., Matson, P., Midgley, P., and Wang, M. (2001). Chapter 4: Atmospheric chemistry and greenhouse gases. In *IPCC TAR WG1*, chapter 4. Cambridge University Press.
- Dunlea, E. J., Herndon, S. C., Nelson, D. D., Volkamer, R. M., San Martini, F., Sheehy, P. M., Zahniser, M. S., Shorter, J. H., Wormhoudt, J. C., Lamb, B. K., Allwine, E. J., Gaffney, J. S., Marley, N. A., Grutter, M., Marquez, C., Blanco, S., Cardenas, B., Retama, A., Ramos Villegas, C. R., Kolb, C. E., Molina, L. T., and Molina, M. J. (2007). Evaluation of nitrogen dioxide chemiluminescence monitors in a polluted urban environment. *Atmospheric Chemistry and Physics*, 7(10):2691–2704.
- Environment and Climate Change Canada (2013). National Air Pollution Surveillance Program (NAPS). <http://www.ec.gc.ca/rns-pans/Default.asp?lang=En&n=5C0D33CF-1> accessed 2016-11-14.

- Environment and Climate Change Canada (2016). Canadian Climate Normals 1981-2010 Station Data, Shearwater A, Nova Scotia. http://climate.weather.gc.ca/climate_normals/results_1981_2010_e.html?searchType=stnProv&lstProvince=NS&txtCentralLatMin=0&txtCentralLatSec=0&txtCentralLongMin=0&txtCentralLongSec=0&stnID=6465&dispBack=0 accessed 2017-01-13.
- Environment Canada (2010a). Continuous Measurement of Nitrogen Dioxide (NO₂) in Ambient Air by Chemiluminescence. Technical report, NAPS Operations Unit.
- Environment Canada (2010b). NAPS Stations Map. <http://www.ec.gc.ca/rnsp-naps/default.asp?lang=En&n=8BE12DF0-1> accessed on 2016-11-09.
- Environment Canada (2014). Planning for a Sustainable Future: A Federal Sustainable Development Strategy for Canada 2013-2016. <https://www.ec.gc.ca/ddsd/default.asp?lang=en&n=37A4B580-1> accessed 2016-11-09.
- Fahey, D. W., Eubank, C. S., Hübler, G., and Fehsenfeld, F. C. (1985). Evaluation of a catalytic reduction technique for the measurement of total reactive odd-nitrogen NO_y in the atmosphere. *Journal of Atmospheric Chemistry*, 3(4):435–468.
- Fontijn, A., Sabadell, A., and Ronco, R. (1974). Homogeneous chemiluminescent measurement of nitric oxide with ozone: Implications for continuous selective monitoring of gaseous air pollutant. *Analytical Chemistry*, 46:575–579.
- Gerboles, M., Lagler, F., Rembges, D., and Brun, C. (2003). Assessment of uncertainty of NO₂ measurements by the chemiluminescence method and discussion of the quality objective of the NO₂ European Directive. *J. Environ. Monit.*, 5:529–540.
- Grosjean, D. and Harrison, J. (1985). Response of chemiluminescence NO_x analyzers and ultraviolet ozone analyzers to organic air pollutants. *Environmental Science & Technology*, 19(9):862–865. PMID: 22196613.
- Harrison, R. M., Grenfell, J., Yamulki, S., Clemitshaw, K., Penkett, S., Cape, J., and McFadyen, G. (1999). Budget of NO_y species measured at a coastal site. *Atmospheric Environment*, 33(26):4255 – 4272.
- Heard, D., editor (2006). *Analytical Techniques for Atmospheric Measurement*. Wiley-Blackwell, Oxford.
- Hollingsworth, A. and Lönnberg, P. (1986). The statistical structure of short-range forecast errors as determined from radiosonde data. Part I: The wind field. *Tellus A*, 38A(2):111–136.
- Jacob, D. J. (1999). *Introduction to Atmospheric Chemistry*. Princeton University Press, Princeton.

- Kebabian, P. L., Herndon, S. C., and Freedman, A. (2005). Detection of nitrogen dioxide by cavity attenuated phase shift spectroscopy. *Analytical Chemistry*, 77(2):724–728.
- Kebabian, P. L., Wood, E. C., Herndon, S. C., and Freedman, A. (2008). A practical alternative to chemiluminescence-based detection of nitrogen dioxide: Cavity Attenuated Phase Shift Spectroscopy. *Environmental Science and Technology*, 42(16):6040–6045. PMID: 18767663.
- Keffer, T. (2016). Weewx. <http://weewx.com> accessed April 2016.
- Kitto, A.-M. N. and Harrison, R. M. (1992). Nitrous and nitric acid measurements at sites in South-East England. *Atmospheric Environment. Part A. General Topics*, 26(2):235 – 241.
- Levy, I., Mihele, C., Lu, G., Narayan, J., and Brook, J. (2014). Evaluating multipollutant exposure and urban air quality: Pollutant interrelationships, neighborhood variability, and nitrogen dioxide as a proxy pollutant. *Environmental Health Perspectives*, 122:65–72.
- Lorenz, E. N. (1963). Deterministic nonperiodic flow. *Journal of the Atmospheric Sciences*, 20(2):130–141.
- McClenny, W. A., Williams, E. J., Cohen, R. C., and Stutz, J. (2002). Preparing to measure the effects of the NO_x SIP Call: Methods for ambient air monitoring of NO, NO₂, NO_y, and individual NO_z species. *Journal of the Air and Waste Management Association*, 52(5):542–562.
- Moran, M., , Ménard, S., Gravel, S., Pavlovic, R., and Anselmo, D. (2012). RAQDPS Versions 1.5.0 and 1.5.1: Upgrades to the CMC Operational Regional Air Quality Deterministic Prediction System Released in October 2012 and February 2013. Technical report, Science and technology Branch, Air Quality Research Division, Environment Canada.
- Neuman, J. A., Huey, L. G., Ryerson, T. B., and Fahey, D. W. (1999). Study of inlet materials for sampling atmospheric nitric acid. *Environmental Science & Technology*, 33(7):1133–1136.
- R Core Team (2017). *R: A Language and Environment for Statistical Computing*. R Foundation for Statistical Computing, Vienna, Austria.
- Robichaud, A. and Ménard, R. (2012). Technical Report Regional Deterministic Air Quality Analysis (RDAQA). Technical report, Science and technology Branch, Air Quality Research Division, Environment Canada.
- Ryerson, T. B., Williams, E. J., and Fehsenfeld, F. C. (2000). An efficient photolysis system for fast-response NO₂ measurements. *Journal of Geophysical Research: Atmospheres*, 105(D21):26447–26461.

- Seinfeld, J. H. and Pandis, S. N. (2006). *Atmospheric Chemistry and Physics - From Air Pollution to Climate Change*. John Wiley & Sons, Inc., Hoboken, New Jersey, second edition.
- Steinbacher, M., Zellweger, C., Schwarzenbach, B., Bugmann, S., Buchmann, B., Ordóñez, C., Prevot, A. S. H., and Hueglin, C. (2007). Nitrogen oxide measurements at rural sites in Switzerland: Bias of conventional measurement techniques. *Journal of Geophysical Research: Atmospheres*, 112(D11):2156–2202.
- Stieb, D. M., Burnett, R. T., Smith-Doiron, M., Brion, O., Shin, H. H., and Economou, V. (2008). A new multipollutant, no-threshold air quality health index based on short-term associations observed in daily time-series analyses. *Journal of the Air and Waste Management Association*, 58(3):435–450.
- Vaisala Oyi (2013). Humidity conversion formulas B210973en-F. [www.vaisala.com/Vaisala Documents/Application notes/Humidity_Conversion_Formulas_B210973EN-F.pdf](http://www.vaisala.com/Vaisala_Documents/Application_notes/Humidity_Conversion_Formulas_B210973EN-F.pdf) accessed 2017-06-23.
- Villena, G., Bejan, I., Kurtenbach, R., Wiesen, P., and Kleffmann, J. (2012). Interferences of commercial NO₂ instruments in the urban atmosphere and in a smog chamber. *Atmospheric Measurement Techniques*, 5(1):149–159.
- Volz-Thomas, A., Berg, M., Heil, T., Houben, N., Lerner, A., Petrick, W., Raak, D., and Pätz, H.-W. (2005). Measurements of total odd nitrogen (NO_y) aboard MOZAIC in-service aircraft: instrument design, operation and performance. *Atmospheric Chemistry and Physics*, 5(3):583–595.
- Wilcoxon, F. (1945). Individual comparisons by ranking methods. *Biometrics Bulletin*, 1(6):80–83.
- Williams, E. J., Baumann, K., Roberts, J. M., Bertman, S. B., Norton, R. B., Fehsenfeld, F. C., Springston, S. R., Nunnermacker, L. J., Newman, L., Olszyna, K., Meagher, J., Hartsell, B., Edgerton, E., Pearson, J. R., and Rodgers, M. O. (1998). Intercomparison of ground-based NO_y measurement techniques. *Journal of Geophysical Research: Atmospheres*, 103(D17):22261–22280.
- Wilson, A., Waugh, D., Chisholm, L., Beauchamp, S., Stroud, C., Appleby, B., Howe, M., Gibson, M., and Savoie, R. (2014). Preliminary Results from the Northern New Brunswick AQHI Evaluation Study. Presented at the 48th Annual Canadian Meteorological and Oceanographic Society Symposium, Rimouski, Quebec.
- Winer, A. M., Peters, J. W., Smith, J. P., James, N., and Pitts, J. (1974). Response of commercial chemiluminescent NO-NO₂ analyzers to other nitrogen-containing compounds. *Environ. Sci. Technol*, 8(13):1118–1121.

Appendices

Appendix A

Calibration Valve Code

The following code was written for Python 3.x. It was installed on a Raspberry Pi model B with the PiFace Digital board. Further details are described in Section 2.4.

```
1 #!/usr/bin/env python3
2
3 # using piface digital to poll for change of a 5V digital
   output on T700 cal
4 # on digital input 0 and then report and log status
5 # piface digital relay used to switch three way valve to
   introduce cal gas
6 # to sample stream
7
8 import pifacedigitalio as pfdio, logging
9 from time import sleep, asctime
10
11 pfdio.init()
12 pfd = pfdio.PiFaceDigital()
13
14 global pin0_val
15 pin0_val = pfd.input_pins[0].value
16
17 #set up logging to file and some basic formatting
18 logging.basicConfig(format = '%(asctime)s %(name)-12s %(
   levelname)-8s %(message)s',
19                       filename = '/home/pi/NOz_cal_status.log',
20                       level = logging.DEBUG,
21                       datefmt='%y-%m-%d %H:%M')
```

```
22
23 #set up some logs for program and actual status
24 logger1 = logging.getLogger('pgm')
25 logger2 = logging.getLogger('status')
26
27 #file handlers for same
28 fh1 = logging.FileHandler('pgm.log')
29 fh2 = logging.FileHandler('status.log')
30
31 #formatter for the handlers
32 formatter1 = logging.Formatter('%(asctime)s - %(name)s - %(
    levelname)s - %(message)s')
33 formatter2 = logging.Formatter('%(asctime)s - %(name)s - %(
    levelname)s - %(message)s : ')
34
35 #define a Handler that writes to sys.stderr at level
    specified
36 ch1 = logging.StreamHandler()
37 ch1.setLevel(logging.DEBUG) # change this to INFO after it
    works
38
39 #add formatter
40 ch1.setFormatter(formatter1)
41
42 #set levels for file handlers
43 fh1.setLevel(logging.DEBUG)
44 fh2.setLevel(logging.INFO)
45
46 #set formatters for same
47 fh1.setFormatter(formatter1)
48 fh2.setFormatter(formatter2)
```

```

49
50 #add the handlers for both logs
51 logger1.addHandler(fh1)
52 logger1.addHandler(ch1)
53 logger2.addHandler(fh2)
54 logger2.addHandler(ch1)
55
56 logger1.info('pgm started')
57 print('Control-C to exit program . . .')
58
59 while True:
60     try:
61
62         def status_ch(pin0_new):
63             pin0_new = pin0_new
64             logger2.info('Stream changed to %d' % pin0_new)
65             pfd.leds[0].value = pin0_new
66             pfd.relays[0].value = pin0_new
67             sleep(1)
68             return
69
70         pin0_new = pfd.input_pins[0].value
71
72         if pin0_new == pin0_val:
73             sleep(1)
74             continue
75
76         if pin0_new != pin0_val:
77             status_ch(pin0_new)
78             pin0_val = pfd.input_pins[0].value
79             continue

```

```
80
81     except KeyboardInterrupt:
82         break
83
84 logger1.warning('Program Terminated by keyboard!')
85 pfdio.deinit()
86 sleep(0.25)
87 print('Good bye!')
88 sleep(0.1)
89
90 print('exit at end')
```

To ensure the calibration relay script was running in the case of an accidental reboot (power outage, accidentally disconnecting the power supply cable, etc.), a short bash shell script was written, and set to run on reboot using the linux crontab (cron table).

```
1 #!/bin/sh
2 screen
3 sudo python3 /home/pi/cal_relay.py
```

Screen is a linux package that allows for running a detached terminal. Giving the python calibration relay script its own terminal generally prevented other processes and tasks from interfering with the running of the script. It could then essentially run in the background and allow other work to continue on the Raspberry Pi, such as updating packages.

Appendix B

Certifications

B.1 Calibration Gas

The calibration gas mixture was sent for certification by NAPS prior to the start of the measurement campaign. The calibration certificate is shown below. NO is NIST traceable.

Certificate of Analysis

NAPS Quality Assurance
Environment Canada
335 River Road, Ottawa, ON K1A 0H3

Certificate Number: 16-M003

Certification Request:

Air Quality Sciences Section
Environment Canada
16th Floor, Queen Square
45 Alderney Drive
Dartmouth, NS
B2Y 2N6

Cylinder Identification:

Cylinder Code: MIX 076
Supplier: Linde
Serial Number: SD 11483
Pressure: 1900 psi

<u>Component *</u>	<u>Certified Concentration</u>	<u>Certification Date:</u>	<u>Expiration:</u>
Carbon Monoxide	506.0 ppm ± 2%	April 13, 2016	Apr-2018
Nitric Oxide	41.2 ppm ± 2%	April 19, 2016	Apr-2018
NO2 Impurity	ND ppm		
Sulphur Dioxide **	NA ppm ± 2% with Thermo NA ppm ± 2% with API		

* balance is nitrogen

** use SO2 concentration value corresponding to make of analyzer to be calibrated. Presence of Nitric Oxide in mixture results in different apparent SO2 concentration seen by Thermo analyzer versus API analyzer


Traceable to *National Institute of Standards & Technology (NIST)* Standard Reference Material:

Carbon monoxide in Nitrogen
Standard Reference Material® 2637a
Cylinder Number: CAL017994
Carbon monoxide = 490.4 µmol/mol ± 2.0 µmol/mol
Expiration of Certification: February, 2017

Nitric Oxide in Nitrogen
Primary Reference gas Mixture (PRM)
Cylinder Number: CAL018113
Nitric Oxide = 48.79 µmol/mol ± 0.34 µmol/mol
Expiration of Certification: March 2019

The product listed above has been tested according to Environment Canada method 2.02/2.03/2.04, *Certification of Calibration Gas Mixtures for Ambient Air Analyzers*, and found to contain the component concentrations listed above. The reported uncertainties of the certified values have been determined according to the requirements of ISO/IEC 17025 using a Type 'A' approach and a coverage factor of k=2, corresponding to a 95 % confidence interval.


Analyst:


 Claude Tremblay
 Technologist, NAPS Operations

Date:

20 Apr 2016

Reviewed by:



Form No. 2.02M / F4a - ver 9 Sept. 22, 2011

B.2 T700U Calibrator Mass Flow Controllers (MFCs)

The following is the calibration certificate for the dilutant (zero air) and calibration gas mass flow controllers. The trace level 0-10 cc/min MFC was not calibrated, and was therefore not used in calibration of the instruments.

Certification of
API T700U
s/n 194
Mass Flow Controllers

Certificate No: [MTU 16-04-38](#)
[21-Apr-16](#)

NAPS Applied Metrology Laboratory
Analysis & Air Quality Section
Air Quality Research Division
Atmospheric Science and Technology Directorate
Science and Technology Branch



Environment
Canada

Environnement
Canada

Certification of
API T700U
s/n 194
Certificate Number MTU 16-04-38

21-Apr-16

This is to certify that the instrument indicated below has been compared with the reference standard of the National Air Pollution Surveillance (NAPS) Network Applied Metrology Laboratory.

Certificate Issued To: Environment Canada - Atlantic Region

Date of Calibration: 21-Apr-16 **Next Calibration Required by:** 21-Apr-17

Identification of Instrument Calibrated:

Ownership: Environment Canada - Atlantic Region

Manufacturer / Model / Serial Number: API T700U
s/n 194

Calibration Reference Standard Used:

DHI Molbox/Molbloc RFM™
Manufacturer: DH Instruments Inc.
Molbox RFM-M (tm) s/n 407
Mass Flow Element 3E4-VCR-V-Q Molbloc s/n 1355 (range 0.3 - 30 lpm)
Mass Flow Element 5E2-VCR-V-Q Molbloc s/n 1426 (range 5 - 500ccm)

All certifications were performed by the NAPS Applied Metrology Laboratory of the Analysis and Air Quality Section in a controlled environment by qualified personnel using established instrumentation and methods. The instrument was set up according to the procedures and specifications of Environment Canada and/or the stated manufacturer.
This certification is traceable to the International System of Units (SI) through recognized national metrology institutes that can be provided upon request.

Certification of
 API T700U
 s/n 194
 Certificate Number MTU 16-04-38

Verification Audit of Diluent Mass Flow Controller As Received: 21-Apr-16

Gas Used for Calibration: **Air**
 Average Ambient Temperature: 23.1 °C
 Average Ambient Pressure: 748.2 mmHg

API T700U s/n 194 Diluent MFC Control Flow (slpm)	API T700U s/n 194 Diluent MFC Monitor Flow (slpm)	Reference Unit Molbloc 1355 (slpm)	% Difference	Acceptance Criteria
1.0000	1.0053	0.9935	1.19	+/- 4.0
2.0000	2.0021	1.9779	1.22	+/- 4.0
3.0000	3.0057	2.9622	1.47	+/- 4.0
4.0000	4.0044	3.9476	1.44	+/- 4.0
5.0000	5.0033	4.9318	1.45	+/- 4.0
6.0000	6.0062	5.9123	1.59	+/- 4.0
7.0000	7.0113	6.8993	1.62	+/- 4.0
8.0000	8.0082	7.8757	1.68	+/- 4.0
9.0000	9.0097	8.8613	1.67	+/- 4.0

Verification Audit of Source Mass Flow Controller As Received: 21-Apr-16

Gas Used for Calibration: **Air**
 Average Ambient Temperature: 24.0 °C
 Average Ambient Pressure: 751.45 mmHg

API T700U s/n 194 Source MFC Control Flow (slpm)	API T700U s/n 194 Source MFC Monitor Flow (slpm)	Reference Unit Molbloc s/n 1426 (slpm)	% Difference	Acceptance Criteria
0.0100	0.0100	0.0097	3.09	+/- 4.0
0.0200	0.0200	0.0198	1.01	+/- 4.0
0.0300	0.0300	0.0296	1.35	+/- 4.0
0.0400	0.0401	0.0394	1.78	+/- 4.0
0.0500	0.0501	0.0491	2.04	+/- 4.0
0.0600	0.0600	0.0589	1.87	+/- 4.0
0.0700	0.0701	0.0686	2.19	+/- 4.0
0.0800	0.0801	0.0784	2.17	+/- 4.0
0.0900	0.0901	0.0883	2.04	+/- 4.0

Certification of
 API T700U
 s/n 194
 Certificate Number MTU 16-04-38

Interactive Calibration of Diluent Mass Flow Controller:

Gas Used for Calibration: **Air**
 Average Ambient Temperature: 23.0 ° C
 Average Ambient Pressure: 748.35 mmHg

API T700U s/n 194 Diluent MFC DRV (mv)	Reference Unit Molbloc s/n 1355 (slpm)
250	0.5751
500	1.1048
750	1.6305
1000	2.1521
1250	2.6753
1500	3.1983
1750	3.7213
2000	4.2401
2250	4.7589
2500	5.2801
2750	5.7975
3000	6.3164
3250	6.8279
3500	7.3449
3750	7.8561
4000	8.3709
4250	8.8879
4500	9.3800
4750	9.9130
5000	10.3860

Post Calibration Performance Audit of Diluent Mass Flow Controller:

Gas Used for Calibration: **Air**
 Average Ambient Temperature: 23.4 ° C
 Average Ambient Pressure: 748.42 mmHg

API T700U s/n 194 Diluent MFC Control Flow (slpm)	API T700U s/n 194 Diluent MFC Monitor Flow (slpm)	Reference Unit Molbloc s/n 1355 (slpm)	% Difference	Acceptance Criteria
1.0000	1.0000	1.0022	-0.22	+/- 2.0
2.0000	2.0000	2.0036	-0.18	+/- 2.0
3.0000	3.0000	3.0027	-0.09	+/- 2.0
4.0000	4.0015	4.0019	-0.01	+/- 2.0
5.0000	5.0026	5.0039	-0.03	+/- 2.0
6.0000	6.0013	6.0041	-0.05	+/- 2.0
7.0000	7.0012	7.0012	0.00	+/- 2.0
8.0000	8.0021	8.0021	0.00	+/- 2.0
9.0000	9.0029	9.0029	0.00	+/- 2.0

Certification of
 API T700U
 s/n 194
 Certificate Number MTU 16-04-38

Interactive Calibration of Source Gas Mass Flow Controller:

Gas Used for Calibration: **Air**
 Average Ambient Temperature: 22.6 ° C
 Average Ambient Pressure: 747.96 mmHg

API T700U s/n 194 Source MFC DRV (mv)	Reference Unit Molbloc s/n 1426 (slpm)
250	0.0058
500	0.0112
750	0.0165
1000	0.0216
1250	0.0269
1500	0.0321
1750	0.0373
2000	0.0425
2250	0.0476
2500	0.0528
2750	0.0580
3000	0.0631
3250	0.0684
3500	0.0738
3750	0.0790
4000	0.0841
4250	0.0899
4500	0.0954
4750	0.1009
5000	0.1064

Post Calibration Performance Audit of Source Gas Mass Flow Controller:

Gas Used for Calibration: **Air**
 Average Ambient Temperature: 22.8 ° C
 Average Ambient Pressure: 747.99 mmHg

API T700U s/n 194 Source MFC Control Flow (slpm)	API T700U s/n 194 Source MFC Monitor Flow (slpm)	Reference Unit Molbloc s/n 1426 (slpm)	% Difference	Acceptance Criteria
0.0100	0.0099	0.0099	0.00	+/- 2.0
0.0200	0.0199	0.0199	0.00	+/- 2.0
0.0300	0.0300	0.0302	-0.66	+/- 2.0
0.0400	0.0400	0.0402	-0.50	+/- 2.0
0.0500	0.0500	0.0500	0.00	+/- 2.0
0.0600	0.0600	0.0601	-0.17	+/- 2.0
0.0700	0.0700	0.0701	-0.14	+/- 2.0
0.0800	0.0800	0.0802	-0.25	+/- 2.0
0.0900	0.0900	0.0900	0.00	+/- 2.0

Calibrated by: _____ Date: _____

Peter Howes , NAPS Applied Metrology Laboratory
 (613)-991-4052

Reviewed by: _____

B.3 T700U Calibrator Ozone Generator Certification

Key sections of the calibration certificate for the calibrator ozone generator are included below. the individual pre and post calibration runs are excluded for the sake of brevity. A calibrated ozone generator was required, as NO_2 was generated by gas phase titration of O_3 in excess NO .

Certification of
Ozone Photometer and
Calibration of Ozone Generator
API T700 U Dilution Calibrator
(s/n 194)

Certificate No: [MTU 16-04-23](#)

[11-Apr-16](#)

NAPS Applied Metrology Laboratory

Analysis & Air Quality Section

Air Quality Research Division

Atmospheric Science and Technology Directorate

Science and Technology Branch



Environment
Canada

Environnement
Canada

**Certification of
Ozone Photometer and
Calibration of Ozone Generator
Certificate Number : MTU 16-04-23**

This is to certify that the instrument indicated below has been calibrated against the primary reference standard of the National Air Pollution Surveillance Network.

All certification testing was performed in the NAPS Applied Metrology Laboratory of the Analysis and Air Quality Section by qualified personnel using established and reliable instrumentation and methods in a controlled environment. The reference standard employed for calibration of this transfer standard belongs to a set of equivalent reference standards manufactured by the United States National Institute of Standards and Technology (NIST). Traceability to other reference ozone photometers from among the NIST set of instruments is currently established by direct intercomparison on a periodic basis.

Certificate Issued To: Environment Canada - Atlantic Region

Date of Calibration: 11-Apr-16 **Next Calibration Required by:** 11-Apr-2017

Identification of Instrument Calibrated:

Ownership: Environment Canada - Atlantic Region

Manufacturer / Model / Serial Number: API T700 U Dilution Calibrator (s/n 194)

Calibration Reference Standard Used:

NIST Standard Reference Photometer (SRP) Serial Number: 16

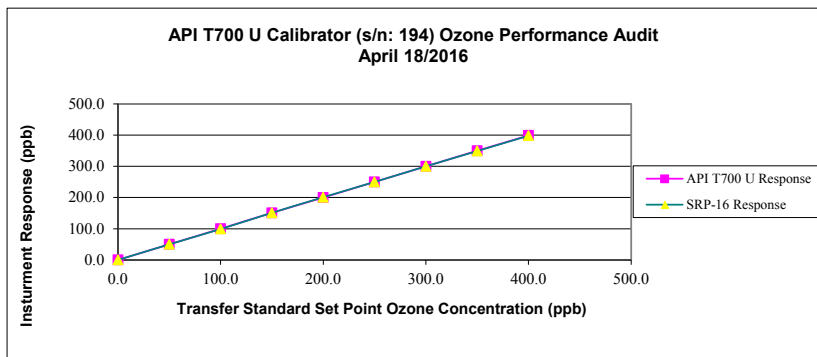
API T700 U Pre Verification Diagnostics: (with Zero Air)

Dilution Flow (LPM)	4.9927
Ozone Flow (LPM)	0.1250
Ozone Lamp Temp. (°C)	48.0
Box Temp. (°C)	26.3
Photo Meas. (mV)	3184.8
Photo Ref. (mV)	3184.8
Photo Flow (LPM)	0.7867
Photo Lamp Temp. (°C)	58.0
Photo Sample Press. (in Hg A)	28.6
Photo Sample Temp. (°C)	37.3

Audit of Transfer Standard Ozone Operation
API T700U (s/n: 194)

Audit Institute: Environment Canada **Date:** 25-Mar-15
Operator: Peter Howes
Instrument: SRP-16
Comment: API T700 U (s/n: 194) Generating Ozone Set Point
 With Photometer Servo Control "ON" vs SRP-16

API T700 U O3 Set Pt. (PPB)	API T700 U Photo. Resp. (PPB)	SRP-16 Resp. (PPB)	% Difference of Transfer Standard vs SRP-16	Acceptance Criteria (%)
0.0	0.0	0.0		
50.0	50.0	50.0	0.0	+/- 3.0
100.0	100.0	99.0	1.0	+/- 3.0
150.0	151.0	151.0	0.0	+/- 3.0
200.0	200.0	201.0	-0.5	+/- 3.0
250.0	250.0	250.0	0.0	+/- 3.0
300.0	300.0	300.0	0.0	+/- 3.0
350.0	350.0	349.0	0.3	+/- 3.0
400.0	399.0	398.0	0.3	+/- 3.0
450.0	449.0	446.0	0.7	+/- 3.0



Final Ozone Transfer Standard Diagnostics: (with Zero Air)

Dilution Flow (LPM)	4.9902	Photo Flow (LPM)	0.7954
Ozone Flow (LPM)	0.1250	Photo Lamp Temp. (°C)	58.0
Ozone Lamp Temp. (°C)	48.0	Photo Sample Press. (in Hg A)	28.9
Box Temp. (°C)	29.3	Photo Sample Temp. (°C)	40.0
Photo Meas. (mV)	3166.2	Photo Slope	0.991
Photo Ref. (mV)	3166.0	Photo Offset	-0.4

Certified by: _____ Date: _____

Peter Howes, NAPS Quality Assurance
(613)-991-4052

Reviewed by: _____

Appendix C

Traffic Volume

The following is an example of the traffic volume records as provided by the Municipality of Halifax on request of the author. They represent an number of intersections surrounding the measurement site.

HALIFAX REGIONAL MUNICIPALITY
 TRANSPORTATION & PUBLIC WORKS
 TRAFFIC & RIGHT OF WAY

CODE NO. 13-TM-191

MANUAL TRAFFIC COUNTS

INTERSECTION: ALDERNEY DRIVE AT PORTLAND STREET AND PRINCE ALBERT ROAD

DAY: TUESDAY DATE: 5 MONTH: NOV YEAR: 2013

WEATHER: SUNNY
 RECORDER: DL

STREET:		PORTLAND STREET			PORTLAND STREET			PRINCE ALBERT ROAD			ALDERNEY DRIVE			TOTAL
		FROM THE EAST			FROM THE WEST			FROM THE NORTH			FROM THE SOUTH			
15 MIN INTERVALS		L	S	R	L	S	R	L	S	R	L	S	R	
04:30:00 PM	04:45:00 PM	89	65	4	15	30	1	0	14	13	3	23	182	439
04:45:00 PM	05:00:00 PM	70	62	4	6	54	2	0	16	9	0	22	142	387
05:00:00 PM	05:15:00 PM	66	49	4	9	40	0	0	11	18	3	29	165	394
05:15:00 PM	05:30:00 PM	51	53	8	6	39	0	0	14	3	0	25	162	361

TOTAL	276	229	20	36	163	3	0	55	43	6	99	651	1581
PEAK	525			202			98			756			
15 MIN PEAK	632			248			116			832			
PEAK HOUR FACTOR	0.83			0.81			0.84			0.91			PEAK HR
TWO WAY TOTALS	1339			480			253			1090			FACTOR
													1.01
													1597

VEHICULAR GRAPHIC SUMMARY SHEET
 INTERSECTION : ALDERNEY DRIVE AT PORTLAND STREET AND PRINCE ALBERT ROAD

